PEOPLE'S DEMOCRATIC REPUBLIC OF ALGERIA
MINISTRY OF HIGHER EDUCATION AND SCIENTIFIC RESEARCH
UNIVERSITY OF M'HAMED BOUGUERRA OF BOUMERDES

FACULTY OF SCIENCE ENGINEERING
DEPARTMENT OF INDUSTRIAL MAINTENANCE
DYNAMICS MOTORS AND VIBROACOUSTICS
LABORATORY

IN PARTIAL FULFILLMENT OF THE REQUIREMENTS FOR THE

MASTERDEGREE IN MECHANICS AND ENGINEERING SYSTEMS

TOPIC

Computational analysis for wing geometry optimization

Realized by:

KHERROUBI Abdelkader

BENOUEREKHOU Tarek

Supervised by:

Mme.F.BRAHIMI

2016/2017

ACKNOWLEDGEMENT

First and foremost, we must acknowledge our limitless thanks to Allah, the Ever-Magnificent, the Ever-Thankful, for His help and bless. We are totally sure that this work would have never become truth, without his guidance.

Most importantly, none of this would have been possible without the love and patience of our Parents has been a constant source of love, concern, support and strength all these years. Particularly through the process of pursuing the master degree. Because of their unconditional love and prayers, we had the chance to complete this thesis.

We have been amazingly fortunate to have an advisor ***Mme. F. BRAHIMI*** *who gave us the freedom to explore on our own, and at the same time the guidance to recover when our steps faltered.* ***Mme. F. BRAHIMI*** *taught us how to question thoughts and express ideas. His patience and support helped us overcome many crisis situations and finish this dissertation. We hope that one day we would become as good an advisor as* ***Mme. F. BRAHIMI*** *has been to us.*

Besides our advisor, we would like to thank the responsible of Mechanics and Engineering Systems option ***Prof. NOUR Abd-el-Kader*** *who gave his life and availability for this field. We would like also to thank the jury members for their interest in our work and who honored us by their presence. And thank all the teachers of mechanical engineering system for their encouragement, insightful comments and teaching assistant.*

Finally, we appreciate the mental support of our close friends and thank all our friends and classmates for their support and encouragement through the hard times.

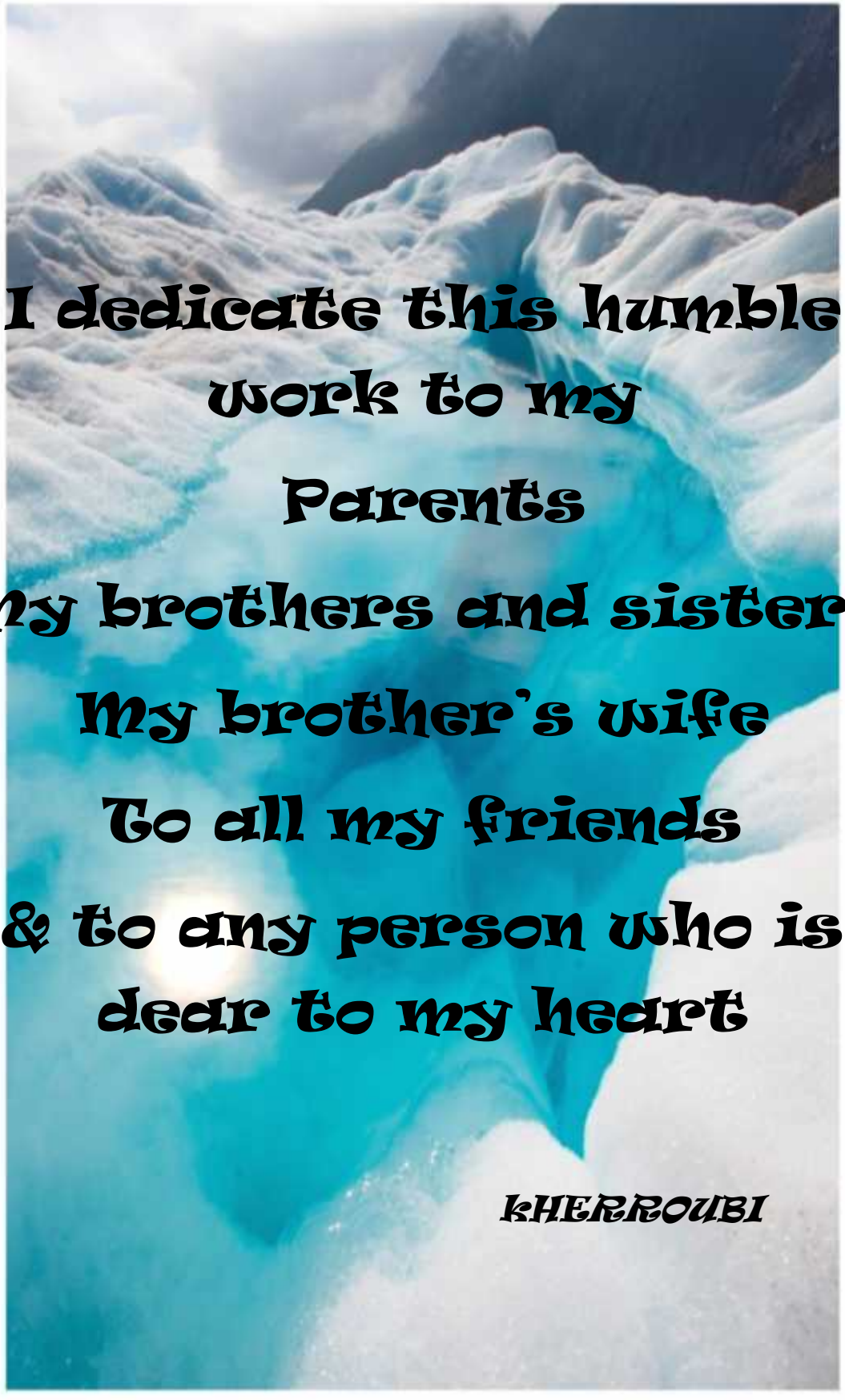

I dedicate this humble work to my

Parents

My brothers and sisters

My brother's wife

To all my friends

& to any person who is dear to my heart

kHERROUBI

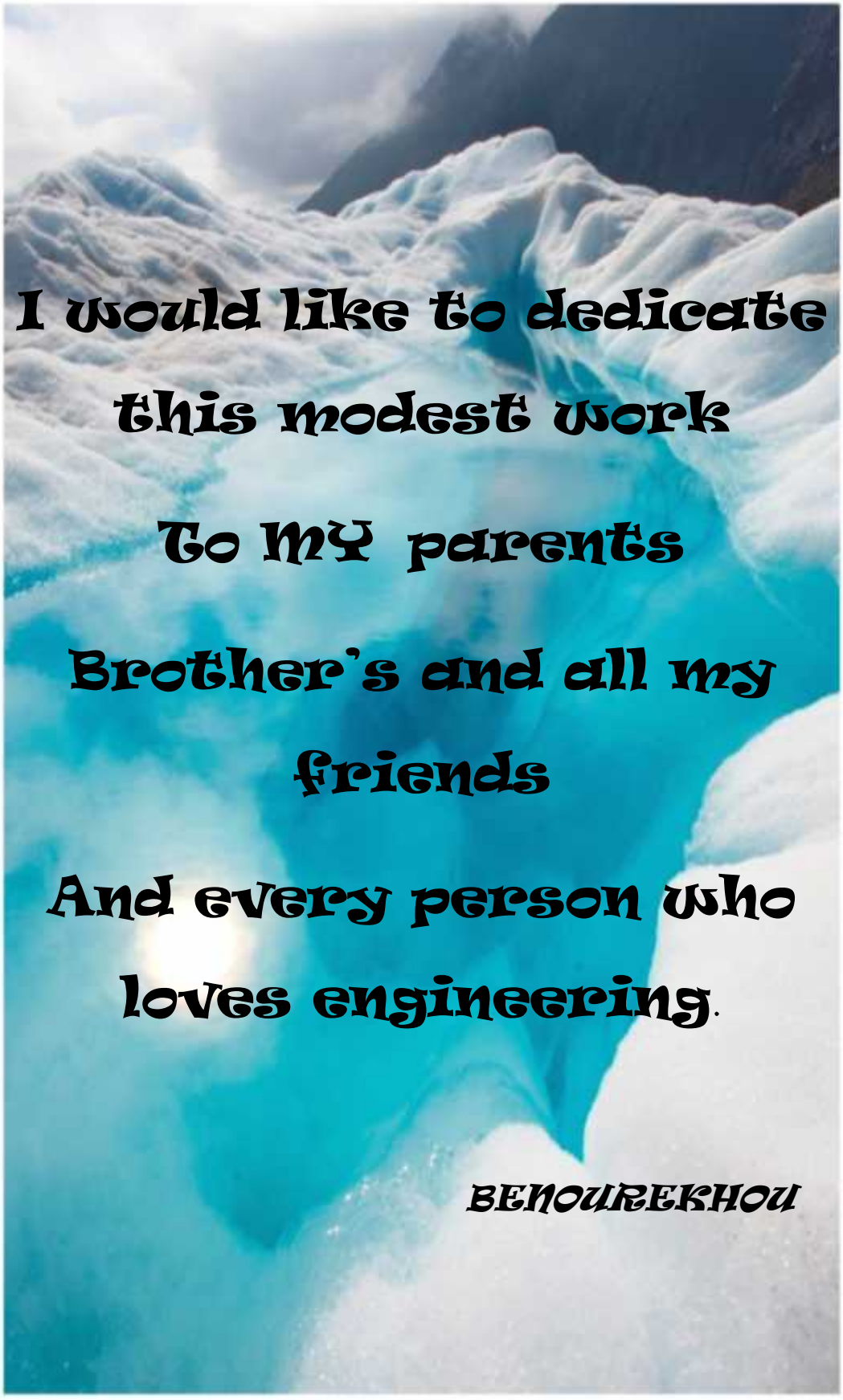
I would like to dedicate
this modest work
To MY parents
Brother's and all my
friends
And every person who
loves engineering.
BENOUREKHOU

Abstract:

In order to optimize the geometry of aircraft wings, the aim of the work is to highlight the effect of the geometric parameters of these wings such as wing span, chord and camber on the one hand on the behavior of the fluid around the wing and, on the other hand, the behavior of the wing against the forces exerted by the fluid. The tool used in this work is ANSYS software which is highly reputed for its effectiveness in several fields.

In the first step of the work we performed the simulation of the air flow around the wing in the fluid part of the software in a three-dimensional configuration. The flow is stationary and compressible with an upstream Mach number of 0.29. This allows us to determine the forces exerted by the fluid on the wing. These forces are represented by the aerodynamic coefficients of lift and drag.

In the second part of the work we carried out simulations in the structural part of the software. The wing being subjected to the force exerted by the fluid, we have determined the Von-Mises stress, the elastic deformation, the deformation energy and the maximum deformation undergone by the wing. The simulations were carried out for different configurations corresponding to wings with different wingspans, chords and different camber.

The results obtained have clearly shown that the geometrical parameters of the wings have a considerable effect on the evolution of the various variables used.

Résumé :

Dans le but d'optimiser la géométrie des ailes d'avion, l'objectif du travail consisteà mettre en évidence l'effet des paramètres géométriques de ces ailes tels que l'envergure, la corde et la cambrure d'une part sur le comportement du fluide autour de l'aile et d'autre part sur le comportement de l'aile face aux efforts exercés par le fluide. L'outil utilise dans ce travail est le logiciel ANSYS qui est très réputé pour son efficacité dans plusieurs domaines.

Dans la première étape du travail nous avons effectué la simulation de l'écoulement d'air autour de l'aile dans la partie fluide du logiciel dans une configuration tridimensionnelle. L'écoulement étant stationnaire et compressible avec un nombre de Mach amont de 0.29. Ceci nous permet de déterminer les efforts qui sont exercés par le fluide sur l'aile. Ces efforts sont représentés par les coefficients aérodynamiques de portance et de traînée.

Dans la deuxième partie du travail nous avons réalisé des simulations dans la partie structure du logiciel. L'aile étant soumise à l'effort exercé par le fluide nous avons déterminé la contrainte de Von-Mises, la déformation élastique, l'énergie de déformation et la déformation maximale subies par l'aile. Les simulations ont été réalisées pour différentes configurations correspondant à des ailes avec différentes envergures, cordes et différentes cambrures.

Les résultats obtenus ont bien montré que les paramètres géométriques des ailes ont un effet considérable sur l'évolution des différentes variables utilisées.

ملخص:

الهدف من هذا العمل هو تسليط الضوء على تأثير المعايير الهندسية لهذه الأجنحة مثل الحجم، والحل واحدودلب الأجنحة من أجل تحسين هندسة أجنحة الطائرات. من جهة سلوك السوائل حول الجناح والآخر على سلوك الجناح التي تواجه قوات السوائل المبذولة. الأداة المستخدمة في هذا العمل هي برنامج انسيس التي تشتهر فعاليته في العديد من المجالات.

في المرحلة الأولى من العمل نقوم بدراسة محاكاة لتدفق الهواء حول الجناح في الجزء السائل من البرنامج في تكوين ثلاثي الأبعاد. تدفق غير ثابتة وانضغاط مع عدد ماخ من المنبعيساوي.0.29 وهذا يسمح لنا لتحديد الجهود المبذولة من قبل السائل على الجناح. يتم تمثيل هذه القوى عن طريق المعاملات الهوائية الرفع والسحب.

في الجزء الثاني من العمل قمنا بتنفيذ المحاكاة في الجزءالمخصصلبنية البرمجيات. نناقش فيه مدى تأثير القوى الأيروديناميكية الناتجة عن تدفق الهواء على سطح الجناح وتأثيرها على الإجهاد والتشوه المرن والحد الأقصى من التشوه.

أجريت محاكاة لتكوينات مختلفة الأجنحة مع مختلفة الأحجام، السلاسل والأحداب وقد أظهرت النتائج أن المعاييرالهندسية من الأجنحة لها تأثير كبير على تطور المتغيرات المختلفةالمستعملة.

0

SUMARRY

THEORETICAL PART

A.WING GENERALITIES

B.REVEIW OF FLUID MECHANICS AND AERODYNAMICS

SUMARRY

C.REVIEW OF STRUCTURE MECHANICS

NUMERICAL SUMILATION PART

SUMARRY

SUMARRY

LISTE OF FIGURES

PART I

LISTE OF FIGURES

PART II

LISTE OF FIGURES

LISTE OF FIGURES

LISTE OF FIGURES

LIST OF SYMBOLS

A: Axial Force

a_c : Critical Crack length

C_A : Axial force Coefficient

C_D : Drag coefficient

C_f : Skin Friction Coefficient

C_l : Lift coefficient

C_N : Normal coefficient

C_M : Moment coefficient

C_p : Pressure coefficient

C_a : Viscous Matrix of Cushion

C_{r} : Chord root length

C_{ti} : Chord root length

$c\dot{x}$: Viscous resistance force

E: Young Modulus

e: Internal energy

K: Stiffness

K_m : Maximum Stress Intensity Factor

K_m : Minimum Stress Intensity Factor

kx: Elastic force

L: Wing length (m)

$m\ddot{x}$: Inertia force

N: Normal Force

N_f : Remaining Number of Cycle Factor

P: Pressure

q_∞: Dynamics pressure

$\dot{q}$: Rate volumetric heat addition

LIST OF SYMBOLS

$\dot{Q}'_v$, $\dot{W}'_v$: Proper forms of the viscous terms

$\Re e$: Reynolds number

S_S : Yield Strain in shear

S_y: Tensile Yield Strength

T: Temperature

V: Speed

V_∞: Freestream velocity

α: Angle of attack

χ: Compressibility

Y: Dimensionless Parameter

ρ: Density

τ: Shear stress

$\sigma_{V\ -M}$: Von-Mises stress

σ: Applied Stress

Δk: Range of the Stress Intensity Factor

Δ_ω: Range of Cyclic Stress Amplitude

ε: Strain energy

μ: Dynamic viscosity

λ : Damping coefficient

η: Relative damping (or damping factor)

$\omega_{\mathbb{C}}^2$: Pulse of the conservative system

AOA: Angle of attack

LE: Leading edge

TE: Trailing edge

GENERAL INTRODUCTION

Air transport has an important place in the transit of people or goods through the seas and oceans. The airplane has been the main engine since the first world War. It has a crucial place in modern society today.

Following the first flights made by the Wright brothers in december 1903 the stability and controller problems faced in the early years were sometimes considerable since the flying qualities of their aircrafts were often less than satisfactory, and when we talk about facts we have to start from aircraft wing.

The wing has a leading role in the flight of aircraft. The wing allows the aircraft to fly and to be in an equilibrium position. it creates a force called lift, the lift is obtained by the fact that a vacuum is created on the upper surface and an overpressure on the lower surface, which will cause the aircraft to rise, To ensure a good air plane conditions, relatively to the wing, we must have great aerodynamic forces such as high lift and samall drag and wing material with the best geometrical caracteristcs to can bear these forces .

After knowinng that lift is created by the wing, we should ask if this force varies according to different parameters related to the wing.

In that context this work based on a numerical simulation of the air flow over an aircraft wing will show in a first step the influence of the geometrical parameters of the wing as the span, the chord and the camber on the aerodynamic forces (lift and drag).

Secondly a structural analysis, is foreseen to show the structure response to the aerodynamic forces. It is represented by the deformation, elastic strain, Von-Mises stress and the strain energy.

To acheive our purpose the paper is organized into two main parts as fallow:

- Theoritical part in which we present some generalities obout the wings, a review of fluid mechanics and aerodynamics and we end with some notions of the solids.
- Numerical part: it contains a numerical simulation for the fluid and a numerical simulation for the structure. In each part we desribe the different steps followed to use the software, the simulation conditions and the results obtained. All simulations are carried out by ANSYS softwar.
  And we finish with a general conclusion.

A. WING GENERALITIES

A wing is a type of fin with a surface that produces aerodynamic forces facilitating movement through air and other gases, or water and other liquids. As such, wings have an airfoil shape, a streamlined cross-sectional shape producing lift. The word "wing" from the Old Norse vængr for many centuries referred mainly to the foremost limbs of birds (in addition to the architectural aisle). But in recent centuries the word's meaning has extended to include lift producing appendages of insects, bats, pterosaurs, boomerang, some sail boats and aircraft, or the inverted airfoil on a race car that generates a downward force to increase traction.

Various species of penguins and other flighted or flightless water birds such as auks, cormorants, guillemots, shearwaters, eider and scoter ducks and diving petrels are avid swimmers, and use their wings to propel through water [1].

I. Geometry of wing

The figure 1 gives technical definitions of a wing's geometry, which is one of the chief factors affecting airplane lift and drag. The figure shows a wing viewed from three directions; the upper left shows the view from the top looking down on the wing, the lower left shows the view from the front looking at the wing leading edge, and the right shows a side view from the left looking in towards the centerline

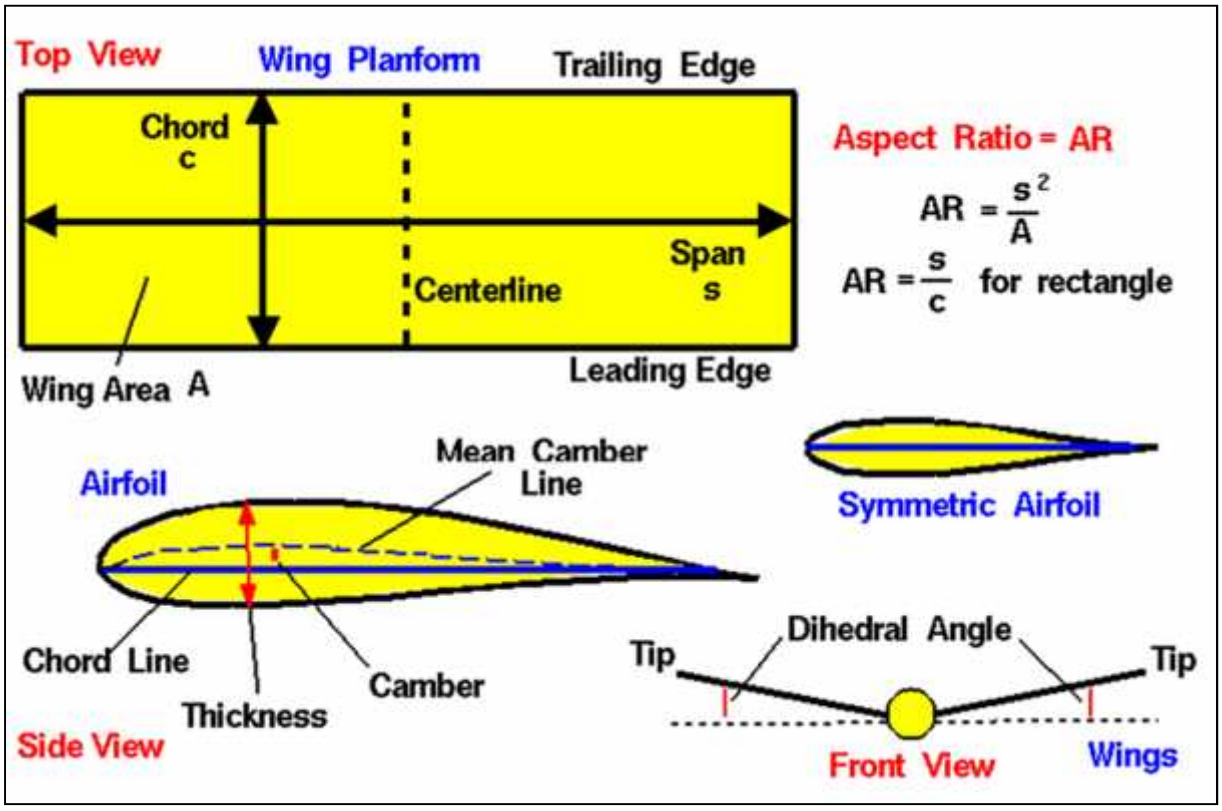

Figure 1: Wing Geometry

THEORETICAL PART

The side view shows an airfoil shape with the leading edge to the left. We defined the wing parameters:

- The mean camber line: is the line joining the mid points between the upper and lower surfaces of an airfoil and measured perpendicular to the mean camber line.
- The chord line: is the straight line which joins the end points of the mean camber line.
- The thickness: is the height of the airfoil measured normal to the chord line. The ratio of maxi-mum thickness to the chord length is called the thickness ratio.
- The camber: is the maximum distance of the mean line from the chord line.
- The leading edge: is the point at the front of the airfoil that has maximum curvature (minimum radius).
- The trailing edge: is defined similarly as the point of maximum curvature at the rear of the airfoil [2].

Top view

The top view shows a simple rectangular wing geometry. The front of the wing (at the bottom) is called the leading edge; the back of the wing (at the top) is called the trailing edge. The distance from the leading to trailing edges is called the chord. The ends of the wing are called the wing tips, and the distance from one wing tip to the other is called the span. The shape of the wing, when viewed from above looking down onto the wing, is called a planform. For a rectangular wing, the chord length at every location along the span is the same. For most modern aircraft, the chord length varies along the span, and the leading and trailing edges may be swept. The wing area is the projected area of the planform and is bounded by the leading and trailing edges and the wing tips. The total surface area includes both upper and lower surfaces. The wing area is a projected area and is almost half of the total surface.

Front view

The front view of this wing shows that the left and right wing do not lie in the same plane but meet at an angle. The angle that the wing makes with the local horizontal is called the dihedral angle if the tips are higher than the root or the an anhedral angle if the tips are lower than the root. Dihedral is added to the wings for roll stability, a wing with some dihedral will naturally return to its original position if it encounters a slight roll displacement. You may have noticed that most large airliner wings are designed with dihedral. The wing tips are farther off the ground than the wing root. Highly maneuverable fighter planes, on the other hand usually have the wing tips lower than the roots giving the aircraft a high roll rate. The Wright brothers designed their 1903 flyer with a slight anhedral to improve the aircraft roll performance [3].

II. Types of wings

II.1 Low aspect ratio

Short and stubby wing more efficient structurally and higher instantaneous roll rate. They tend to be used by fighter aircraft, and by very highspeed aircraft (e.g. North American X 15).
Moderate aspect ratio: general purpose wing (e.g. the Lockheed P80 Shooting Star).
High aspect ratio: long and slender wing. More efficient aerodynamically, having less induced drag. They tend to be used by high altitude subsonic aircraft, subsonic airliners (e.g. the Bombardier Dash 8) and by high performance sailplanes (e.g. Glaser Dirks DG500)

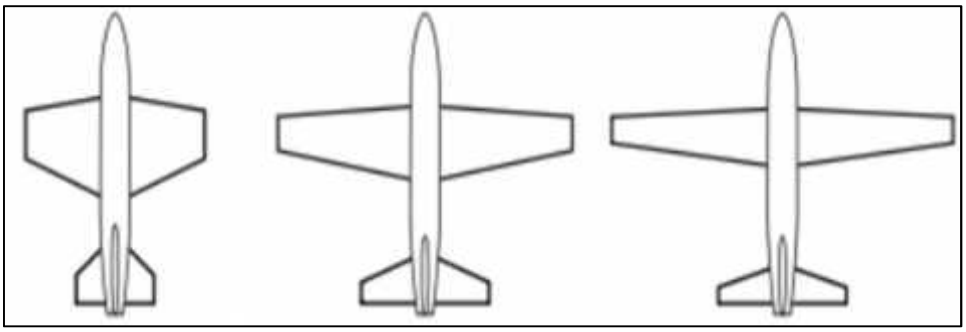

Figure 2: Wings Low aspect ratio, Moderate aspect ratio and High aspect ratio

II.2 Constant chord

Parallel leading and trailing edges, Simplest to make, and common where low cost is important.
Tapered: Structurally and aerodynamically more efficient than a constant chord wing, and easier to make than the elliptical type.

Compound tapered: Typically braced to maintain stiffness, used on the Westland Lysander army cooperation aircraft to increase visibility for the crew.
Constant chord with tapered outer section: common variant seen for example on many Cessna types and the English Electric Canberra.

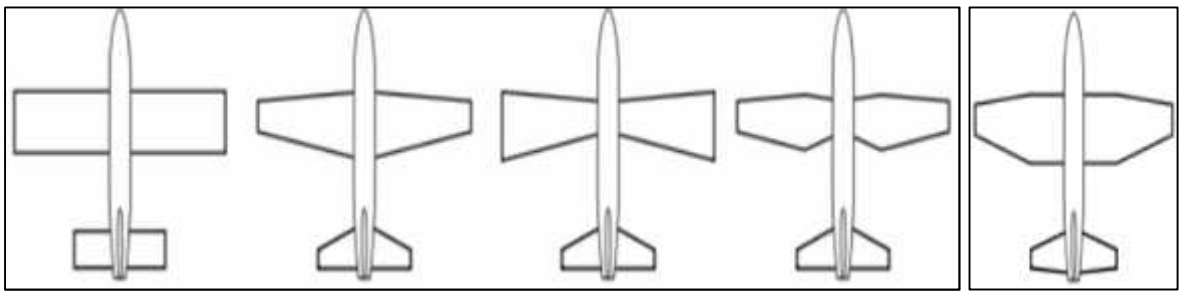

Figure 3: Constant chord, tapered (trapezoidal), reverse tapered, compound tapered, constant chord (tapered outer)

II.3 Elliptical

Leading and trailing edges are curved such that the chord length varies elliptically with respect to span. Theoretically the most efficient, but difficult to make. Famously used on the super marine Spitfire.

II.4 Semielliptical

Only the leading or trailing edge is elliptical with the other being straight.

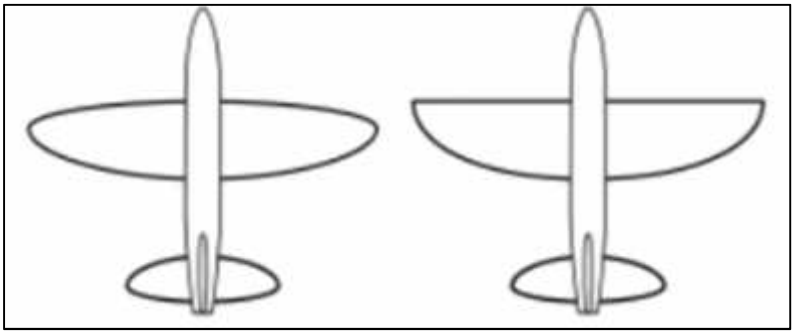

Figure 4: Elliptical and semi-elliptical wing

II.5 Delta

Triangular plan form with swept leading edge and straight trailing edge, offers the advantages of a swept wing, with good structural efficiency and low frontal area. Disadvantages are the low wing loading and high wetted area needed to obtain aerodynamic stability. We have a lot of types of delta wings like Tailless delta, Tailed delta, cropped delta, Compound delta or double delta, ogival delta …

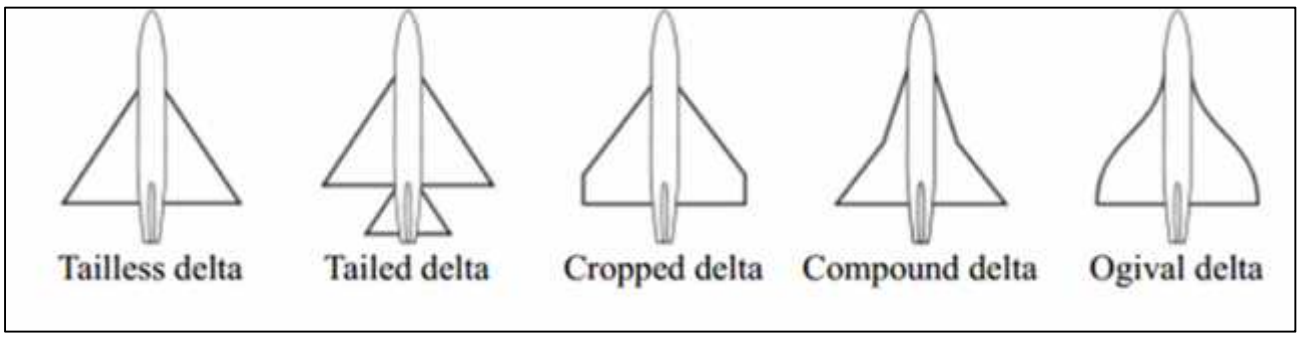

Figure 5: Different types of delta wings.

II.6 Straight and swept

Extends at right angles to the line of flight, the most structurally efficient wing, it is common for low speed designs, such as the P80 Shooting Star and sailplanes. Swept back (aka "swept wing"): The wing sweeps rearwards from the root to the tip. In early tailless examples, such as the Dunne aircraft, this allowed the outer wing section to act like a conventional empennage (tail) to provide aerodynamic stability. At transonic speeds swept

wings have lower drag, but can handle badly in or near a stall and require high stiffness to avoid aero elasticity at high speeds. Common on high subsonic and early supersonic designs e.g. The Hawker Hunter. [4].

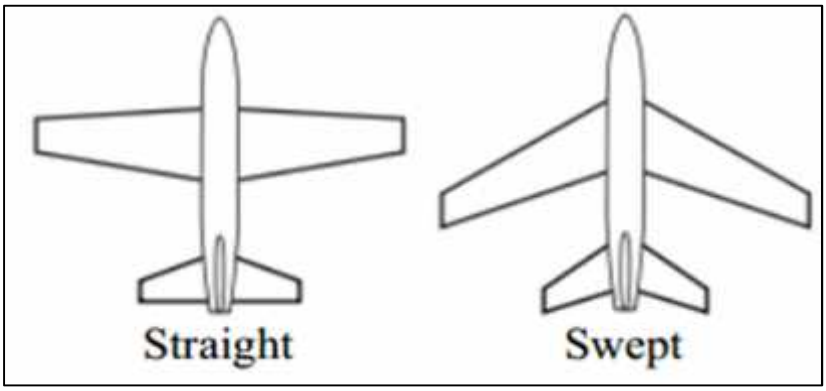

Figure 6: Straight and swept wing.

III. Airfoil

An airfoil is the term used to describe the cross-sectional shape of an object that, when moved through a fluid such as air, creates an aerodynamic force. Airfoils are employed on aircraft as wings to produce lift or as propeller blades to produce thrust. Both these forces are produce perpendicular to the air flow. Drag is a consequence of the production of lift/thrust and acts parallel to the airflow.

The NACA airfoils were designed during the period from 1929 through 1947 under the direction of Eastman Jacobs at the NACA's Langley Field Laboratory. Most of the airfoils were based on simple geometrical descriptions of the section shape, although the 6 and 6A series were developed using theoretical analysis and don't have simple shape definitions. Although a new generation of airfoils has emerged as a result of improved understanding of airfoil performance and the ability to design new airfoils using computer methods, the NACA airfoils are still useful in many aerodynamic design applications [5].

The airfoils are described as NACA xxxx or NACA xxxxx or NACA xx_y-xxx series. Following definitions are given to this nomenclature.

The NACA 4-digit airfoils mean the following: The first digit expresses the camber in percent chord, the second digit gives the location of the maximum camber point in tenths of chord, and the last two digits give the thickness in percent chord. Thus 4412 has a maximum camber of 4% of chord located at 40% chord back from the leading edge and is 12% thick, While 0006 is a symmetrical section of 6% thickness.

The NACA 5-digit series airfoil means the following: The first digit designates the approximate camber in percent chord, the second digit indicates twice the position of the maximum camber in tenths chord, the third (either 0 or 1) distinguishes the type of mean-camber line, and the last two digits give the thickness in percent chord. Thus, the 23012 airfoil has a maximum camber of about 2% of the chord located at 15% of the chord from the leading edge (3 tenths divided by 2) and is 12% thick.

The NACA six, seven and even eight series were designed to highlight some aerodynamic characteristic. For example, NACA 65_3-421 is a 6-series airfoil for which the minimum pressure's position in tenths chord is indicated by the second digit (here, at the 50% chord location), the subscript 3 means that the drag coefficient is near its minimum value over a range of lift coefficients of 0.3 above and below the design lift coefficient, the next digit indicates the lift coefficient in tenths (here, 0.4) and the last two digits give the maximum thickness in percent chord (here, 21% of chord) [5].

IV. Manufacturing material of wings

IV.1 Aluminum

The current material used for aircraft wings is aluminum. This material is currently used to construct aircraft wings [6]. The advantages and the disadvantages of aluminum alloy are presented in table 1:

Advantages	Disadvantages
• Light weight • Easily shaped/cast/forge • Good electrical conductor • Good thermal conductor • Easy to machine	• Expensive to refine (must be done by electrolysis of fused salts) • Poor chemical resistance (acids and base) • Loses strengths when heated

Table 1: Advantages and disadvantages of Aluminum

IV.2 Titanium

This metal has a high strength to weight ratio, a relative density of 4.5 which is 60% heavier than aluminum however it is twice as strong.

Titanium has excellent corrosion resistance properties this is due to the oxide film which forms. Titanium is not normally susceptible to stress, fatigue, intergranular or galvanic corrosion, putting or localized attack. However, under certain circumstances it will burn in air, therefore in order to prevent a reaction with oxygen or nitrogen it may be treated with chloride gas in order to form a protective coating of titanium dioxide.

Titanium and its alloys are classed in 3 categories:

- Alpha (A) - Wieldable, tough, strong both hot and cold and resistant to oxidization.
- Beta (B) - Excellent bend ductility, strong both hot and cold however vulnerable to contamination.

- Combined (C) - Combination of alpha and beta with comprised performance, strong cold and warm but weak when hot, excellent forgeability, good bendability moderate contamination resistance. The melting point of titanium is 1668 degrees Celsius and has low thermal conductibility and a low co efficient of expansion. Its high temperature properties are however disappointing.; the ultimate yield strength falls rapidly above 425 degrees Celsius and atmospheric oxygen and nitrogen absorbent above 540 degrees Celsius makes the metal brittle and worthless after a long-term exposure.

The ideal type of titanium to use on an aircraft wing would be the combined (C) class as it does meet to requirements for an aircraft wings. However, the major drawback for this material is when working with titanium extra care must be taken when making due to its extreme work hardening properties. The advantages and the disadvantages of titanium are presented in table 2:

Advantages	Disadvantages
• Lightweight • Strong • Able to withstand high temperatures • Corrosion resistant	• Expensive • Process for forming and joining titanium are complex and expensive

Table 2: Advantages and disadvantages of titanium

IV.3 Composite

A composite material consists of two or more different materials whose mechanical properties complement each other although maintain their separate identities, unlike alloy.

The reason the composite materials are used on an aircraft and their strength to weight ration and corrosion resistance. Reinforced plastics are much lighter than metals. If the metal part can be as much as 25 times heavier than an equivalent composite part, however that composite part must be as strong and durable as the original.

Therefore, reinforced plastics must have very good strength, stiffness and impact resistance.

Strength- this is the ability of a material to support a load without breaking.

Stiffness- this is the ability of material to support a load without bending too much.

Impact- this is the ability of a material to withstand resistance impact without shattering.

The types of the most reinforced materials used:

- Glass reinforced plastic
- Aramid fibers
- Carbone fibres

IV.4 Aluminum- Lithium

Aluminum- lithium is a new concept within the aviation industry which allows the industry to progress in a new direction, this allows an aircraft to be light, efficient yet have the same amount of or more power to transport both passengers and freight. Also, with aircraft being so light it may allow even bigger aircrafts then the currently produced Airbus A380, and Boeing 787 to be produced. The advantages and the disadvantages of Aluminum-Lithium are presented in table 3:

Advantages	Disadvantages
• 10% denser than aluminium 2024 • Lightweight • 10 - 15% higher modulus than aluminum 2024 • Excellent fatigue and cryogenic toughness properties • Higher stiffness • Superior fatigue crack growth resistance	• Reduced ductility • Low fracture toughness

Table 3: Advantages and disadvantages of Aluminum-Lithium

B. REVIEW OF FLUIDS MECHANICS AND AERODYNAMICS

Review of fluid mechanics

In all real flow situations, the physical laws of conservation apply. These refer to the conservation respectively of mass, momentum and energy. The equation of state completes the set that needs to be solved if some or all of the parameters controlling the flow are unknown. If a real flow can be 'modeled' by a similar but simplified system, then the degree of complexity in handling the resulting equations may be considerably reduced [7].

I. Basic equations of conservation

I.1 Continuity equation

The continuity equation is developed simply by applying the law of conservation of mass to a small volume element within a flowing fluid.

In fluid dynamics, the continuity equation states that, in any steady state process, the rate at which mass enters a system is equal to the rate at which mass leaves the system [8].

The differential form of the continuity equation is

$$\frac{\partial \rho}{\partial t} + \nabla . (\rho.u) = 0 \qquad (1)$$

If the fluid is an incompressible flow (ρ = constant), the mass continuity equation simplifies to a volume continuity equation:

$$\nabla . u = 0 \qquad (2)$$

This means that the divergence of velocity field is zero everywhere.

I.2 Momentum equation

Newton's law states that the rate change of linear momentum of a system is equal to the net force acting on a system

The general momentum equation is also called the equation of motion, when the fluid is Newtonian.

The momentum equation in integral form is written as:

$$\frac{\partial}{\partial} \iiint_v \rho \quad + \oiint_s (\rho \quad . d \,) V = - \oiint_s \rho \, d \; + \iiint_v \rho \quad + F_v \qquad (3)$$

The x, y, and z components of the momentum equation respectively in differential form are:

$$\frac{\partial}{\partial t}(\rho u) + \nabla.(\rho\, u\, V) = -\frac{\partial p}{\partial x} + \rho f_x + (F_x)_v \quad (4)$$

$$\frac{\partial}{\partial t}(\rho\, v) + \nabla.(\rho\, v\, V) = -\frac{\partial p}{\partial y} + \rho f_y + (F_y)_v \quad (5)$$

$$\frac{\partial}{\partial t}(\rho\, w) + \nabla.(\rho\, w\, V) = -\frac{\partial p}{\partial z} + \rho f_z + (F_z)_v \quad (6)$$

Equations (3) and (4,5, and 6) apply to the unsteady, three-dimensional flow of any fluid, compressible or incompressible, viscous or in viscid.

I.3 Energy equation

The energy equation is based on the principle that energy can be neither created nor destroyed it's written as:

$$\iiint_v q\rho dv + \dot{Q}_v - \oiint_s (\rho V\,.ds)\,V + \iiint_v \rho(f.V)dv + \dot{W}_v = \frac{\partial}{\partial t}\iiint_v \rho\left(e + \frac{V^2}{2}\right)dv + \oiint_s \rho\left(e + \frac{V^2}{2}\right) \quad (7)$$

Or:

$$\dot{q}\rho + \rho(f.V) - \nabla.(\rho V) + \dot{Q}'_v + \dot{W}'_v = \nabla.\left(\rho\left(e + \frac{V^2}{2}\right)V\right) + \frac{\partial}{\partial t}\left(\rho\left(e + \frac{V^2}{2}\right)V\right) \quad (8)$$

Where $\dot{Q}'_v$ and $\dot{W}'_v$ represent the proper forms of the viscous terms [12].

- $\boldsymbol{\rho}$: Density of the fluid **(kg/m^3)**
- **f :** Force **(N)**
- **v:** Volume **(m^3)**
- **e:** Internal energy **(J)**
- $\dot{\mathbf{q}}$**:** Rate of volumetric heat addition

I.4 Ideal gas law

The state of an amount of gas is determined by its pressure, volume, and temperature.

$$P.\,V = n.R.T$$

- **P** is the pressure of the gas.
- **V** is the volume of the gas.
- **n** is the amount of substance of gas (number of moles).
- **R** is the universal gas constant.
- **T** is the temperature of the gas.

These equations are at the heart of fluid flow modeling. for a particular set of boundary conditions (such as inlet, outlets, and walls), predicts the fluid velocity and its pressure in a given geometry.

II. Flow types

II.1 Inviscid and Viscous Flow

If there is friction, thermal conduction or diffusion in a flow, it is termed **viscous**. If none of these things is present, the flow is Inviscid flows do not appear in nature, but some flows are almost inviscid [9].

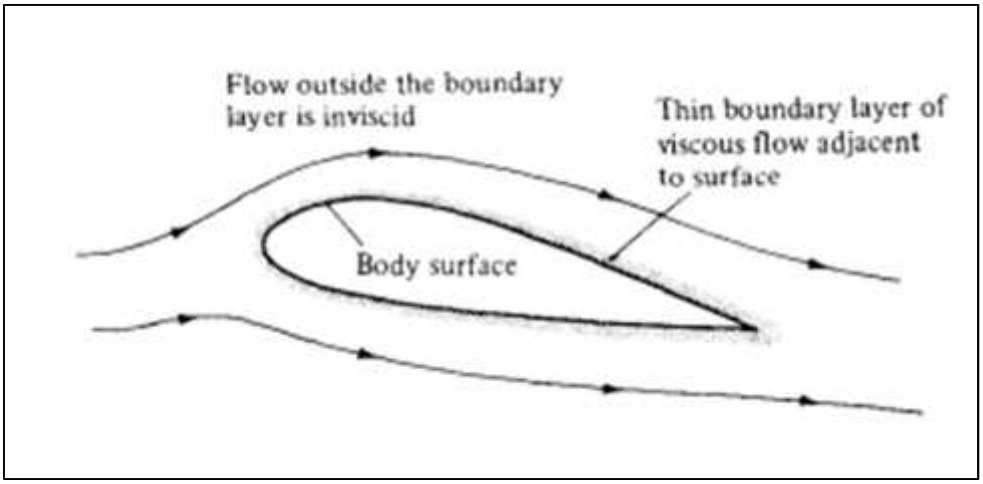

Figure 7: Division of a flow into two regions: (I) the thin viscous boundary layer adjacent to the body surface and (2) the inviscid flow outside the boundary layer

II .2 Incompressible and Compressible Flows

A flow in which the density **ρ**is constant, otherwise a compressible flow is a flow in which the fluid density ***ρ*** varies significantly within the flow field. therefore, *ρ (x, y, z) must* now be treated as a field variable rather than simply a constant. Typically, significant density variations start to appear when the flow **Mach number 0.3.**

The effects become especially large when the Mach number approaches and exceeds unity.

Most problems in incompressible flow have two unknowns:

Pressure and velocity. These unknowns were solved by using the underlying principals from the continuity and linear momentum conservation equations. In compressible flow pressure and velocity remain unknown but density and temperature also become a factor. These hints at the need for two additional equation in order to solve equation of state for gas and the conservation of energy equation [10].

	Incompressible flow	Compressible flow
Variables	$\vec{V}$, P	$\vec{V}$, P,ρ,T
Equations	Mass, momentum	Mass, momentum, energy, state

Table 4: Variables and equation which come into play in compressible and incompressible flows

II.3 Mach Number Regimes

In fluid dynamics, the Mach is a dimensionless quantity representing the ratio of flow velocity past a boundary to the local speed of sound.

The Mach number *M* is defined as ***u/a***, where ***u*** is the airflow velocity and ***a*** is the speed of sound.

- **Subsonic flow (M < 1 everywhere**) A flow field is defined as subsonic if the Mach number is less than 1 at every point. Subsonic flows are characterized by smooth streamlines.
- **Transonic flow (mixed regions where M < 1 and M> 1)** As stated above, if M_∞ is subsonic but is near unity, the flow can become locally supersonic **(M>1).** This is sketched in Fig. 2.b, which shows pockets of supersonic flow over both the top and bottom surfaces of the airfoil.
- **Supersonic flow (M>1 everywhere)** A flow field is defined as supersonic if the Mach number is greater than 1 at every point. Supersonic flows are frequently characterized by the presence of shock waves across which the flow properties and streamlines change discontinuously (in contrast to the smooth, continuous variations in subsonic flows) [11] [12].
- **Hypersonic flow (very high supersonic speeds)** Refer again to the wedge in **Figure 7.d** assume ɵ is a given, fixed value. As M, increases above 1, the shock wave moves closer to the body surface. Also, the strength of the shock wave increases, leading to higher temperatures in the region between the shock and the body (the shock layer). If Mx is sufficiently large, the shock layer becomes very thin, and interactions between the shock wave and the viscous boundary layer on the surface occur

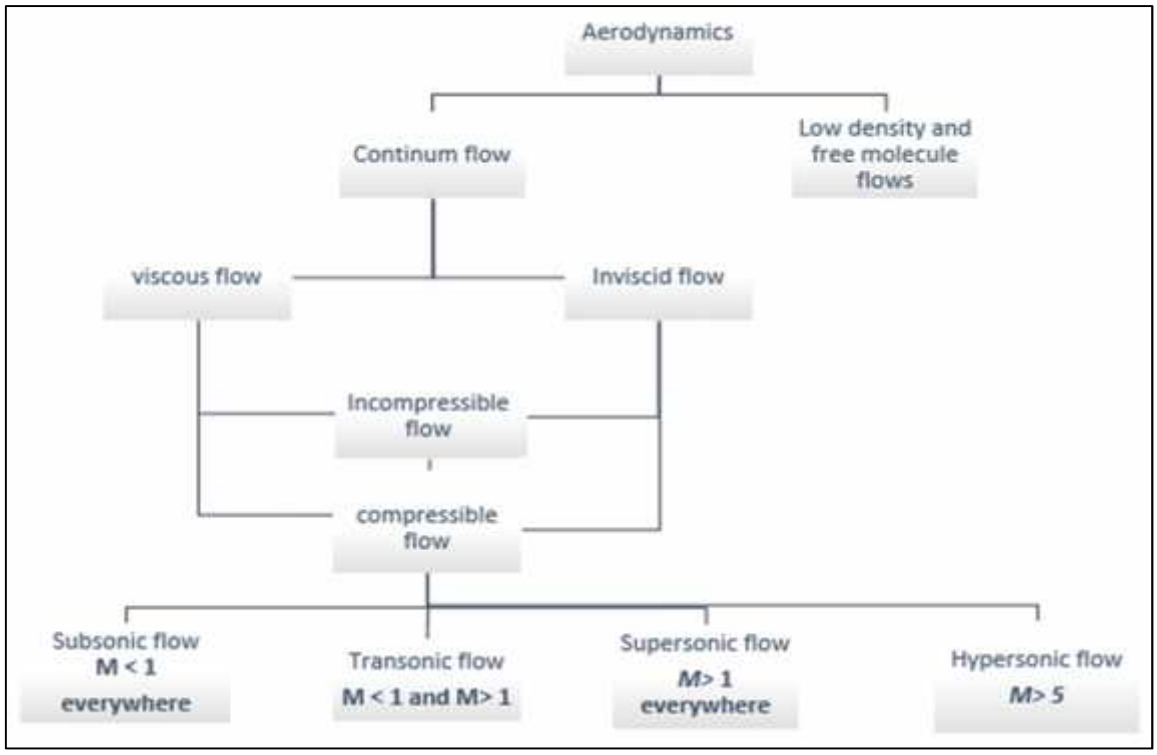

Table 5: Block diagram categorizing the types of aerodynamic flows

II.4 Reynolds number

The Reynolds number is defined as:

$$\Re e = u.\frac{L}{\nu} \qquad \text{or} \qquad \Re e = \frac{\rho.u.L}{\mu} \tag{9}$$

Where:

- $\boldsymbol{\rho}$ is the density of the fluid (SI units: kg/m^3)
- $\boldsymbol{u}$ is the velocity of the fluid with respect to the object (m/s)
- $\boldsymbol{L}$ is a characteristic linear dimension (m)
- $\boldsymbol{\mu}$ is the dynamic viscosity of the fluid (Pa·s or N·s/m^2 or kg/(m·s))
- $\boldsymbol{\nu}$ is the kinematic viscosity of the fluid (m^2/s)

The Reynolds Number can be used to determine if flow is laminar, transient or turbulent. The flow is [13]:

- **laminar** - when Re < 2300
- **transitionnel** - when 2300 < Re < 4000
- **turbulent** - when Re > 4000

II.5.1 Laminar(streamline)flow

Particles of a continuous fluid can be considered to travel along smooth continuous paths which are given the name streamlines, these streamlines can be curved or straight, depending on the flow of the fluid.

Laminar flow is a simple flow, it occurs when a fluid flows is parallel layers, with no disruption between the layers, no cross currents or eddies perpendicular to direction of flow.

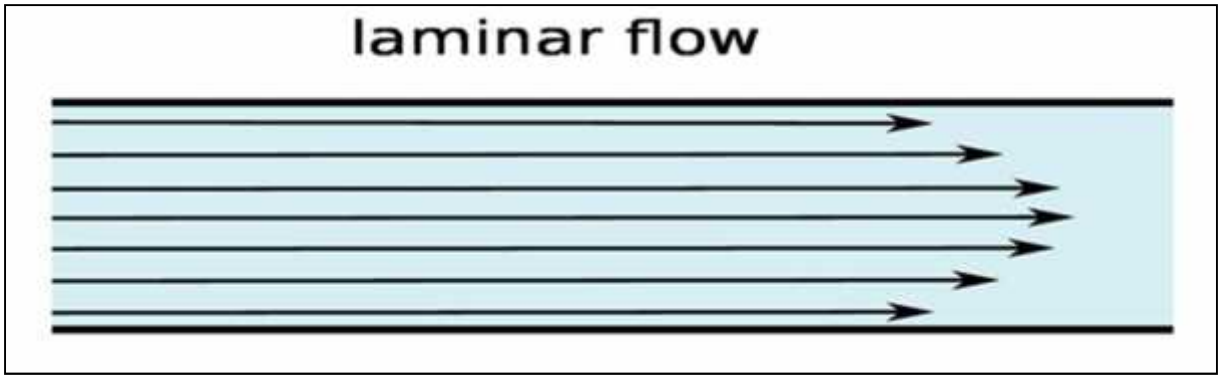

Figure 8: stream line of laminar flow

The laminar flow can be further sub grouped as:

- **Stable laminar flow:** This type of laminar flow prove stable toward imposed disturbances acting from outside.
- **Unstable laminar flow:** a laminar flow is considered unstable when disturbances introduced into it are amplified, but certain “regularity” in the excited disturbances is maintained, in other words, due to the disturbance the investigated flow merges into a new laminar flow state [14].

II.5.2 Transitional flow

When flow is intensified, it tends to switch from laminar to turbulent flow.

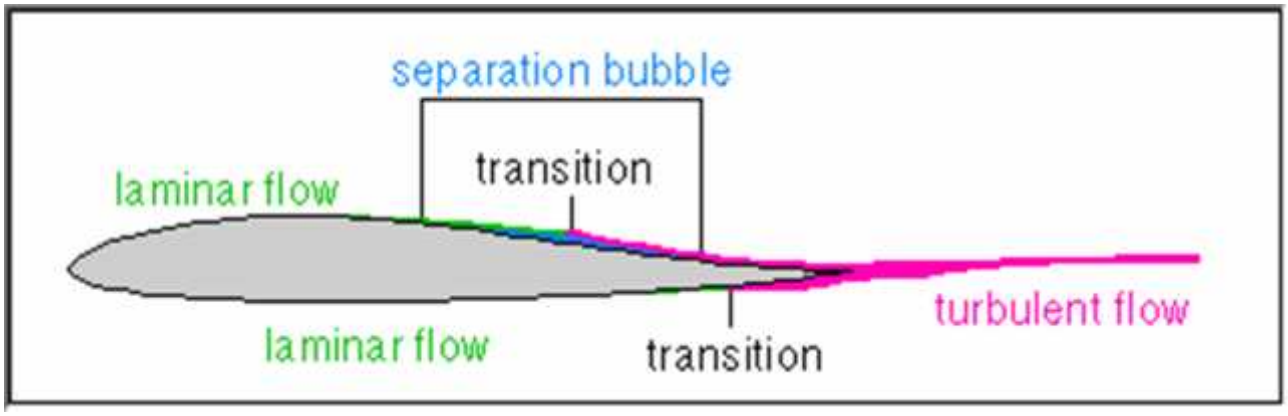

Figure 9: flow regions around an airfoil

II.5.3 Turbulent flow

Is an irregular flaw and is characterized by transfer of small packets of fluid particles layers. Thus, it is accompanied by fluctuations in velocity.

When fluid flow is intensified, it tends to switch from laminar to turbulent flow.

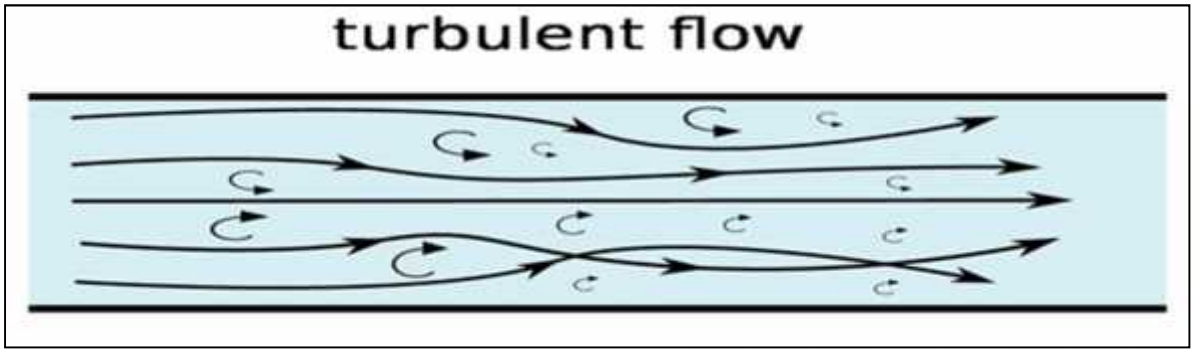

Figure 10: Lines of turbulent flow

II.6 Boundary layer

An assumption was made that air was an ideal fluid, with no viscosity or friction effects. In actually, when air flows across any surface, friction develops. The air immediately next to the surface slows to near zero velocity as it gives up kinetic energy to friction.

As a viscous fluid resists flow or shearing, the adjacent layer of air is also slowed. The **boundary layer** is that layer of airflow over a surface that demonstrates local airflow retardation due to viscosity. It is usually no more than 1mm thick at the leading edge of an airfoil, and grows in thickness as it moves aft over the surface.

The boundary layer has two types of airflow:

In **laminar flow**, the air moves smoothly along in streamlines. A laminar boundary layer produces very little friction, but is easily separated from the surface.

In **turbulent flow**, the streamlines break up and the flow is disorganized and irregular. A turbulent boundary layer produces higher friction drag than a laminar boundary layer, but adheres better to the upper surface of the airfoil, delaying boundary layer separation.

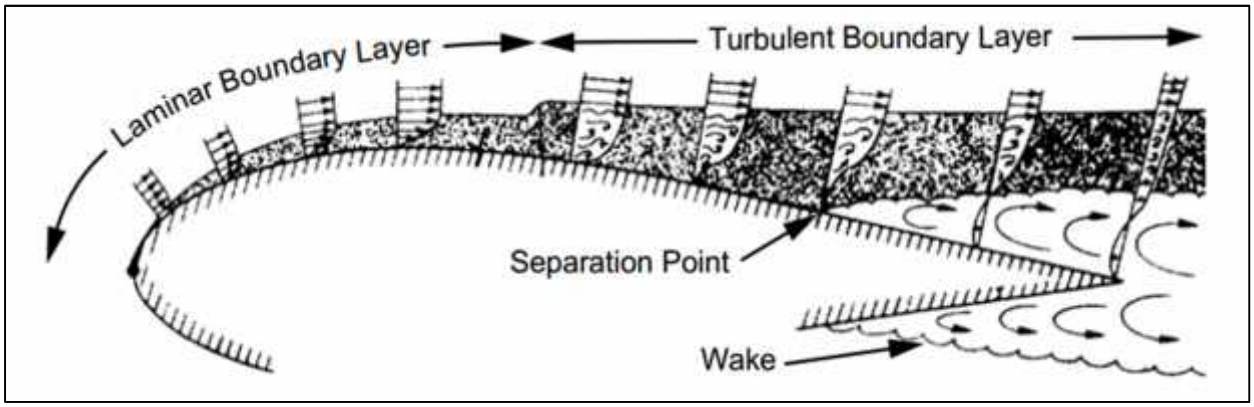

Figure 11: Boundary Layer Separation

Any object that moves through the air will develop a boundary layer that varies in thickness according to the type of surface. The type of flow in the boundary layer depends on its location on the surface. The boundary layer will be laminar only near the leading edge of the airfoil. As the air flows aft, the laminar layer becomes turbulent. The turbulent layer will continue to increase in thickness as it flows aft.

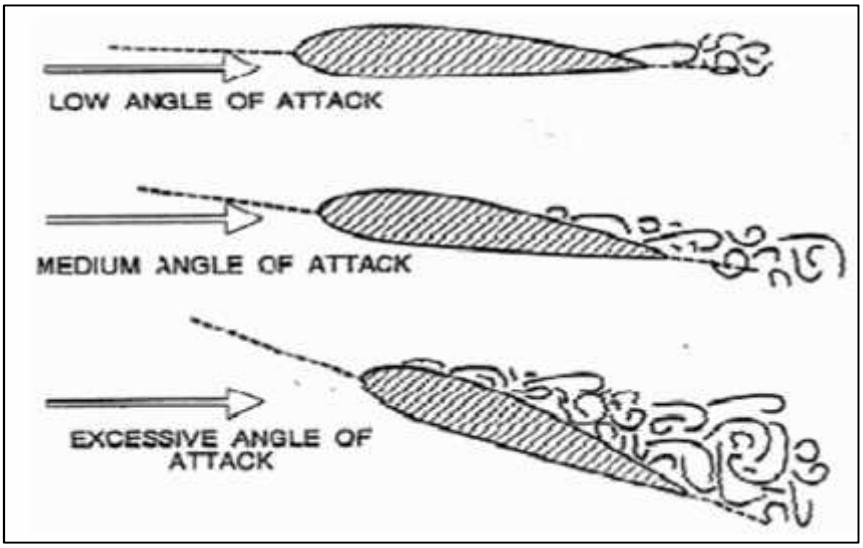

Figure 12: Progression of Separation point Forward with Increasing AOA

Figure 12 shows the boundary layer attached at a normal AOA. The point of separation remains essentially stationary near the trailing edge of the wing, until AOA approaches CL_{max} AOA. The separation point then progresses forward as AOA increases, eventually causing the airfoil to stall. At high angles of attack the airfoil is similar to a flat plate being forced through the air; the airflow simply cannot conform to the sharp turn. Note that the point where stall occurs is dependent upon AOA and not velocity.

III. Aerodynamics of wing

Aerodynamics is concerned with how the motion of air or other gaseous fluid interacts with a moving object. NASA defines aerodynamics as "the science that deals with the motion of air and other gaseous fluids and with the forces acting on bodies when the bodies move through such fluids or when such fluids move against or around the bodies"[15].

The design and analysis of the wings of aircraft is one of the principal applications of the science of aerodynamic, which is a branch of fluid mechanics. The properties of the airflow around any moving object can-in principle- be found by solving the Navier-Stokes equations of fluid dynamics.

III.1 Characteristic of air

In motion, a fluid such as air is characterized by seven magnitudes [16]:

- ρ: Density
- P: Pressure
- T: Temperature
- χ: Compressibility
- V: Speed
- P_∞: Dynamic pressure
- μ : Dynamic viscosity

Density ρ

The density is the mass per unit volume. It is expressed in kg / m^3 and varies with altitude.

Pressure P

The pressure is the force exerted on a unit surface perpendicular to this surface $\mathbf{p} = \frac{F}{S}$. It is expressed in N /m^2 or Pascal (Pa) and is very small, or the bar, which is equal to 105 Pa, is therefore commonly used.

Temperature T

The temperature is expressed in degrees and has no dimensions. Two scales are used: the Celsius ° C and the Kelvin ° K (T(k) = (°C) + 273).

Compressibility χ

Compressibility accounts for the fact that the density varies when the pressure varies. It is the ratio between a variation of effect (difference of ρ) and a variation of cause (difference of P)

Speed V

The speed is of course, the distance traveled per unit of time. It is expressed in m / s but the node Kt can also be used.

Dynamics pressure P_∞

Dynamic pressure characterizes the kinetic energy of a fluid.

A body at rest: $P_\infty = \frac{1}{2} P_\infty V_\infty^2$

Dynamic viscosity μ

In a real fluid, the molecules do not behave independently of one another, there are intermolecular forces.

Viscosity is a property of the fluid which opposes the relative motion between the two surfaces of the fluid in a fluid that are moving at different velocity

In aerodynamics, the viscosity is never used directly, but a dimensionless coefficient. The number of Reynolds (ℜe) it counts the influence of the viscosity.

III.2 Aerodynamic forces and moments

The aerodynamic forces and moments on the body are due to only 2 basic sources **[17] [18]:**

1. Pressure distribution over the body surface

2. Shear stress distribution over the body surface.

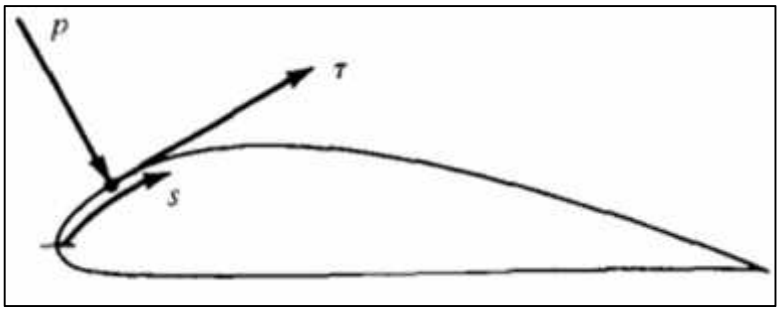

Figure 13: Pressure and shear stress on an aerodynamic surface

P=P(s)=surface pressure distribution τ = τ(s)=surface shear stress distribution

as sketched in **figure 13** pacts normal to the surface and τ acts tangential to the surface.

Shear stress is due to the tugging action on the surface, which is caused by friction between the body and the air.

The net effects of p and τ distributions integrated over the complete body surface have a resultant aerodynamic force R and moment M the body, as sketched in **figure 14**

The resultant R can be split into components, two sets of which are shown in fig 15, $V_\infty$is the relative wind, defined as the flow velocity far ahead of the body. The flow far away from the body is called the freestream, and hence V_∞ is also called the freestream velocity.

L= lift= component of *R* perpendicular to V_∞

D= drag= component of *R* parallel to V_∞

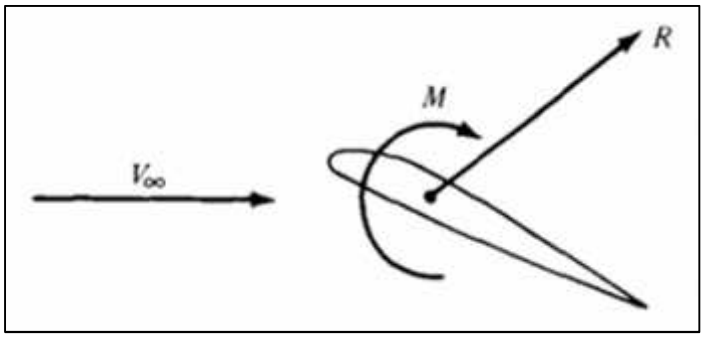

Figure 14: Resultant aerodynamic force moments on the body

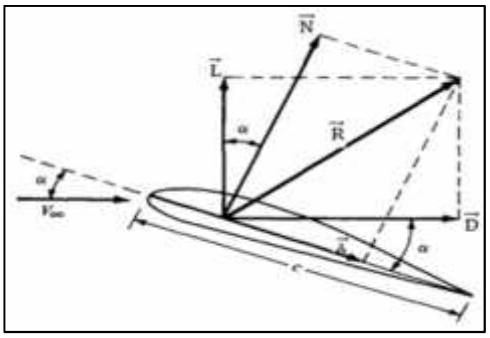

Figure15: Resultant aerodynamic force and the Components into which it splits

N = normal force = component of *R* perpendicular to C.

A = axial force =component of *R* parallel to C.

The angle of attack α is defined as the angle between **C** andV_∞. Hence, **a** is also the angle between L and N and between D and A. The geometrical relation between these two sets of components is, from **figure 16.** [19].

The geometrical relations between these 2 sets of components are:

L = N cos a - A sin a

D = N sin a + A cos a

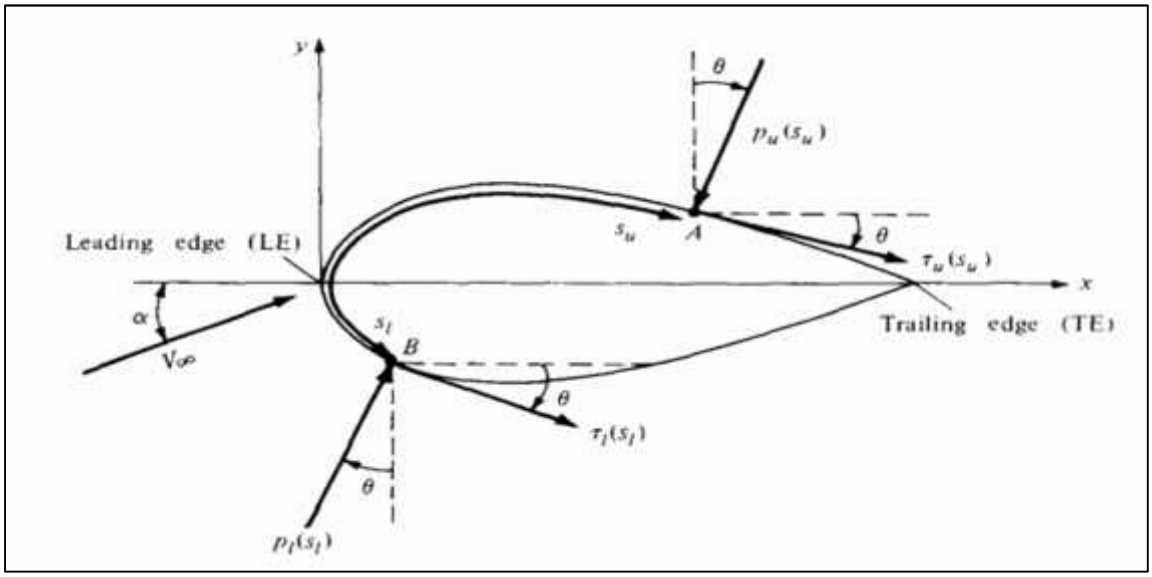

Figure 16: Nomenclature for the integration of pressure and shear stress distribution over a two-dimensional surface

The elemental normal force dN and axial force dA acting on the elemental surface ds on the upper body surface are [17]:

$$dN_u = -p_u dS_u \cos(\theta) - \tau_u dS_u \sin(\theta) \quad (10)$$

$$dA_u = -p_u dS_u \sin(\theta) + \tau_u dS_u \cos(\theta) \quad (11)$$

In the same way on the lower surface we have:

$$dN_l = -p_l dS_l \cos(\theta) - \tau_l dS_l \sin(\theta) \quad (12)$$

$$dA_l = -p_l dS_l \sin(\theta) + \tau_l dS_l \cos(\theta) \quad (13)$$

To determine the normal force N and the axial force A, equations (10) to (13) must be integrated from the leading edge (LE) to the trailing edge (TE)

$$N = -\int_L^T (p_u \cos(\theta) + \tau_u \sin(\theta)) dS_u + \int_L^T (p_l \cos(\theta) + \tau_l \sin(\theta)) dS_l \quad (14)$$

$$A = \int_L^T (-p_u \cos(\theta) + \tau_u \sin(\theta)) dS_u + \int_L^T (p_l \cos(\theta) + \tau_l \sin(\theta)) dS_l \quad (15)$$

The aerodynamic moment exerted on the body depends on the point about which moments are taken. The moment per unit span about the leading-edge due to p and τ on the elemental area (ds) on the upper and lower surfaces are:

$$dM_u = [p_u \cos(\theta) + \tau_u \sin(\theta)]\, x.dS_u + [p_u \sin(\theta) + \tau_u \cos(\theta)]\, y.dS_u \quad (16)$$

$$dM_l = [-p_l \cos(\theta) + \tau_l \sin(\theta)]\, x.dS_l + [p_l \sin(\theta) + \tau_l \cos(\theta)]\, y.dS_l \quad (17)$$

$$M_L = \int_L^T [dM_{u,L} + dM_{l,L}]$$

III.2.1 Lift

Aerodynamic lift is the component of the force undergone by a moving body in a fluid that is perpendicular to the direction of movement. It is the lift of the aerodynes (machines denser than the air).

A cambered airfoil is able to produce an uneven pressure distribution even at zero AOA. Because of the positive camber, the area in the stream tube above the wing is smaller than area in the stream tube below the wing and the airflow velocity above the wing is greater than the velocity below the wing.

the static pressure on both surfaces is less than atmospheric pressure, and thus will produce a lifting force on both upper and lower surfaces. The static pressure on the upper surface will be less than the static pressure on the lower surface, creating a pressure differential. The lower static pressure on the upper surface will "pull" the wing upward, creating a lifting force.

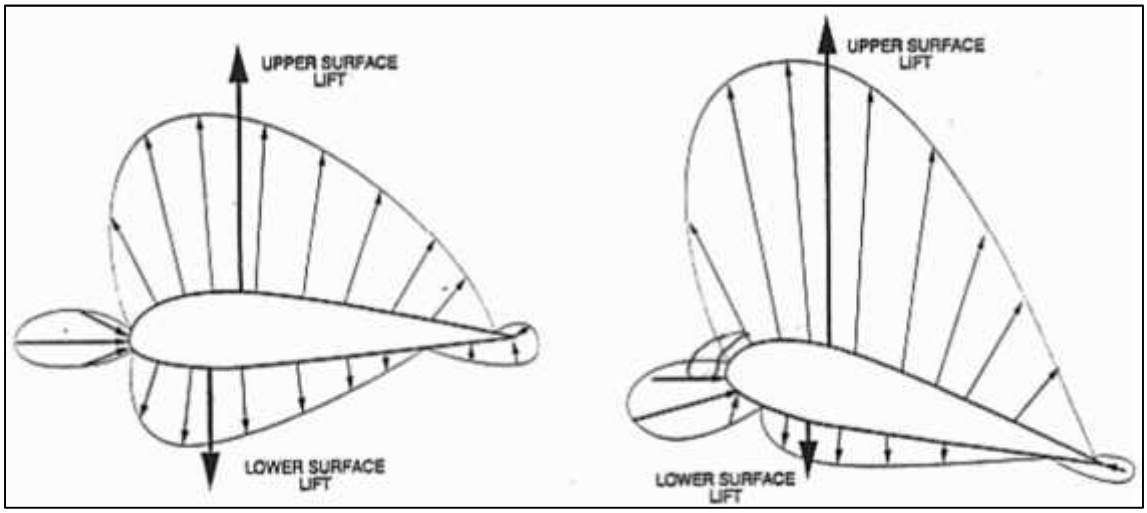

Figure 17: Pressure distribution around Positively Cambered Airfoil at Zero and Positive angle of attack

As the angle of attack of an airfoil is increased, the leading-edge stagnation point will move to a lower point on the leading edge. This shift has the effect of causing the area of the stream tube above the airfoil to decrease. As with an increase in camber, the velocity of the airflow above the airfoil will increase, lowering the static pressure above the airfoil, increasing the differential pressure and, therefore increasing lift [20].

The lift is expressed by the relation shown below:

$$L=\frac{1}{2}\rho S V^2 C_L \qquad (18)$$

Note that there are eight factors that affect lift. The first three are readily apparent: Density (ρ), velocity (V), and surface area (S). The five remaining factors are all accounted for within the coefficient of lift. As stated, both angle of attack (α) and camber affect the production of lift. The remaining three factors are not so easily discernable. They are aspect ratio (AR), viscosity (μ) and compressibility.

When an airfoil is exposed to greater dynamic pressure (q), it encounters more air particles and thus produces more lift. Therefore, lift is dependent upon the density of the air (i.e., the altitude) and the velocity of the airflow. An increase in density or velocity will increase lift.

Since lift is produced by pressure, which is force per unit area, it follows that a greater area produces a greater force. Therefore, an increase in wing surface area produces greater lift.

The Aspect ratio deals with the shape of the wing. Viscosity affects the aerodynamic force since it decreases the velocity of the airflow. Although we consider subsonic airflow to be incompressible, it does compress slightly when it encounters the wing. there is no way to control aspect ratio, viscosity, or compressibility. The coefficient of lift depends essentially on the shape of the airfoil and the angle of attack [21].

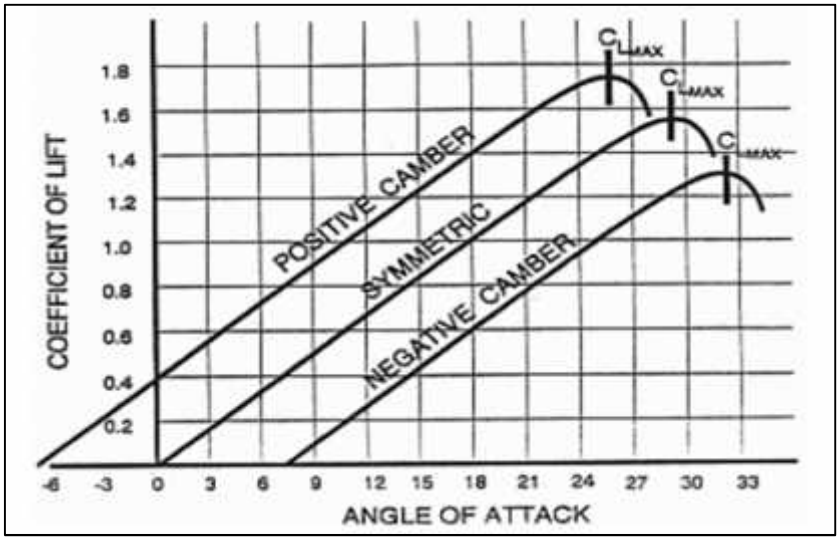

Figure 18: Variation of lift vs AOA

Figure (II.18) plots C_L as it varies with AOA. These curves are for three different airfoils: One symmetric, one negative camber and one positive camber. The shape of the C_L curve is similar for most airfoils. At zero angle of attack, the positive camber airfoil has a positive CL, and the negative camber airfoil has a negative C_L. The point where the curves cross the horizontal axis is the AOA where the airfoil produces no lift (C_L = 0). At zero AOA the symmetric airfoil has C_L = 0. The positive camber airfoil must be at a negative AOA, and the negative camber airfoil must be at a positive AOA for the CL to equal zero. As angle of attack increases, the coefficient of lift initially increases. In order to maintain level flight while increasing angle of attack, velocity must decrease. Otherwise, lift will be greater than weight and the airplane will climb. Velocity and angle of attack are inversely related in level flight.

III.2.2 Drag

Drag is the component of the aerodynamic force that is parallel to the relative wind, and acts in the same direction. The drag equation is the same as the aerodynamic force equation, except that the coefficient of drag (C_D) is used.

$$L=\frac{1}{2}\rho SV^2C_D \quad (19)$$

Note that C_D is low and nearly constant at very low angles of attack. As angle of attack increases, C_D rapidly increases. Since there is always some resistance to motion, drag will never be zero, so C_D will never be zero.

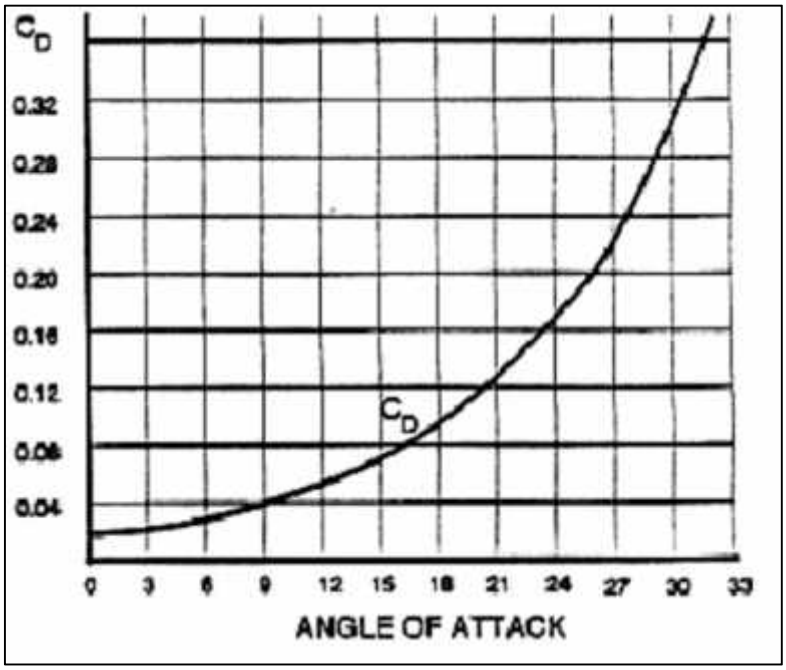

Figure 19: Variation of Drag coefficient with AOA.

Drag is divided into parasite drag and induced drag.

$$D_T = D_P + D_I \quad (20)$$

- **PARASITE DRAG**

Parasite drag (D_P) is drag that is not associated with the production of lift. It is composed of form drag, friction drag and interference drag.

- **Form drag**: also, known as pressure drag or profile drag, is caused by airflow separation from a surface and the low-pressure wake that is created by that separation. It is primarily dependent upon the shape of the object.
- **Friction drag:** Due to viscosity, a retarding force called friction drag is created in the boundary layer. Turbulent flow creates more friction drag than laminar flow. Friction drag is usually small per unit area.

- **Interference drag:** is generated by the mixing of streamlines between components. An example is the air flowing around the fuselage mixing with air flowing around an external fuel tank. We know the drag of the fuselage and the drag of the fuel tank individually. The total drag after we attach the fuel tank will be greater than the sum of the fuselage and the fuel tank separately. Roughly 5 to 10 percent of the total drag on an airplane can be attributed to interference drag.

Total parasite drag (D_P) can be found by multiplying dynamic pressure by an area. Equivalent parasite area (f)is the area of a flat plate perpendicular to the relative wind that would produce the same amount of drag as form drag, friction drag and interference drag combined. It is not the cross-sectional area of the airplane [22].

The equation for D_P is:

$$D_P = \frac{1}{2}\rho V^2 f = q\, f \tag{21}$$

Parasite drag varies directly with velocity squared (V2), so a doubling of speed will result in four times as much parasite drag figure 20.

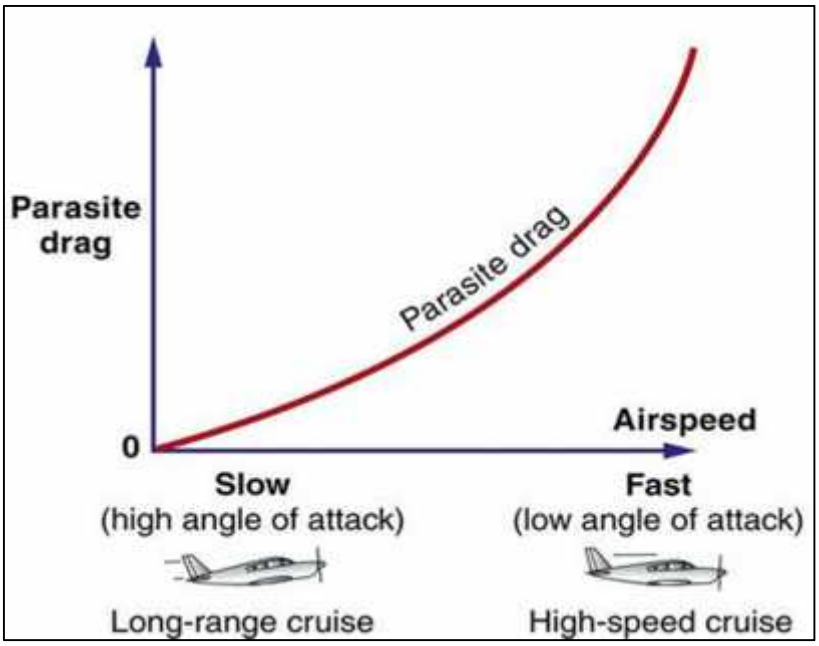

Figure 20: Drag parasite vs. Velocity

- **Induced drag (DI)**

Induced drag (DI) is that portion of total drag associated with the production of lift, or it is the parallel component of total lift.

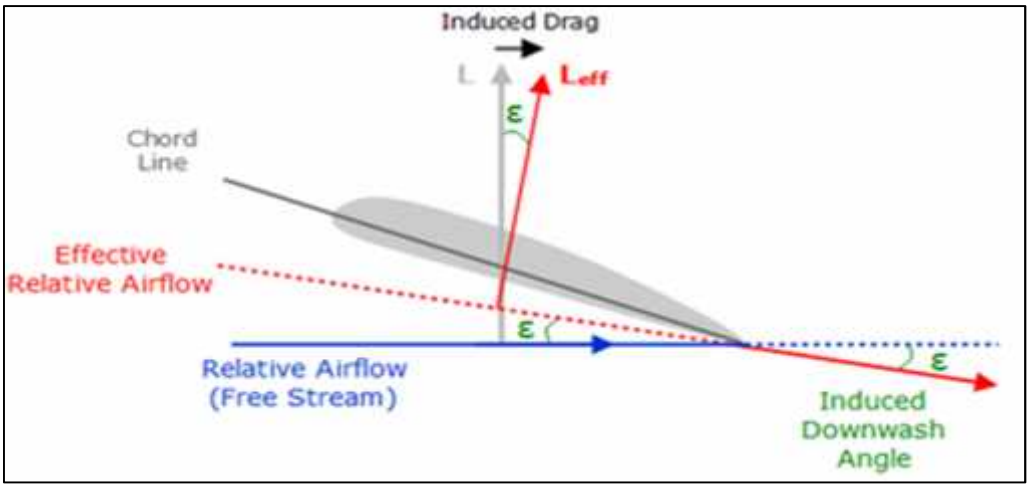

Figure 21: Induced Drag

The D_I equation is derived from the aerodynamic force equation and the assumption that weight equals lift in equilibrium level flight

$$D_I = \frac{KL^2}{\rho V^2 b^2} = \frac{KW^2}{\rho V^2 b^2} \quad (22)$$

Analyzing the equation shows that increasing the weight of an airplane will increase induced drag, since a heavier airplane requires more lift to maintain level flight. Induced drag is reduced by increasing density (ρ), velocity (V), or wingspan (b). In level flight where lift is constant, induced drag varies inversely with velocity, and directly with angle of attack. Another method to reduce induced drag is to install devices that impede the span wise airflow around the wingtip. These devices include winglets, wingtip tanks, and missile rails.

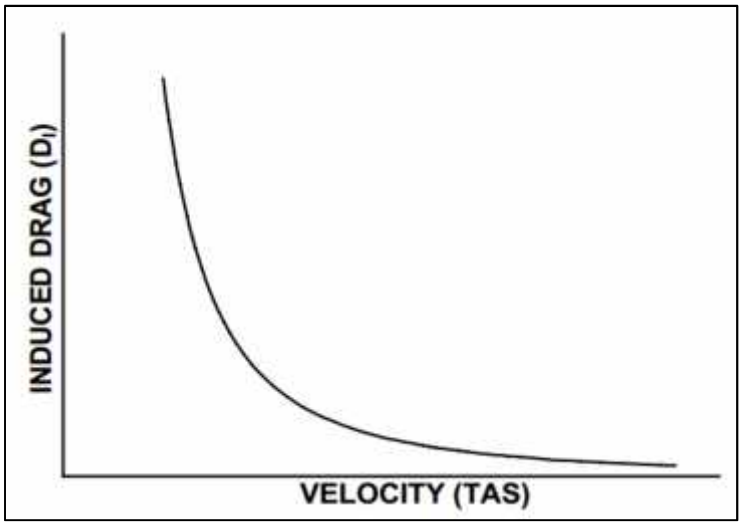

Figure 22: Drag induced vs. Velocity

Parasite and induced drag can be added together to create a total drag curve.

By superimposing both drag curves on the same graph, and adding the values of induced and parasite drag at each velocity, the total drag curve of Figure 23 is derived. The drag curve depicted is particular to one weight, one altitude and one configuration. As weight, altitude and configuration change, the total drag curve will shift.

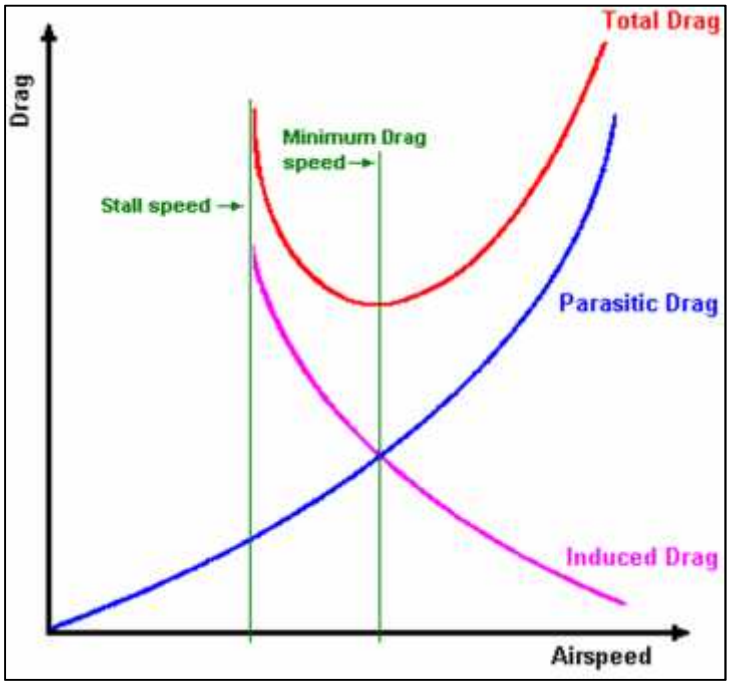

Figure 23: Total drag vs. Velocity

III.2.3. LIFT TO DRAG RATIO

An airfoil is designed to produce lift, but drag is unavoidable. An airfoil that produced the desired lift but caused excessive drag would not be very useful. We use the lift to drag ratio (L/D) to determine the efficiency of an airfoil. A high L/D ratio indicates a more efficient airfoil.[23].

L/D is calculated by dividing lift by drag. All terms except C_L and C_D cancel out:

$$\frac{L}{D} = \frac{\frac{1}{2}\rho V^2 S C_L}{\frac{1}{2}\rho V^2 S C_D} = \frac{C_L}{C_D} \qquad (23)$$

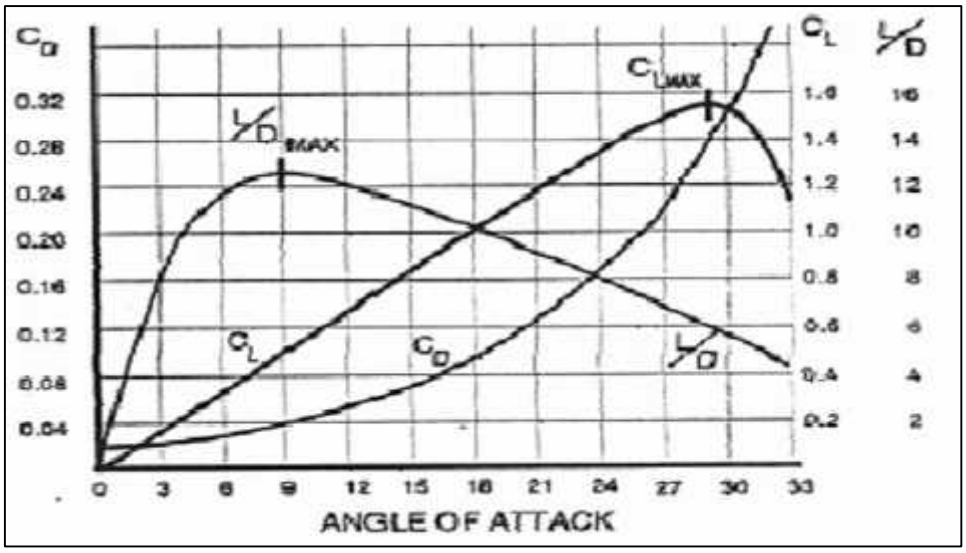

Figure 24: Lift to Drag Ratio

A ratio of the coefficients at a certain angle of attack determines the L/D ratio at that angle of attack. The L/D ratio can be plotted against angle of attack along with C_L andC_D Figure 24

The maximum L/D ratio is called L/D_m .

L/D_m AOA produce the minimum total drag.

L/D_m is located at the bottom of the total drag curve. Any movement away from L/DMAX will increase drag.

- At L/D_m AOA, parasite drag and induced drag are equal. At velocities below L/D_m , the airplane is affected primarily by induced drag, while at velocities above L/D_m , the airplane is affected primarily by parasite drag.
- L/D_m AOA produce the greatest ratio of lift to drag. Note that this is not the maximum amount of lift that can be produced, nor does it correspond to the airplanes maximum speed.
- L/D_m AOA is the most efficient angle of attack. Note that L/D is the efficiency of the wing, not the engine.

III.3 Dimensionless force and moment coefficients

The dimensionless force and moment coefficients are defined as follows [24]:

Lift coefficient : $$C_L = \frac{L}{q_\infty S}$$

Drag coefficient : $$C_D = \frac{D}{q_\infty S}$$

Normal force coefficient : $$C_N = \frac{N}{q_\infty S}$$

Axial force coefficient : $C_A = \frac{A}{q_\infty S}$

Moment coefficient : $C_M = \frac{M}{q_\infty S}$

S = reference area

l = reference length

For an airplane wing, “S” is the planform area, and” l” is the mean chord length, as illustrated in figure 25.

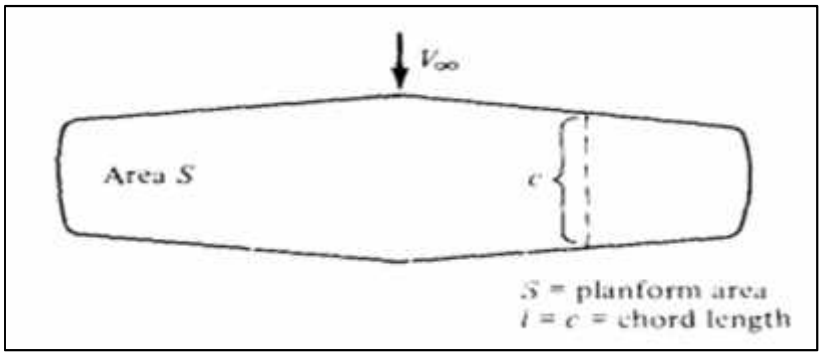

Figure 25: Reference area and length for an airplane wing

C. REVIEW OF STRUCTUR MECHANICS

I. Notions of solid mechanics

I.1Equation of motion

If an external force f (t) acts on the mass, the law of Newton is written as:

$$m\ddot{x} = -k\,x - c\dot{x} + f(t)$$

$$m\ddot{x} + c\dot{x} + k\,x = f(t) \qquad (24)$$

where :

m: The masse

$\ddot{x}$: The acceleration

$\dot{x}$: Velocity

x: Displacement

k:

c: Damping factor

It is indeed a second-order differential equation, linear and with constant coefficients, of which it is worthwhile to study in detail the solutions, for two reasons:

- Many systems of practice can be described by an equation of this kind

- A good understanding of the elementary oscillator facilitates the study of the more complex systems that will be addressed [25]

- **Modified form of the equation of motion**

Let us return to equation (1). It expresses the fact that the external force f (t) is equal to the sum of the three internal forces of the system, namely the inertia force $m\ddot{x}$, the viscous resistance force $c\dot{x}$ and the elastic force $\mathbf{kx}$.

$$m\ddot{x} + c\dot{x} + k\,x = f(t)$$

Division by mass:

$$\ddot{x} + 2\frac{c}{2m}\dot{x} + \frac{K}{m}x = \frac{1}{m}f(t) \qquad (25)$$

And introduce the notations:

$$\omega_0^2 = \frac{K}{m} \Rightarrow \omega_0 = \sqrt{\frac{K}{m}} \quad \text{Pulse of the conservative system}$$

$$\lambda = \frac{c}{2m} \quad \text{damping coefficient}$$

$$\eta = \frac{c}{2m\omega_0} = \frac{\lambda}{\omega_0} \quad \text{relative damping (or damping factor)}$$

Therefore, the differential equation is written as:

$$\ddot{x} + 2\lambda\dot{x} + \omega_0^2 x = \frac{1}{m}f(t) \qquad (26)$$

The four terms have the physical dimension of an acceleration.

If we now divide (24) the stiffness K, the equation includes terms having the dimension of a displacement.

$$\frac{m}{k}\ddot{x} + \frac{c}{k}\dot{x} + x = \frac{1}{k}f(t) \qquad (27)$$

The second member represents the displacement caused by the external force if the system had only the stiffness k

$$x_e(t) = \frac{1}{k}f(t)$$

Using the above definitions, the equation becomes

$$\frac{1}{\omega_0^2}\ddot{x} + \frac{2\lambda}{\omega_0^2}\dot{x} + x = x_e(t) \qquad (28)$$

This last form of the equation of motion is well adapted when the forced regime is sought by a displacement imposed on the system.

I.2 The displacement

Displacement is the difference between the final and initial position of a point (for instance, the center of mass of a moving object).

The actual path covered to reach final position is irrelevant. It can simply be fined as the shortest path between the final point and initial point of body, displacement field

(mechanics), an assignment of displacement vectors for all points in a body that is displaced from one state to another.

I.3 The deformation

Deformation is a change in the shape or size of an object due to an applied force.

Deformation in continuum mechanics is the transformation of a body from a reference configuration to a current configuration ,a configuration is a set containing the position of all particles of the body, a deformation may be caused by external loads body forces (such as gravity) or another forces, or changes in temperature, chemical reaction, …etc. deformation is often described as strain is a description of deformation in terms of relative displacement of particles in the body that excludes rigid body motions [26].

The engineering normal strain or engineering extensional strain or nominal strain ε of a material line element of fiber as axially loaded is expressed as the change in length ΔL per unit of the original length L of the line element or fibers. The normal strain is positive is the material fibers are stretched and negative if they are compressed. This, we have:

$$\varepsilon = \frac{\Delta L}{L} = \frac{l-L}{L} \qquad (30)$$

where ε is the engineering normal strain, **L** is the original length of the fiber l is the final length. Depending on the type of material, size and geometry of the object, and the forces applied, various types of deformation may result.

The imagine to the right shows the engineering modes vs. strain diagram for a typical ductile condition, as can be depicted using a deformation mechanism.

I.3.1 Elastic deformation

This type of deformation is reversible. Once the forces are in longer applied, the object returns to its original shape. Elastomers and shape memory metals such as National exhibit large elastic deformation ranges, as does rubber. However, elasticity is nonlinear in these materials. Normal metals, ceramics and most crystals show linear elasticity and smaller elastic range. Linear elastic deformation is governed by Hooke's low, which states: [27]

$$\sigma = E \quad \text{(Mpa)} \qquad (31)$$

Where σ is the applies stress, E is the material constant called young's modulus, and ε is the resulting strain. This relationship only applies in the elastic range and indicates that the slope of the stress vs. strain curve can be used to find young's modulus. Engineers often use this calculation in tensile. The elastic range ends when the material reaches its yield strength at this point plastic deformation begins.

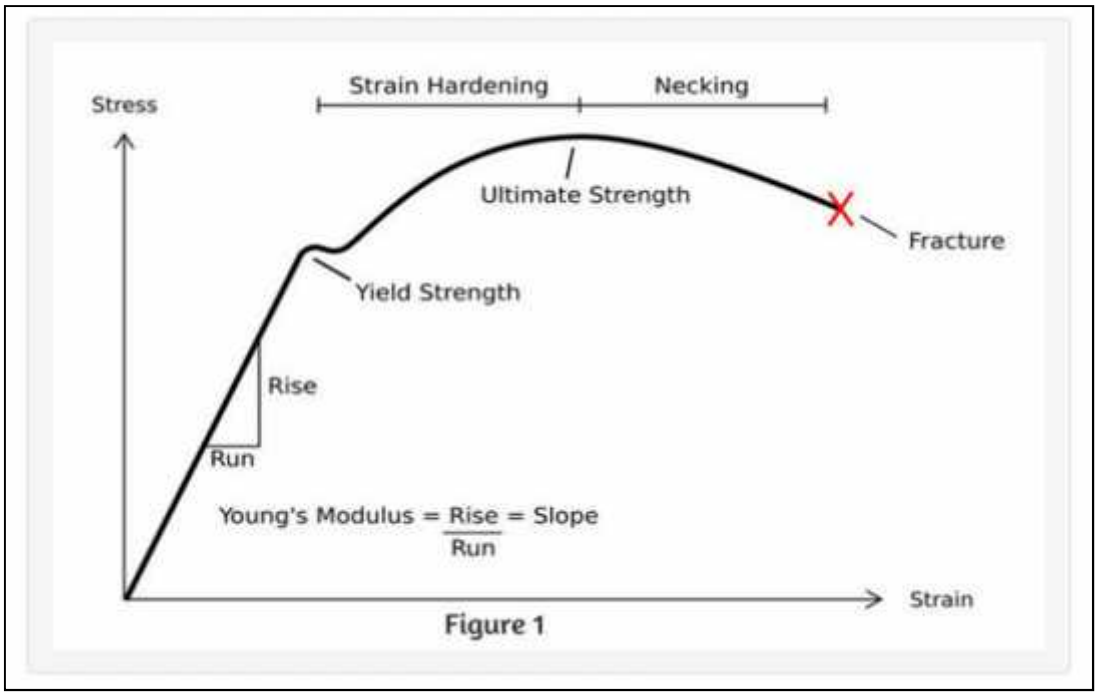

Figure 26: Strain diagram with the variation stages of deformation

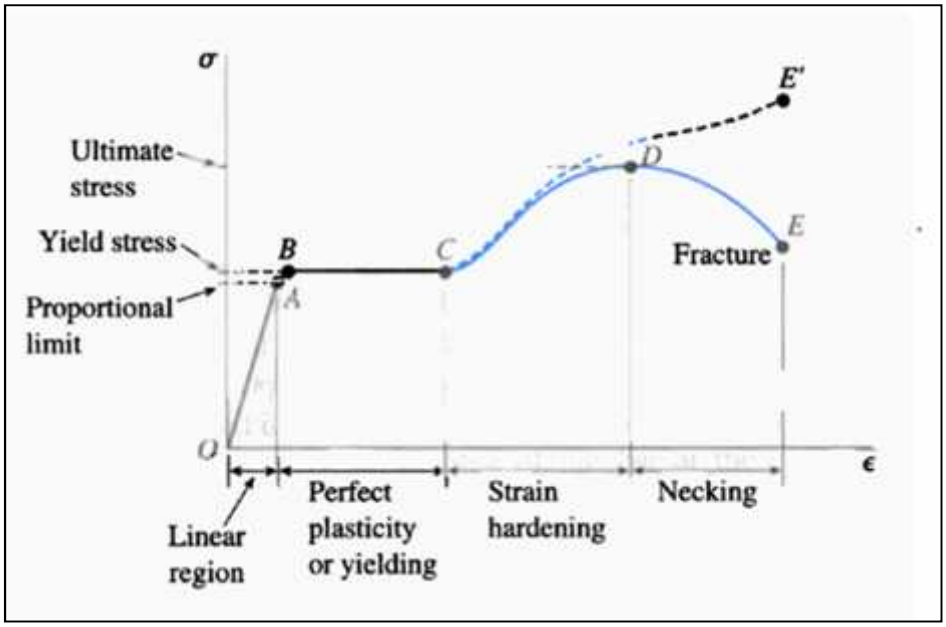

Figure 27: The behavior of stresses

Where:

- Yield strength or the max stress: is the stress at which a slight increase in stress will resent in appreciably increase in strain without increasing in stress.
- Proportional limit: the upper stress limit that the strain varies linearly with stress material follow Hooke's law.
- Elastic limit: the upper stress level of which the material behaves elastically.

I.3.2 Plastic deformation

This type of deformation is irreversible. However, an object in the plastic deformation range will first have undergone elastic deformation, which is reversible, so the object will return part way to its original shape. Soft thermoplastics have a rather large plastic deformation range as to ductile metals such as copper, silver and gold. Steel does, too, but not cast iron. Hard thermosetting plastics, rubber, crystals, and ceramics have minimal plastic deformation ranges. One material with a large plastic deformation range is wet chewing gun, which can be stretched dozens of times its original length [28].

Under tensile stress, plastic deformation is characterized by a strain hardening region and a necking region and finally, fracture, (also called ruptured). During strain hardening the material becomes stronger through the movement of atomic dislocations. The necking phase is indicated by a reduction in cross-sectional area of the specimen. Necking begins after the ultimate strength is reached. During necking, the material can no longer withstand the maximum stress and the strain in the specimen rapidly increases. Plastic deformation ends with fracture of the material [29].

I.4 Metal fatigue

Another deformation mechanism is metal fatigue, which occurs primarily in ductile metals. It was originally thought the material is deformed only within the elastic range return completely to its original state once the forces were removed [30].

II. Resistance criterion

II.1 Von-Mises stresses

Von-Mises stress is widely used by the designers to cheek whether their design will withstand a given load condition. Von-Mises stress is considered to be safe haven for the design engineers. Using this information an engineer can say his design will fail, if the maximum value of Von-Mises stress induced in the material is more than strength of the material. It works well for the most of the case, especially when the material is ductile in nature. [31].

The condition of failure will be as follows.

$$\left[\frac{(\sigma_1-\sigma_2)^2+(\sigma_2-\sigma_3)^2+(\sigma_3-\sigma_1)^2}{2}\right]^{1/2} \geq \sigma_y \qquad (32)$$

The left-hand side of the above equation is denoted as Von-Mises stress end in the other side is denoted the yield stress.

So as a failure criterion the engineer can check whether von misses stress inducted in the material exceeds yield strength (for ductile material) of the material. So, the failure condition can be simplified as

$$\sigma_v \geq \sigma_y \qquad (33)$$

II.2 Tresca-yield surface

The Tresca-yield criterion is taken to work of Henri Tresca. It is also known as the maximum shear stress theory (MSST) and the Tresca-Guest (TG) criterion. In terms of the principal stresses the Tresca criterion is expressed as [32]:

$$\frac{1}{2}\max\left(|\sigma_1-\sigma_2|,|\sigma_1-\sigma_2|,|\sigma_1-\sigma_2|\right)=s_S=\frac{1}{2}s_y \quad (34)$$

Where S_{xy} is the yield strength is shear, and S_y is the tensile yield strength. Figure 28 shows the Tresca-Guest yield surface in the three-dimensional space of principal stresses. It is a prism of six sides and having infinite length. This means that the material remains elastic when all three principal stresses are roughly equivalent (a hydrostatic pressure), no matter how much it is compressed or stretched. However, when one of the such situations, if they become smaller (or larger) than the others material is subject to shearing. In domain. Figure 30 shows the Tresca-Guest yield surface in dimensional stress space, it is a cross section of the prism along the σ_1, σ_2 plane [33].

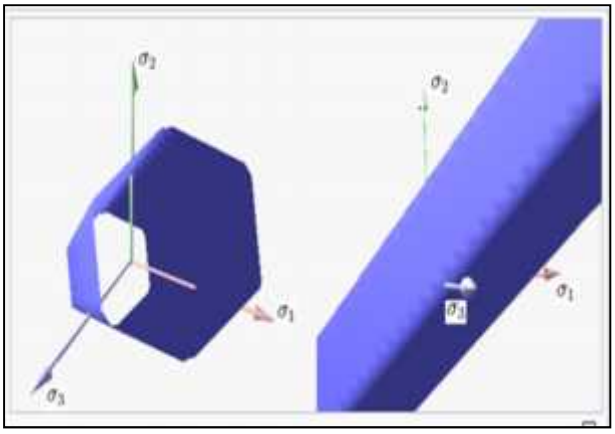

Figure 28: View of Tresca-Guest yield surface in 3D space of principal stresses.

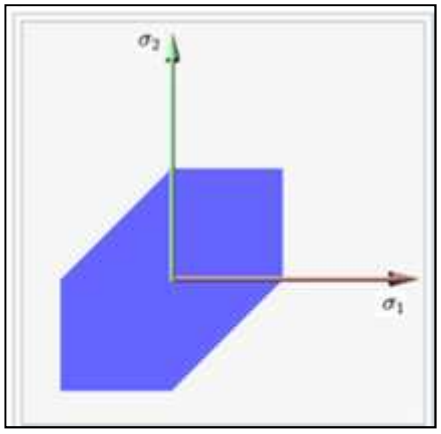

Figure 29: Tresca-Guest yield surface in 2D space (σ_1, σ_2)

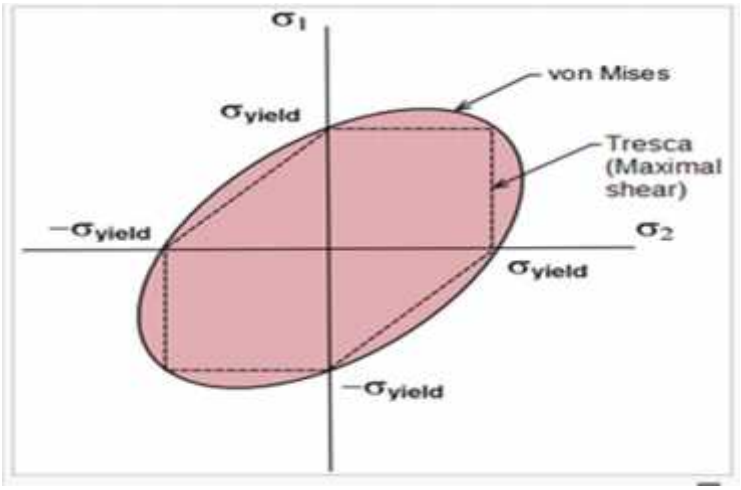

Figure 30: Tresca, von Mises criterion

Conclusion:

We have seen in theoretical part three important steps.

In the first step, we address to the definition of wing, its types, its advantages and disadvantages. We discussed also the geometry of the wing and its manufacturing material.

In the second step, we have seen an overview about fluid mechanics a basic equation of conservation than the flow types around wings all those effects are governed by norms represented by different parameters (Reynolds number, the Mach number), and the boundary layer. We have also defined what means aerodynamic, the characteristic of air and the aerodynamics forces and moments. Finally, we address to the forces applied on the wing (lift and drag), its definition and its types and the relation between them.

In the last step, we have seen the notions of solid mechanics, which are the deformation, elastic deformation, plastic deformation and. Also, we have shown the resistance criterion, which concludes the Von-Mises stresses and the Tresca yield surface.

Aerodynamicists have long realized that the flow over a wing is more complex, in order to study the effect of air on the wing surface with different chord, span and wing profile. there is a fast and accurate analysis method called the computational fluid dynamic (CFD).

CED has been made around the early 20th century, it includes the use of applied mathematics, physics and computational software to visualize how a gas or liquid flows as well as how it effects objects as it flows past.

In this chapter, we will see a numerical simulation of the flow behavior around a wing and the effect of aerodynamic forces on the wing surface.

This simulation is done by different geometry with help of ANSYS 16.0 software.

I. Steps of simulation

I. 1Drawing geometry

This step consists of drawing the geometry of the problem, the wing profile and the surrounding fluid domain, using the ANSYS Design Modeler software which allows to import CAD, 2d (Sketch) plots, 3d object sketch (extrusion etc....) and manipulate 3d objects.

The study was performed in terms of the wing length, the chord root and the camber (different profiles).

The profiles used are:

- NACA 4412, It is the same profile for the wing of Airbus A321.

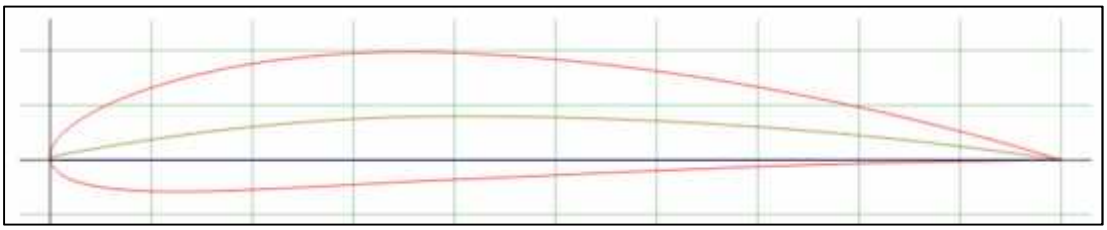

Figure 1: Profile NACA 4412

- NACA 4318 which is the same profile for the wing of ATR 72.

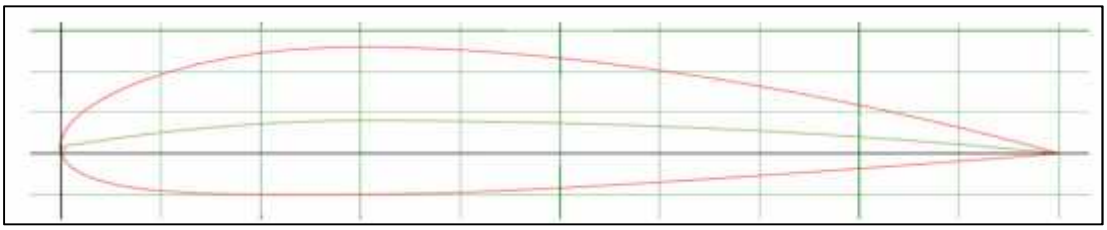

Figure 2: Profile NACA 4318

- NACA 4415which is the same profile for the wing of Airbus A321.

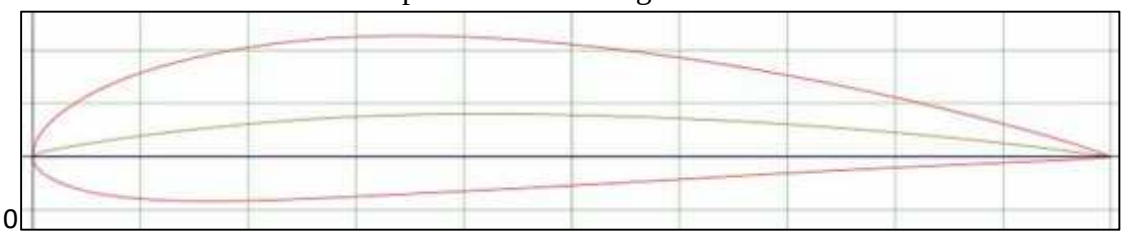

Figure 3: Profile NACA 4415

The geometry is done by ANSYS DesignerModler and the mesh by Ansys Designer meshing.

For the geometry, we draw two volumes of control, in order to get a finer mesh on the wing surface.

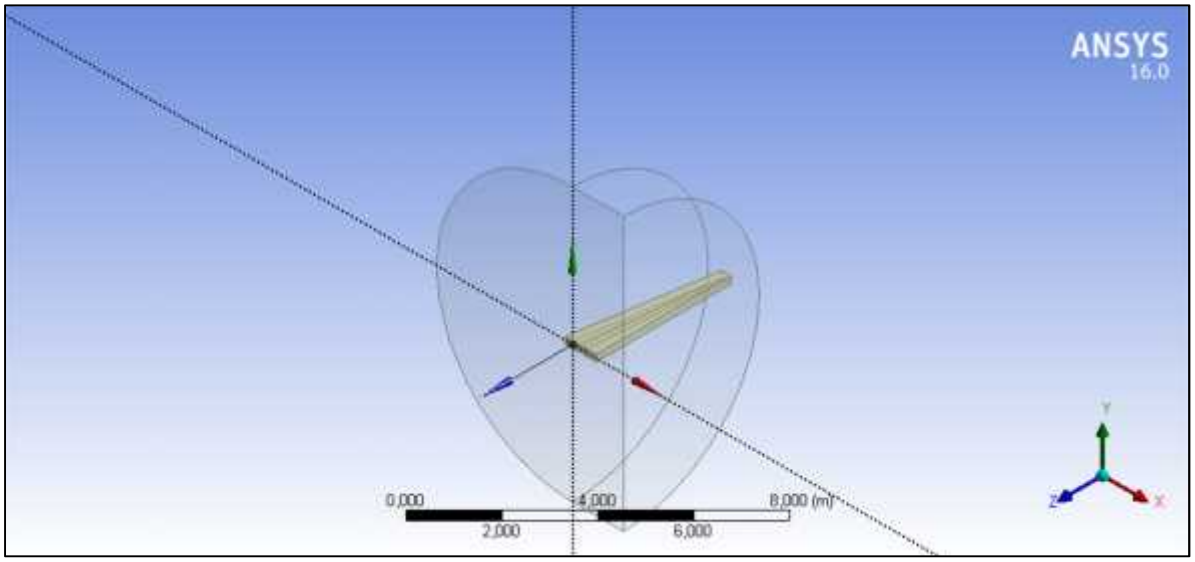

Figure4: Wing geometry

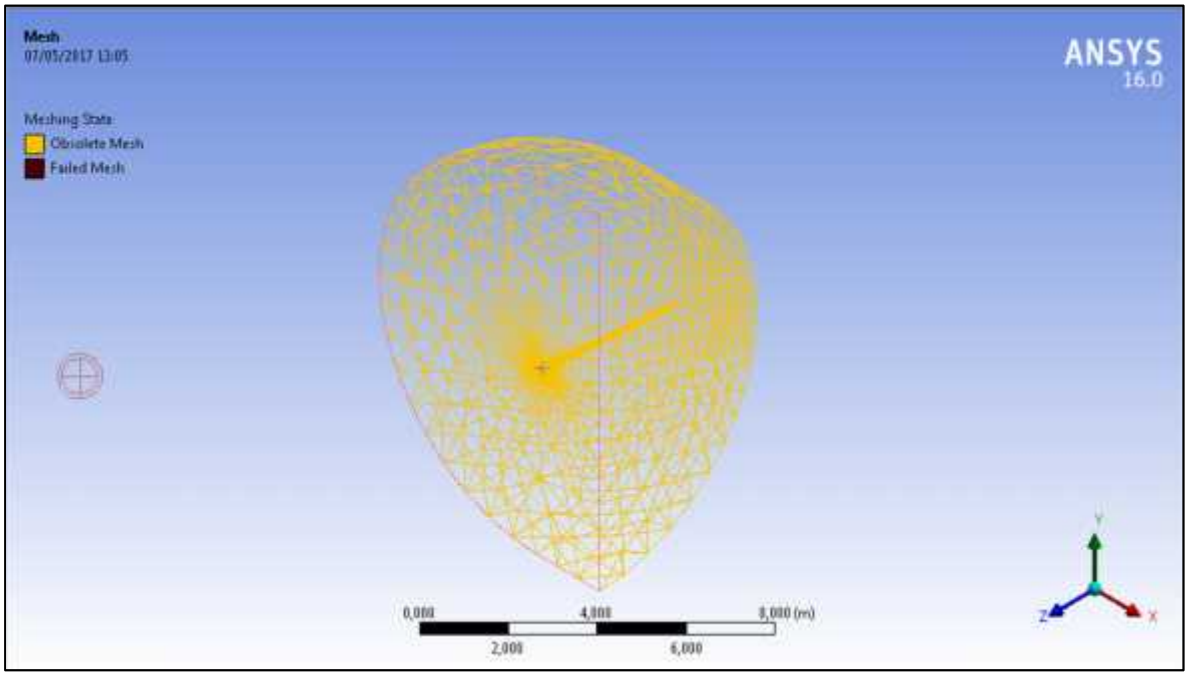

Figure5: Mesh generation

- ✓ **Boundary conditions:**

The boundary conditions used for each simulation are as follow:

Element	Boundary condition
Inlet	Velocity inlet
Outlet	Velocity outlet
Wing tip	Wall
Wing surface	Wall
Symmetry	Wall

Table 1: Boundary conditions

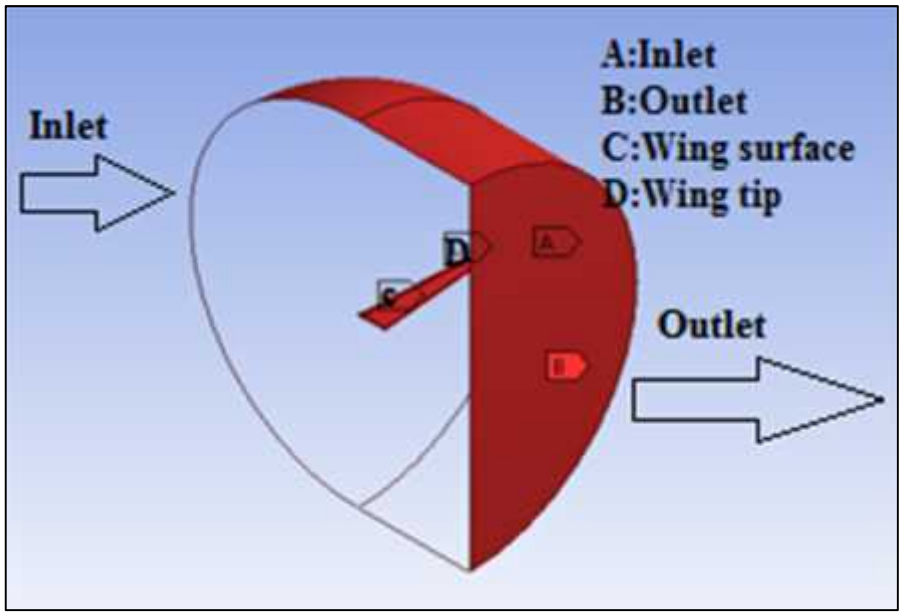

Figure 6: Named of boundary conditions

I.2Fluent simulation software

Ansys Fluent software is one of the most powerful computational fluid dynamics (CFD) software tools available. It contains the broad physical modeling capabilities needed to model flow turbulence, heat transfer, and reaction for industrial applications ranging from air flow over an aircraft wing to combustion in a furnace and much more.

In our work, the software allows us to have the loads (aerodynamic forces) exerted by the fluid (air)on the wing.

The conditions used in fluent software are shown in the **table 2**.

Density	$\rho = 1,2 \quad k / m^3$ (incompressible flow)
Flow type	steady /viscous (Spamlart-Allamars model)
Inlet pressure	Atmospheric pressure 101325 Pa
Inlet velocity	**100 m/s**
Angle of attack	**null angle of attack (0°)**

Table 2: Input conditions for the simulation

I.3 Modal analysis

In modal analysis, we are interested to find the first four modes shapes of vibration. The first fourth natural frequencies of the system will be found using ANSYS workbench (Modal) which will serve as a base for us for transient and vibrational analysis of the system.

The wing geometry in 3D is represented in **figure 4**

The material used is an aluminum alloy. Its characteristics are presented in **table 3.**

Variables	Value	Unit
Density	2770	Kg. m^{-3}
Young's Modulus	7.1 * 10^1	Pa
Poisson's Ratio	0.33	
Shear Modulus	2.6692* 10^1	Pa
Tensile yield strength	2.8* 10^8	Pa
Compressive yield strength	2.8* 10^8	Pa
Tensile ultimate strength	3.1* 10^8	
Reference Temperature	22	C°

Table 3: Characteristics of aluminum alloy

I.4 Static structural analysis

A static analysis calculates the effects of steady loading conditions on a structure, while ignoring inertia and damping effects, such as those caused by time-varying loads. A static analysis can, however, include steady inertia loads (such as gravity and rotational velocity), and time-varying loads that can be approximated as static equivalent loads (such as the static equivalent wind and seismic loads commonly defined in many building codes)

In this section, we are interested to find the maximal deformation, von-Mises stress, strain and the strain energy of the different wing model when it due to the aerodynamic forces.

The boundary conditions used in static structural analysis are the same as the modal analysis and just we add the force applied on the wing surface.

II. Results

We show the results obtained for the different profiles used in our study (NACA4412, NACA4415, NACA4318)

From the fluent software, we obtain the lift, drag and the moment coefficients for each case.

II.1Effect of wing length

The table below shows the result aerodynamic coefficient obtained after different simulation

For NACA 4412 profile and with different wing length and constant chord.

C_t (m)	0,14			
C_r (m)	0,582			
L(m)	3	3.5	3.9	4.5
C_L	0.348	0.357	0.675	0.804
C_D	0.020	0.018	0.028	0.032
C_m	0.046	0.047	0.068	0.081

Table 4: Aerodynamic coefficientswith different wing length

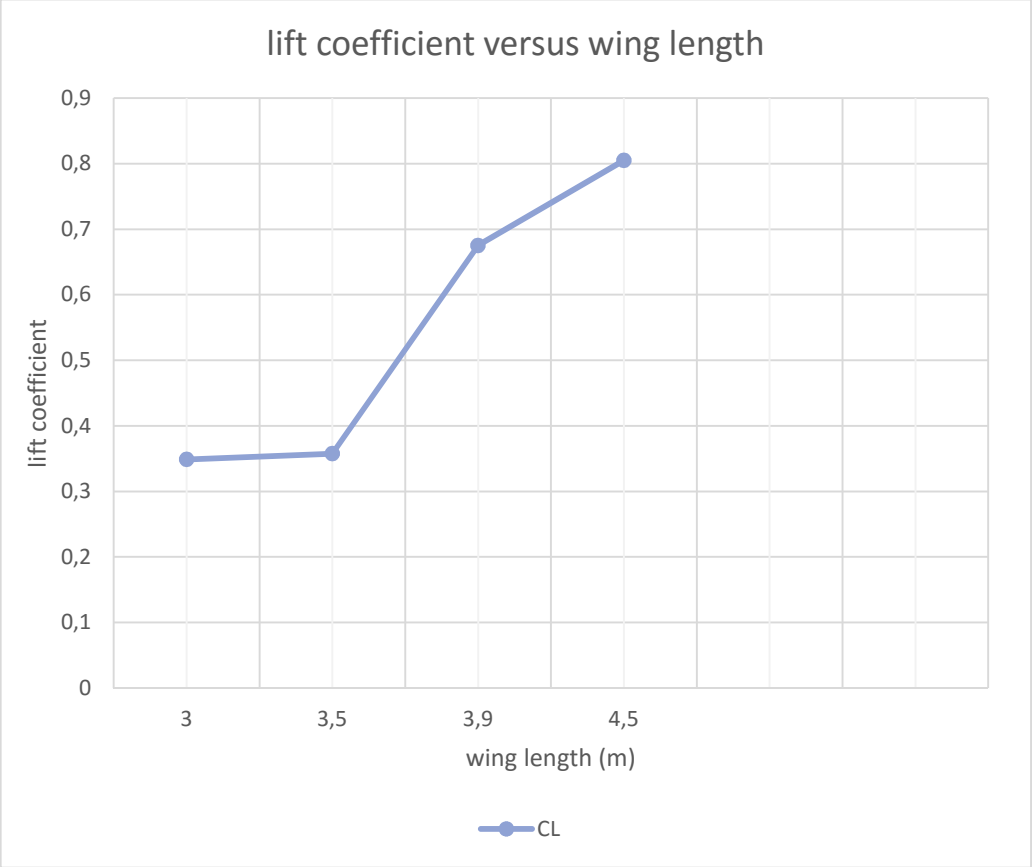

Figure 7: Lift coefficient versus wing length

- We notice in **figure7** that the lift coefficient varies increasingly in function of the wing length. We can see from this figurethat the variation of lift coefficient between L = 3.5m and L= 3m is not important, but it increases sharply from L = 3.5m.

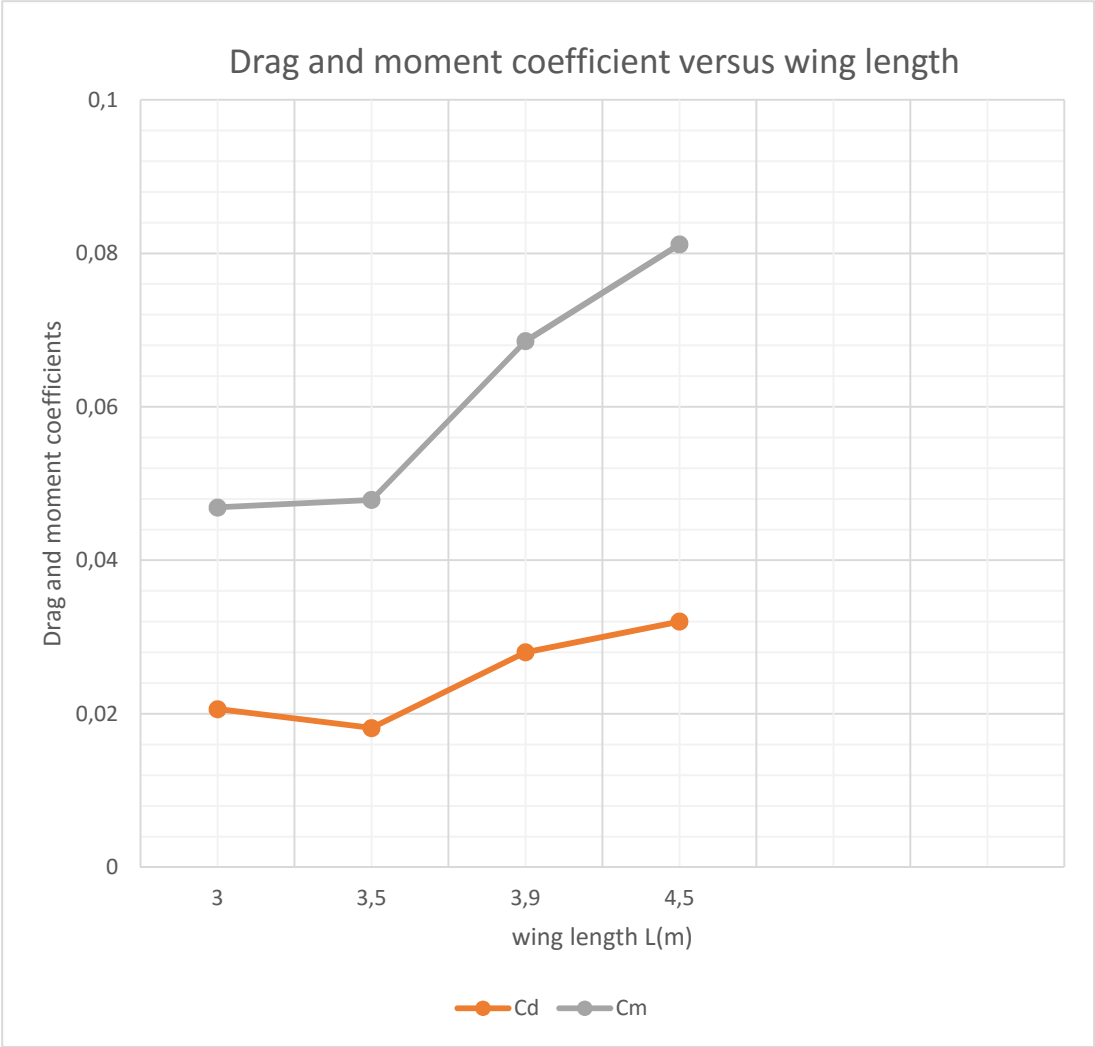

Figure 8: Drag and moment coefficients versus wing length.

- We can see from the **figure 8**that the drag coefficient varies also in function of the wing length, it decreases a little bit to reach the minimum value at L=3.5m, then it increases to reach the maximum value at L=5m, where the highest value reached is 0.036 and the smallest is of 0.018.
- The moment coefficient varies also increasingly in function of the wing length, we notice that the highest absolute value of the moment coefficient is 0.081 for L=4.5m and the smallest value is 0.046 for L=3m.
  The variation of drag and moment coefficients are also not important between L=3m and L=3.5m

After the different simulations for different wing length, we have got a static pressure contours and velocity vectors which are depicted below.

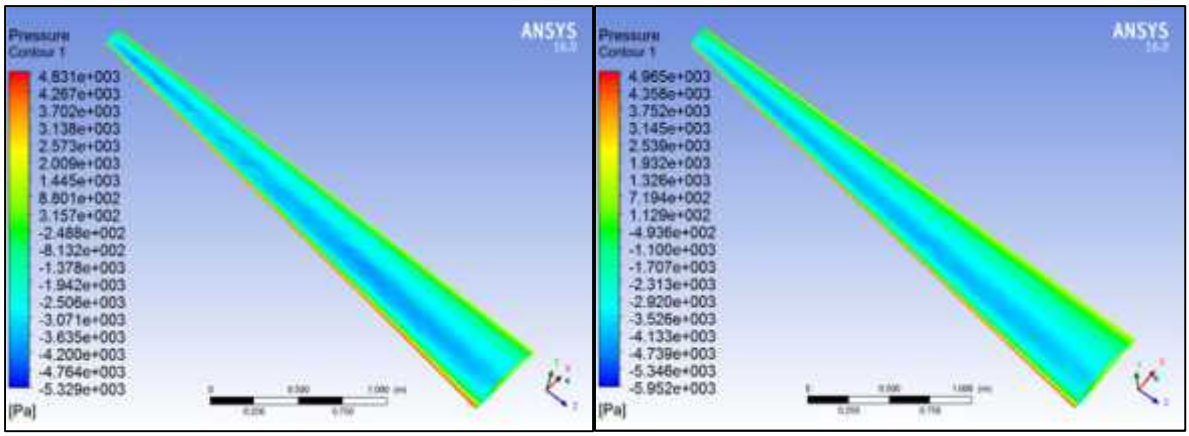

L=3mL=3,5m

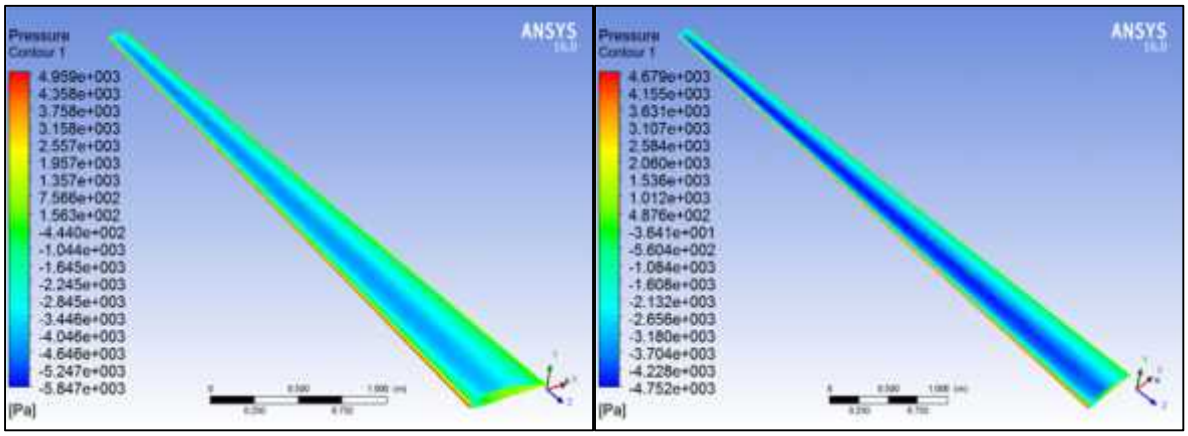

L=3,9m L=4,5m

Figure 9: Contours of static pressure for different wing length

- The **figure 9** shows contours of static pressure for different wing length.We can see from this figure that we almost have the same pressure evolution for the different wing length.

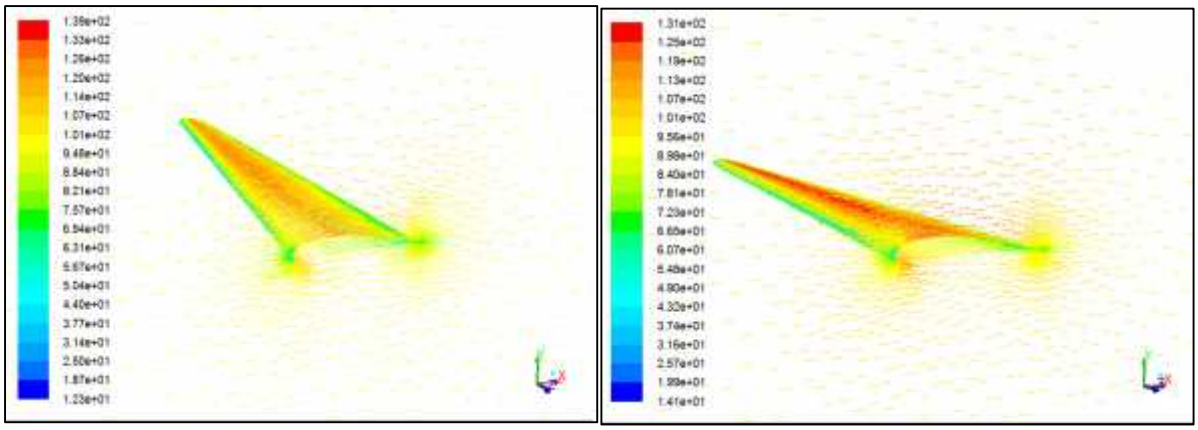

L=3mL=3,5m

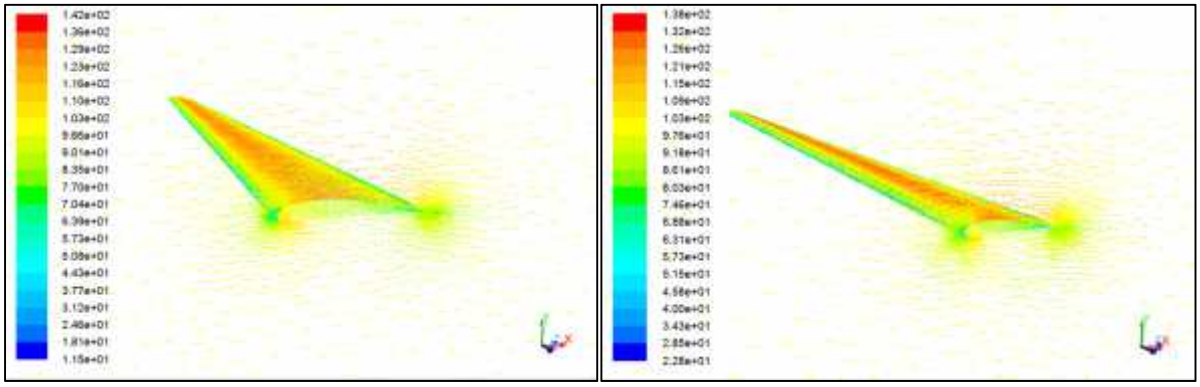

L=3,9mL=4,5m

Figure 10: Velocity vectors (m/s) for different wing length

- The **figures 10** shows velocity vectors for different wing length. We can see from this figure that we almost have the same velocity evolution for the different wing lengths.
  We can also see that there is a sharp decrease in the speed at the leading edge.
  We notice that the flow follows the shape of the profile, there is no separation or reversed flow.

II.1.1Calculation of drag and lift forces

To calculate the drag force: $F_x = \frac{1}{2}\rho V^2 C_d$

And the lift force using: $F_y = \frac{1}{2}\rho V^2 C_L$

The resultant force we can calculate by the relation:

$R = \sqrt{F_x^2 + F_y^2}$

where:

- ρ = 1,225 kg/m^3
- V = 100 m/s

Table 5: Values of lift and drag forces and their resultant. (NACA4412)

L(m)	3	3.5	3.9	4.5
F_y (N)	2307.11	2758.62	5806.48	7986.42
F_x (N)	136.40	140.05	240.97	317.70
R (N)	2311*.38	3863.44	5811.47	7992.73

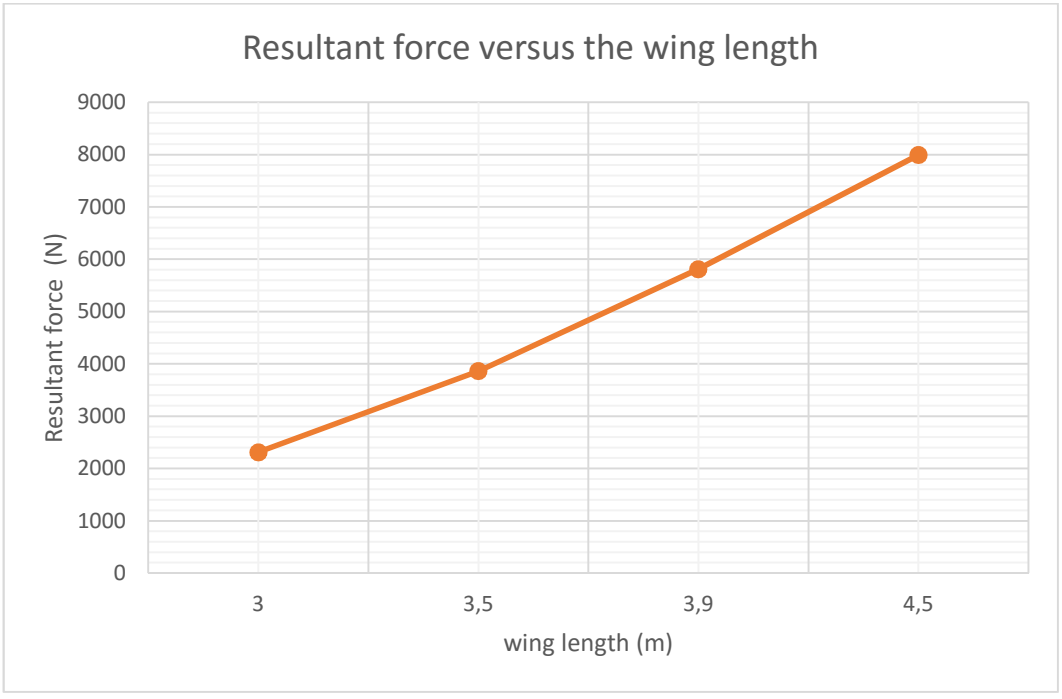

Figure 11: Resultant force according to the wing length.

- The **figure 11** illustratesthe curve of resultant force according to the wing length. We notice that there is a proportional relationship between these two parameters, when we increase the wing length the resultant force also increases.

II.1.2Modal analysis

The **table 6** show the results of modal analysis fordifferent profiles, different wing length and with constant chord ($C_r = 0.582m$ and $C_t = 0.14\,m$).

The modal analysis is characterized by the frequencies and the maximal amplitudes for different wing length

		Profile NACA 4318		**Profile NACA 4415**		**Profile NACA 4412**	
Wing length (m)	Mode shape	Frequency Hz	Maximum amplitude (m)	Frequency Hz	Maximum amplitude (m)	Frequency Hz	Maximum amplitude (m)
L=3	1	26.622	0.260	11.343	0.364	9.803	0.401
	2	72.355	0.430	35.615	0.505	31.373	0.552
	3	136.73	0.248	70.05	0.360	70.248	0.479
	4	148.06	0.514	79.075	0.555	70.457	0.552
L=3.5	1	9.851	0.306	8.3297	0.336	7.065	0.366
	2	30.838	0.427	26.087	0.469	23.181	0.487
	3	52.417	0.303	51.917	0.333	51.818	0.375
	4	68.371	0.474	57.846	0.521	53.023	0.526
L=3.9	1	7.9471	0.290	6.7197	0.318	5.508	0.353
	2	24.886	0.403	21.051	0.443	17.5	0.482
	3	42.374	0.287	41.971	0.316	39.343	0.524
	4	55.207	0.448	46.703	0.492	42.172	0.355
L=4.5	1	5.9769	0.269	5.0594	0.296	4.081	0.332
	2	18.722	0.375	15.855	0.412	12.818	0.461
	3	31.963	0.267	31.635	0.294	28.35	0.509
	4	41,561	0,41561	35,194	0,45684	31.72	0.33132

Table6: Results of modal analysis with different wing lengths.

The first four mode shapes are depicted below

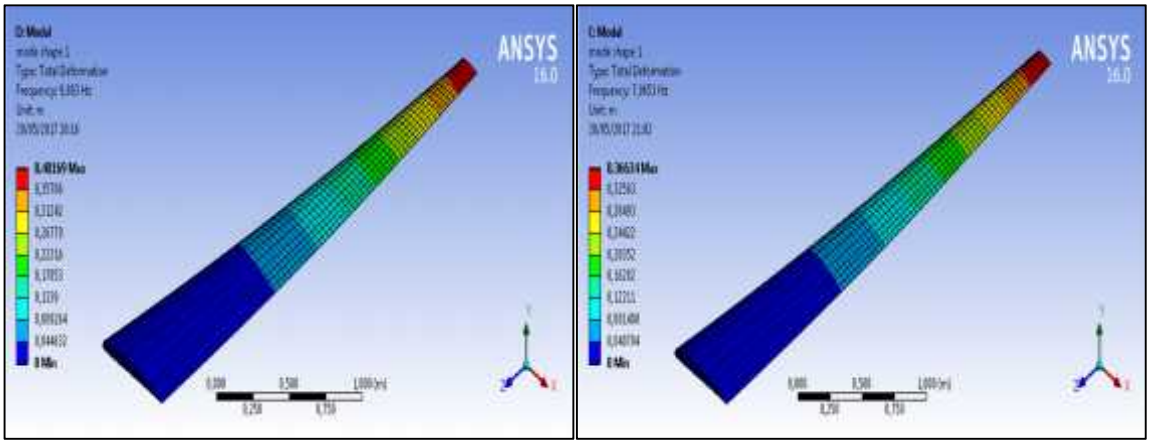

L=3m **L=3.5m**

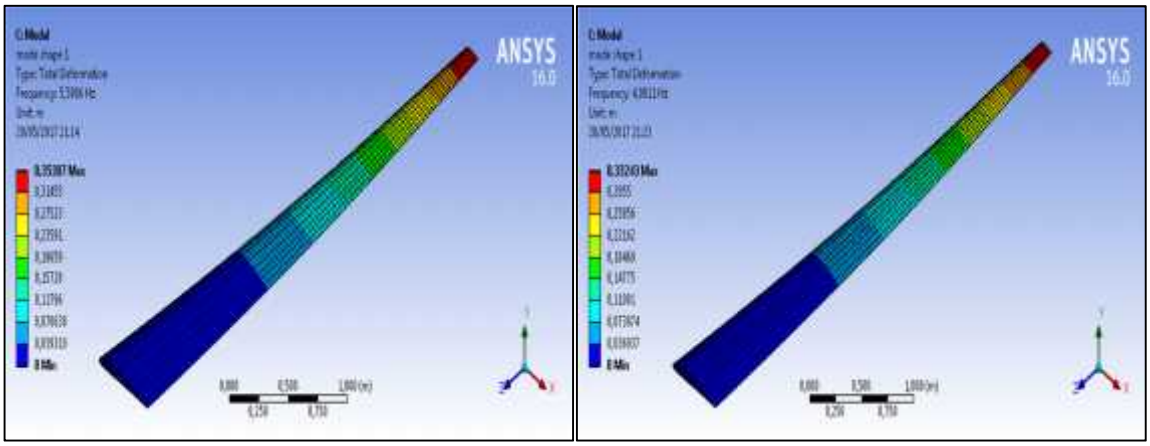

L=3.9 **L=4.5m**

Figure 12: First mode shape for different wing lengths (NACA4412)

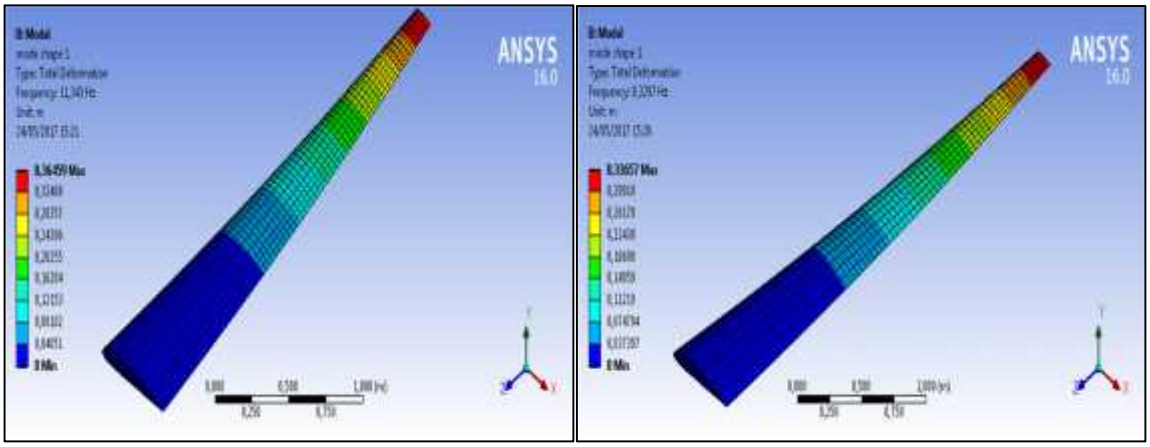

L=3m **L=3.9m**

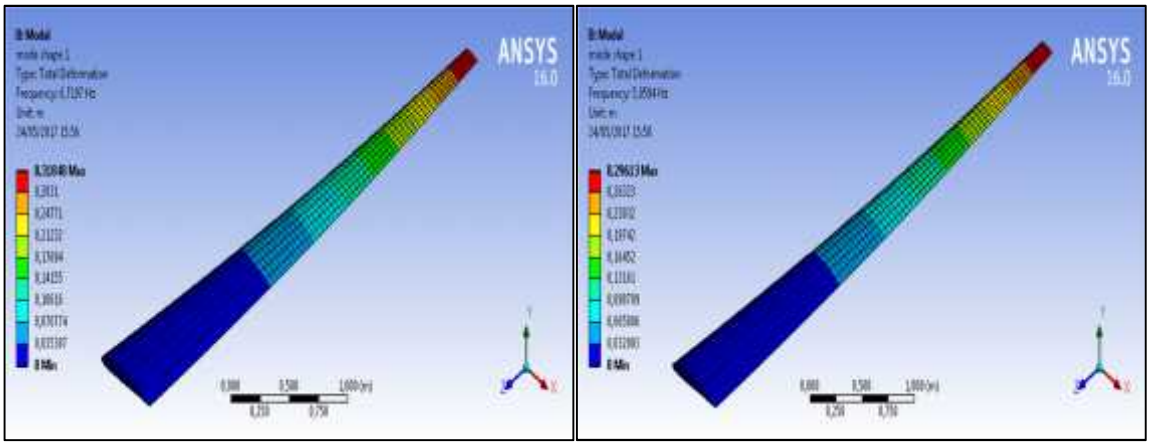

L=3.9m **L=4.5m**

Figure 13: First mode shape for different wing lengths (NACA4415)

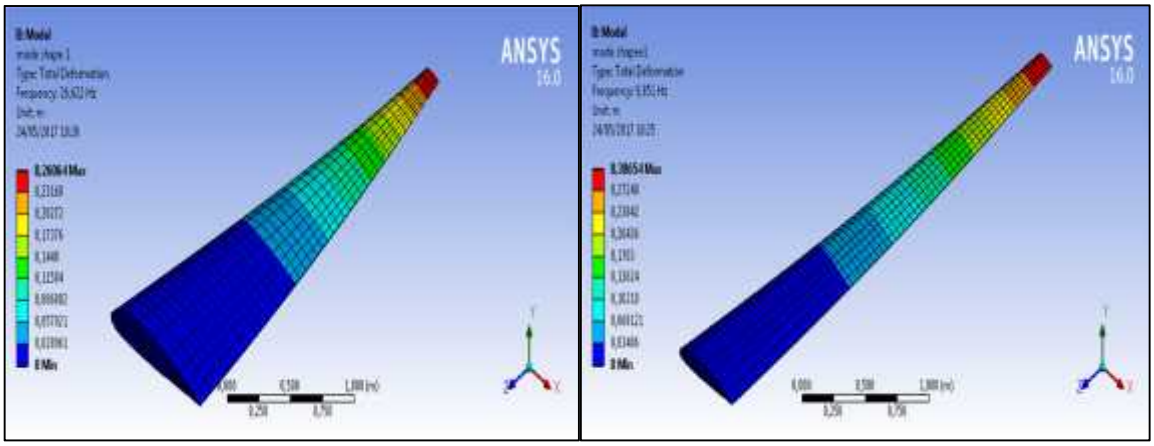

L=3m **L=3.5m**

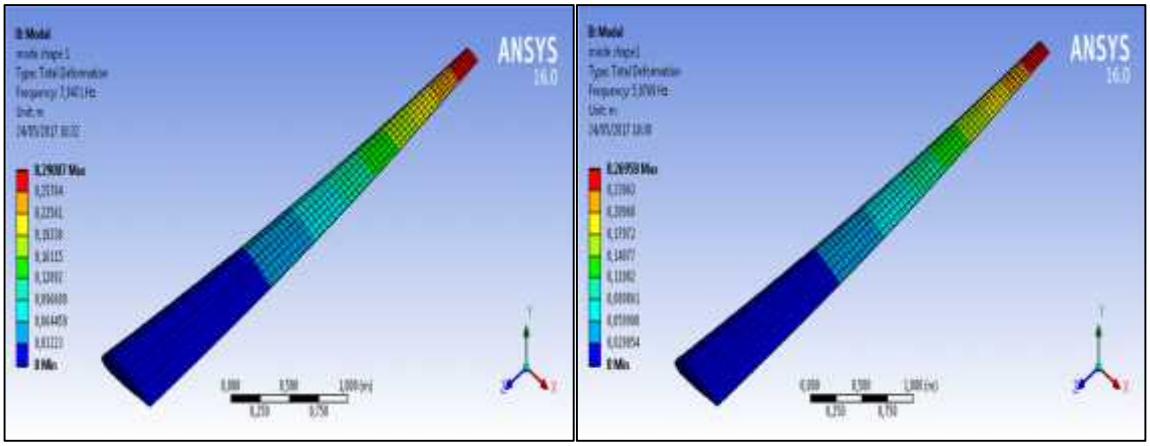

L=3.9m **L=4.5m**

Figure 14: First mode shape for different wing lengths (NACA4318)

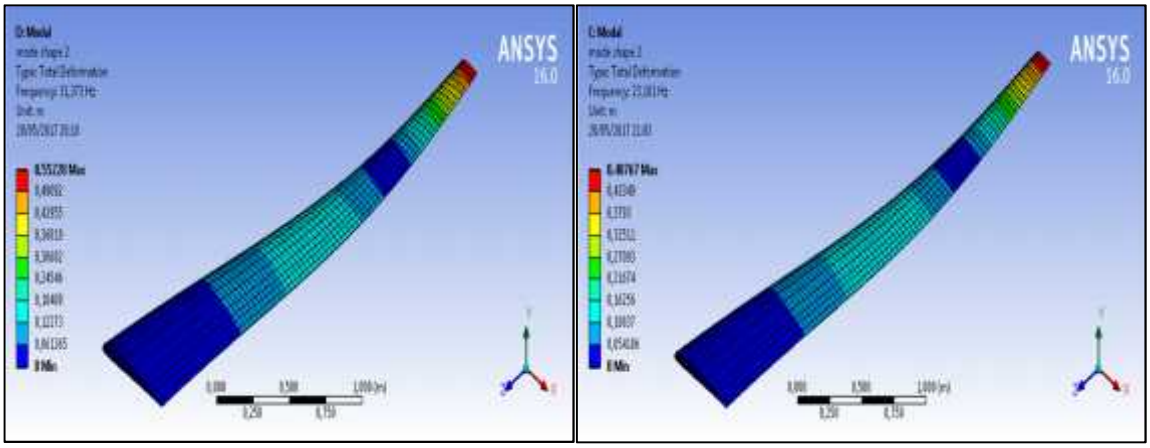

L=3m **L=3.5m**

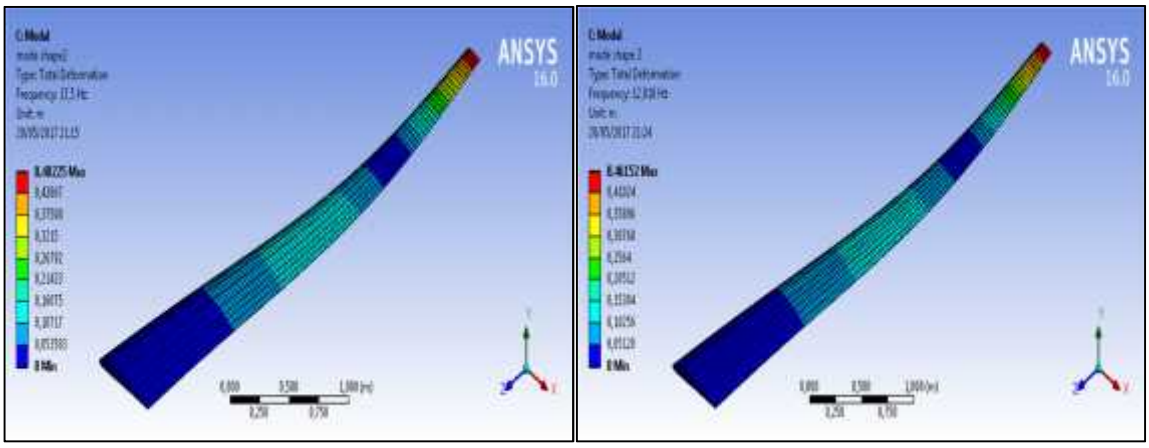

L=3.9m **L=4.5m**

Figure 15: Second mode shape for different wing lengths (NACA4412)

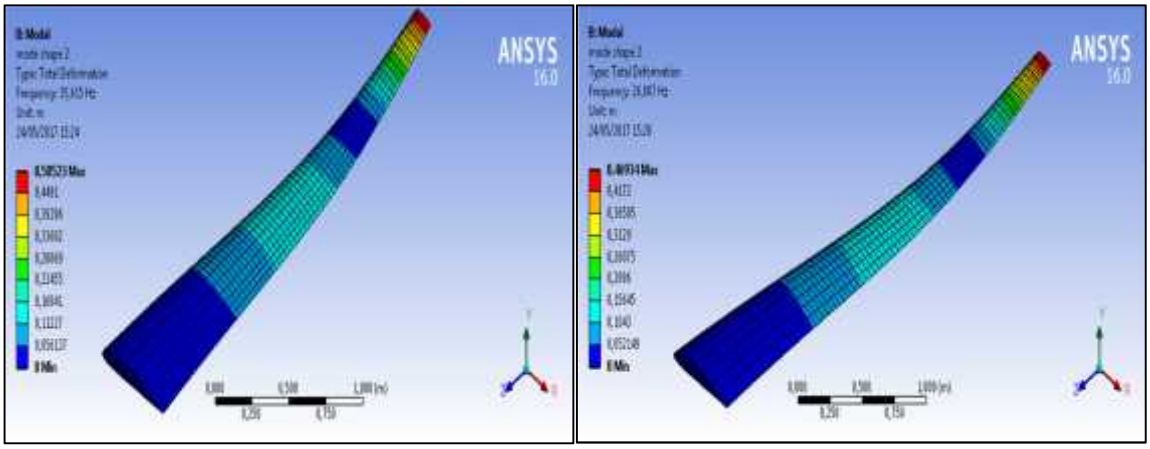

L=3mL=3.5m

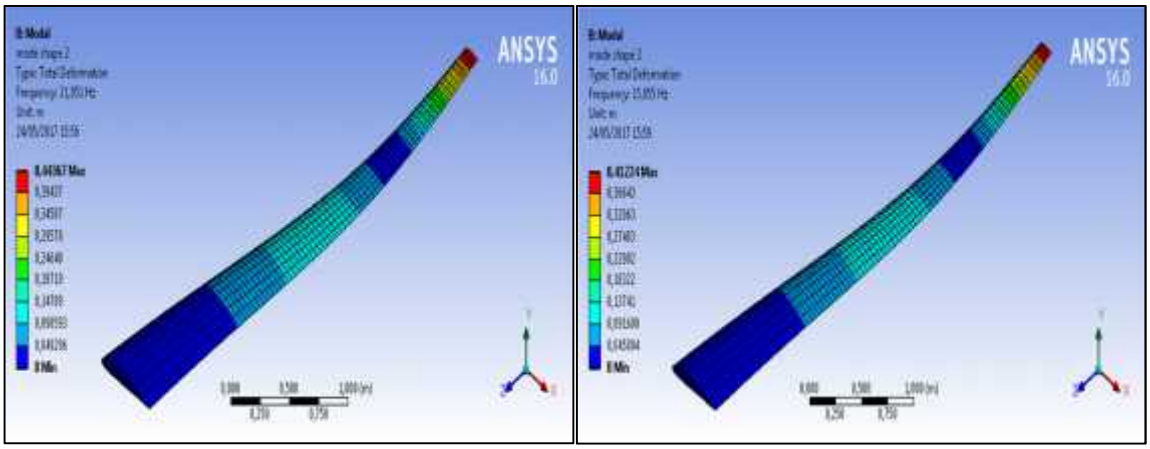

L=3.9m **L=4.5m**

Figure 16: Second mode shape for different wing lengths (NACA4415)

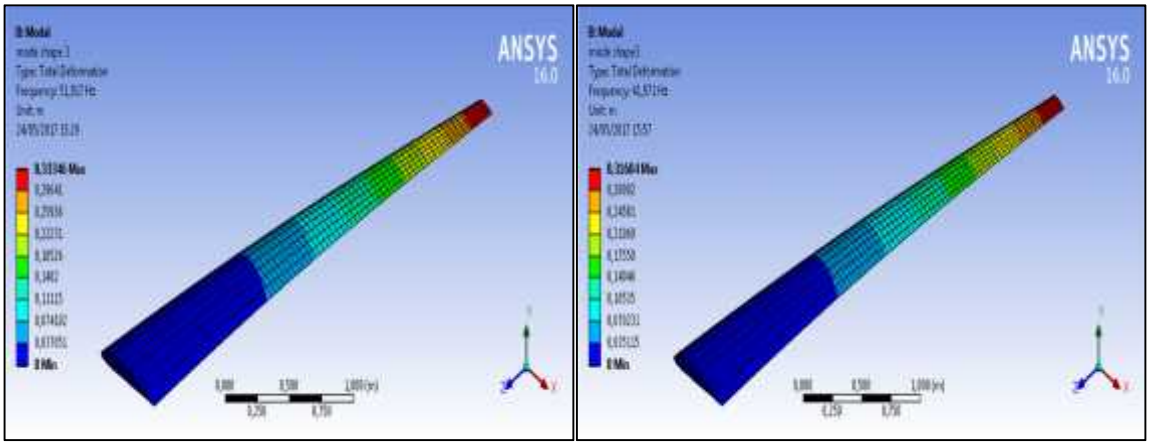

L=3m **L=3.5m**

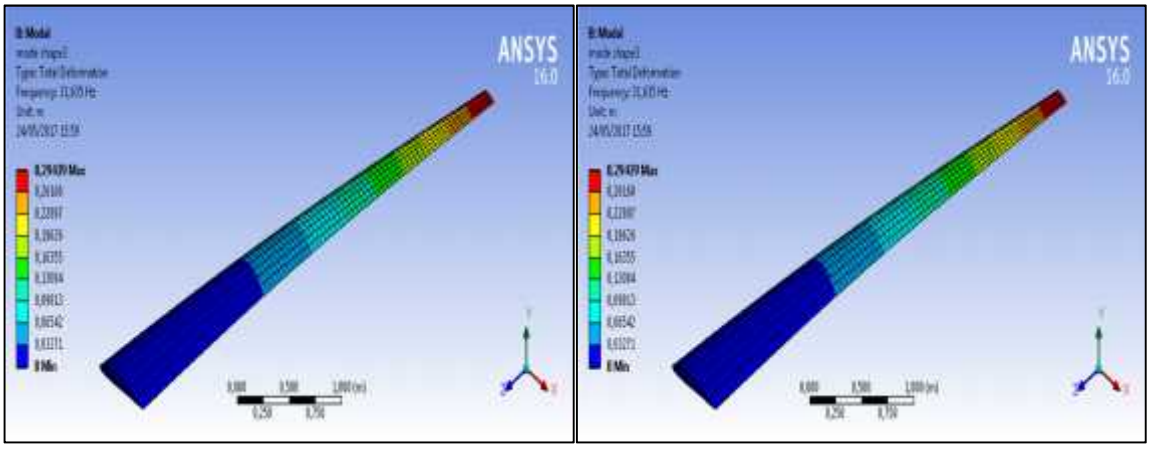

L=3.9m **L=4.5m**

Figure 17: Second mode shape for different wing lengths (NACA4318)

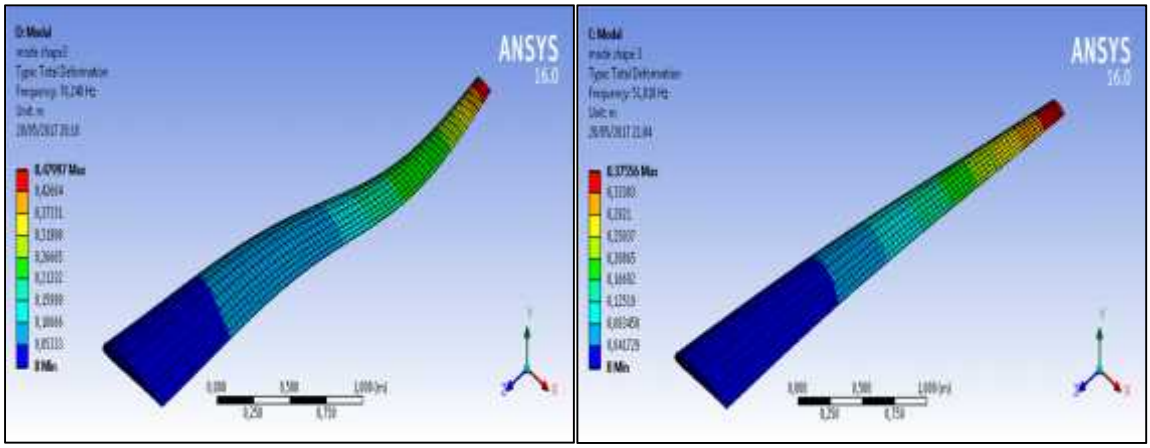

L=3m **L=3.5m**

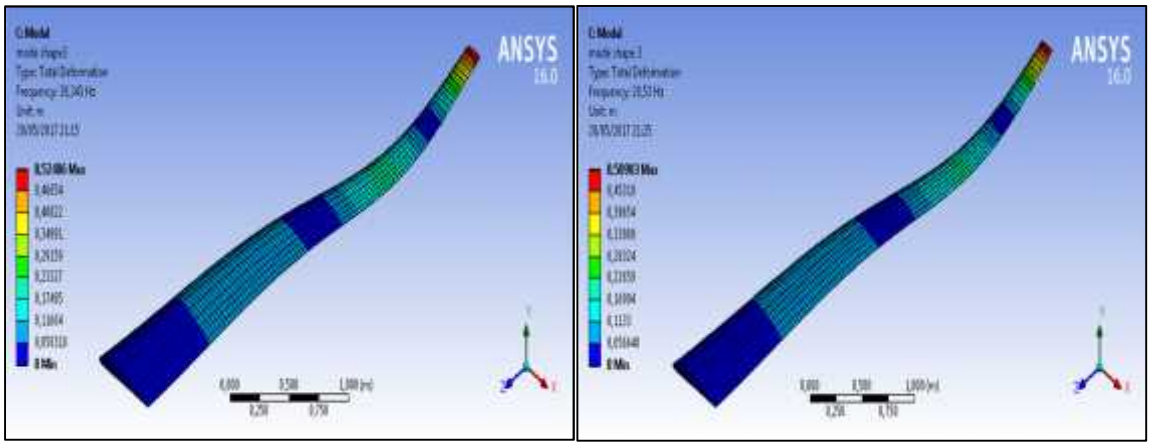

L=3m **L=3.5m**

Figure 18: Third mode shape for different wing lengths (NACA4412)

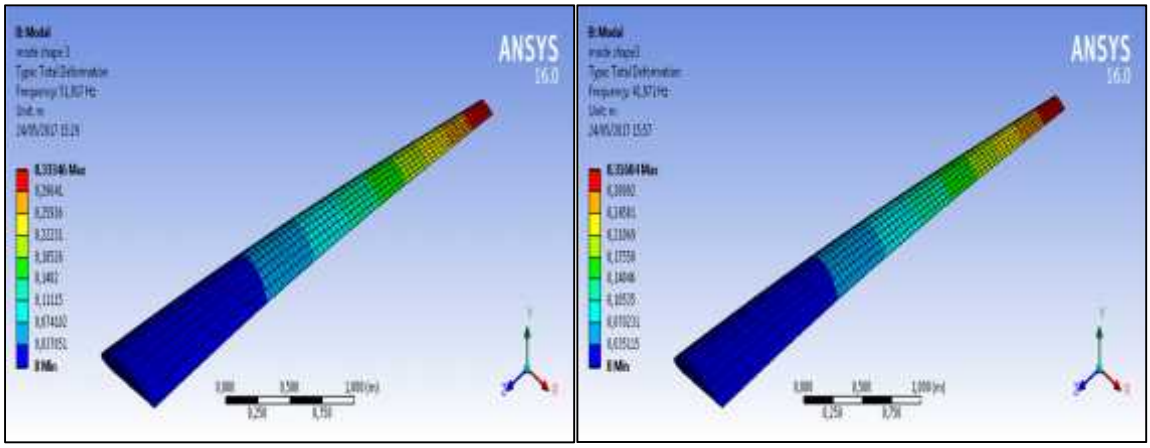

L=3m **L=3.5m**

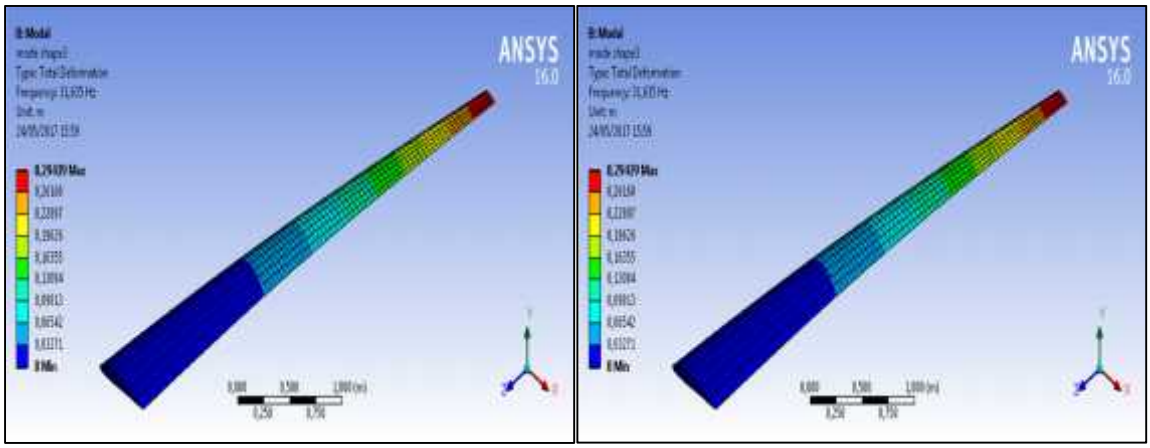

L=3.9m **L=4.5m**

Figure 19: Third mode shape for different wing lengths (NACA4415)

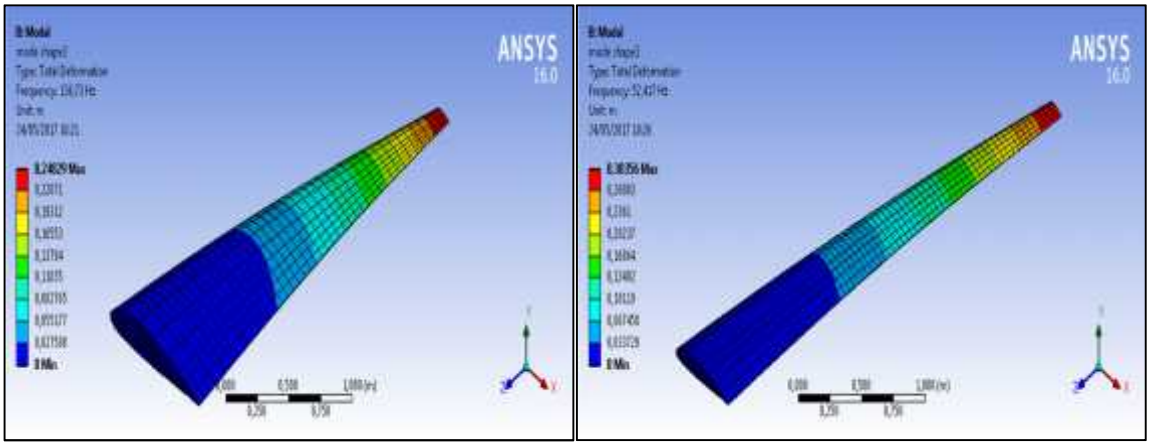

L=3m **L=3.5m**

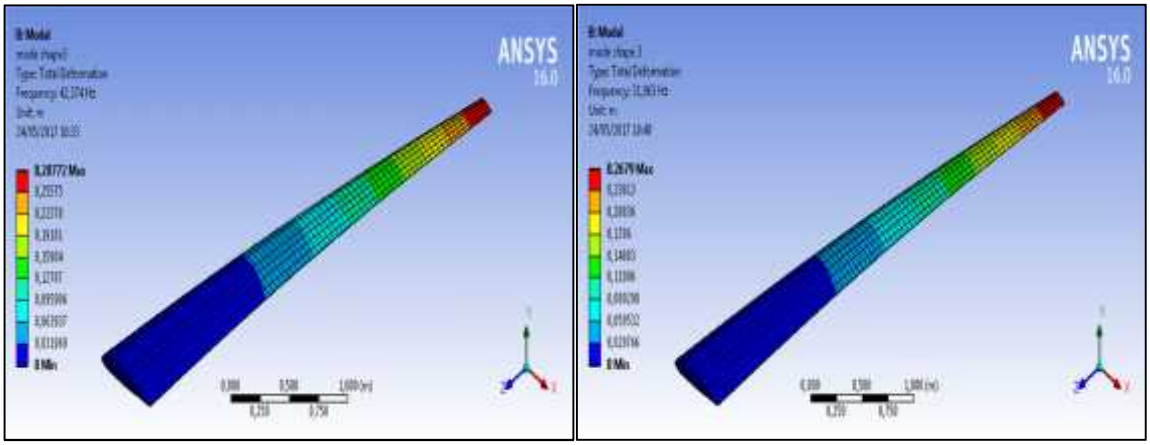

L=3.9m **L=4.5m**

Figure 20: Third mode shape for different wing lengths (NACA4318)

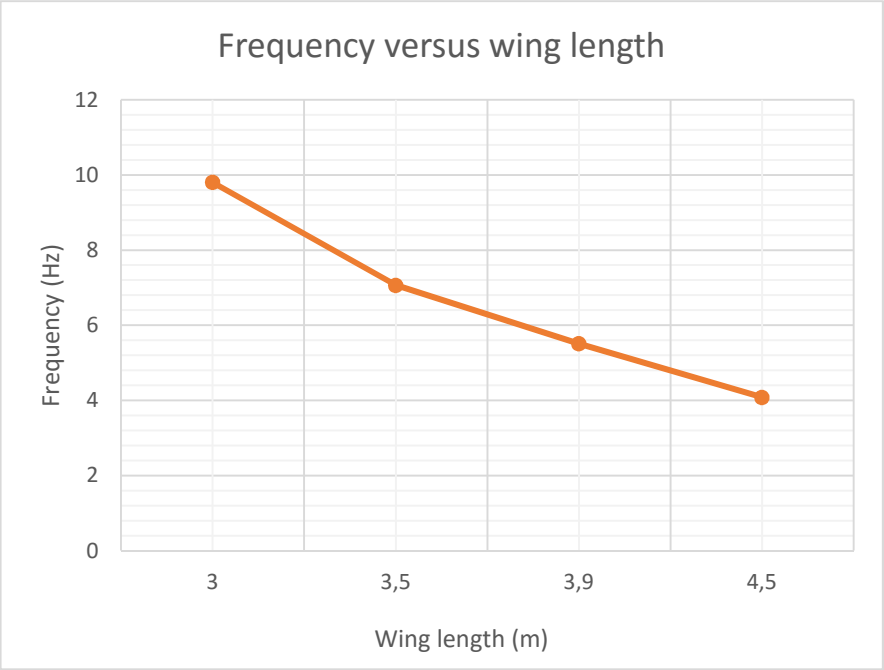

Figure 21: Variation of frequency according to the wing length (NACA 4412) for the first mode

- The **figure 21** illustratescurve of frequency of the first mode shape according to the wing length for NACA 4412 Profile. We observe from this figure that the frequency varies decreasingly in function of the wing length, so when the wing length increases the frequency decreases.

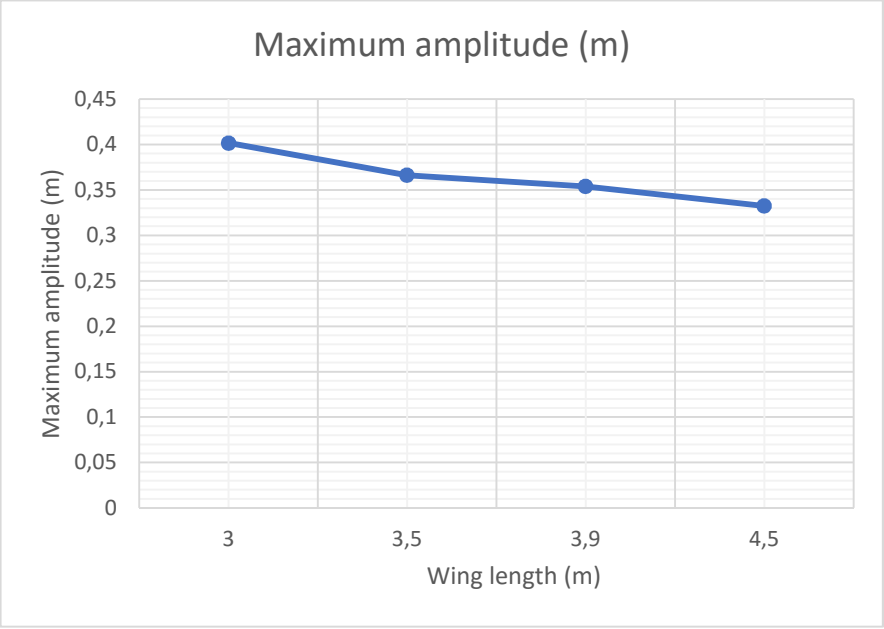

Figure 22: Variation of maximum amplitude of the first mode shape according to different wing length for (NACA 4412)

- The **figure22** representsthe curve of maximum amplitude of the first mode shape according to different wing length for NACA 4412 Profile. We can see from this figure that the maximum amplitude varies also decreasingly in function of the wing length.

Note that we have got the same variation of frequency and maximum amplitude for the other profiles.

II.1.3 Static structural analysis

The tables below show the results of static structural analysis for different wing length and with different profiles.

Wing length (m)	Maximal von-Mises stress (Pa)	Maximal Elastic Strain (m/m)	Maximal Deformation (m)	Maximal Strain Energy (J)
3	$1.021\square 10^{7}$	$1.489\square 10^{-4}$	$2.063\square 10^{-2}$	0.046
3,5	$1.508\square 10^{7}$	$2.157\square 10^{-4}$	$4.037\square 10^{-2}$	0.139
3,9	$4.042\square 10^{7}$	$5.701\square 10^{-4}$	0.126	0.808
4,5	$6.548\square 10^{7}$	$9.232\square 10^{-4}$	0.276	2.405

Table 7: Results of maximal, stress, strain, deformation and strain energy with different wing lengths(NACA 4412)

Wing length (m)	Maximal Elastic Strain (m/m)	Maximal StrainEnergy (J)	Maximal deformation (m)	Maximal Von-Mises stress (Pa)
3	$1.5594\square 10^{-5}$	$4.318\square 10^{-3}$	0.0009312	$1.1071\square 10^{6}$
3.5	$1.1893\square 10^{-4}$	$8.642\square 10^{-2}$	0.01384	$8.4419\square 10^{6}$
3.9	$2.77\square 10^{-4}$	0.479	0.04011	$1.9662\square 10^{7}$
4.5	$4.4410\square 10^{-4}$	0.954	0.084	$3.1508\square 10^{7}$

Table 8: Results of maximal, stress, strain, deformation and strain energy with different wing lengths (NACA 4318)

Wing length (m)	Maximal Elastic Strain (m/m)	Maximal Strain Energy(J)	Maximal deformation (m)	Maximal von-Mises stress (Pa)
3	1.1283×10^{-4}	4.829×10^{-2}	0.012	8.006×10^{6}
3,5	1.767×10^{-4}	7.952×10^{-2}	0.023	1.254×10^{7}
3,9	4.101×10^{-4}	0.434	0.067	2.911×10^{7}
4,5	6.32×10^{-4}	1.309	0.141	4.492×10^{7}

Table 9: Results of maximal, stress, strain, deformation and strain energy with different wing lengths (NACA 4415)

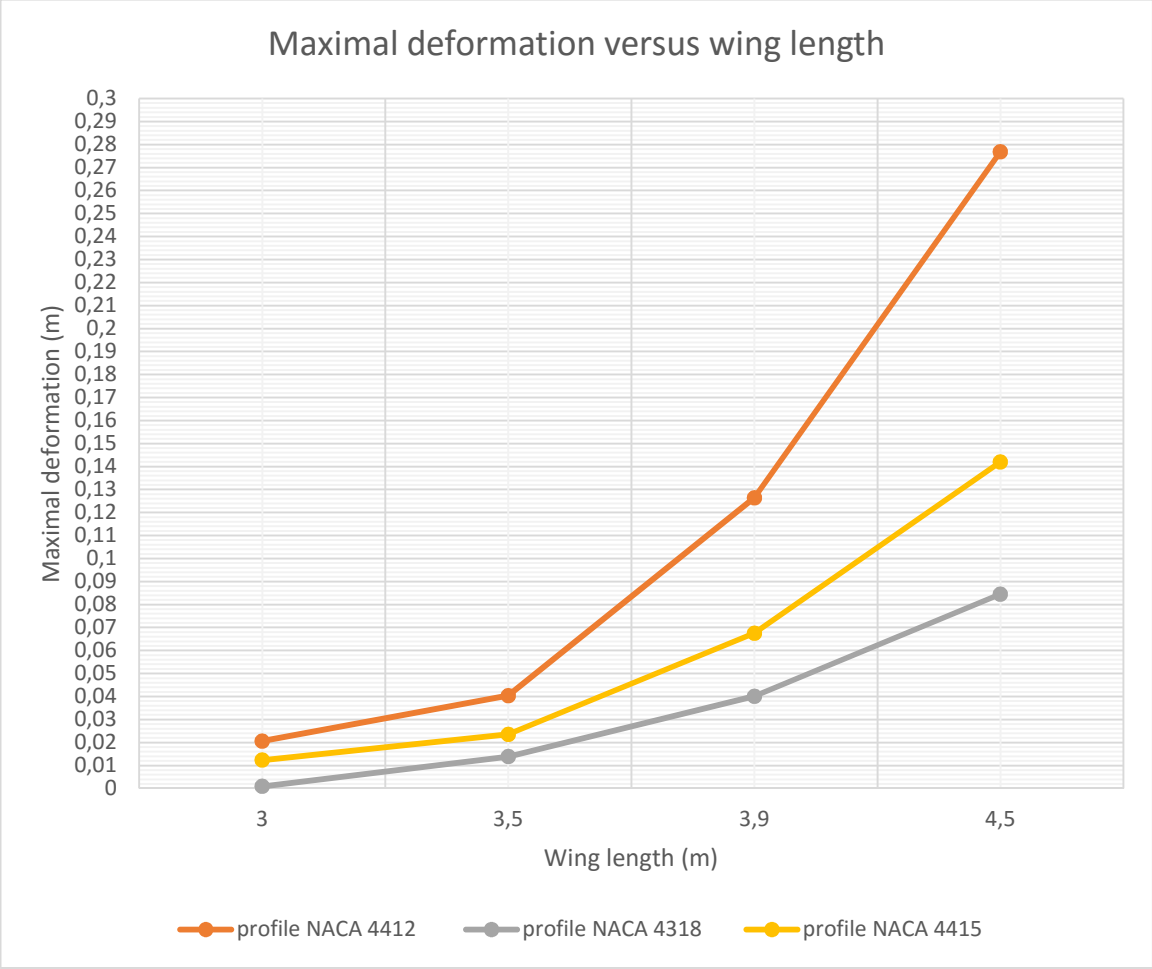

Figure 23: Maximal deformation according to the wing length.

- The **figure 23**illustrates the curve of the maximal deformation values according to the wing length with aluminum alloy material, we observe from this curve that the maximal deformation increases when the wing length increases.

After different simulations, we have got a total deformation, strain, von-Mises stress and stress energy for the three profiles, just those for profile NACA4412 which are depicted below:

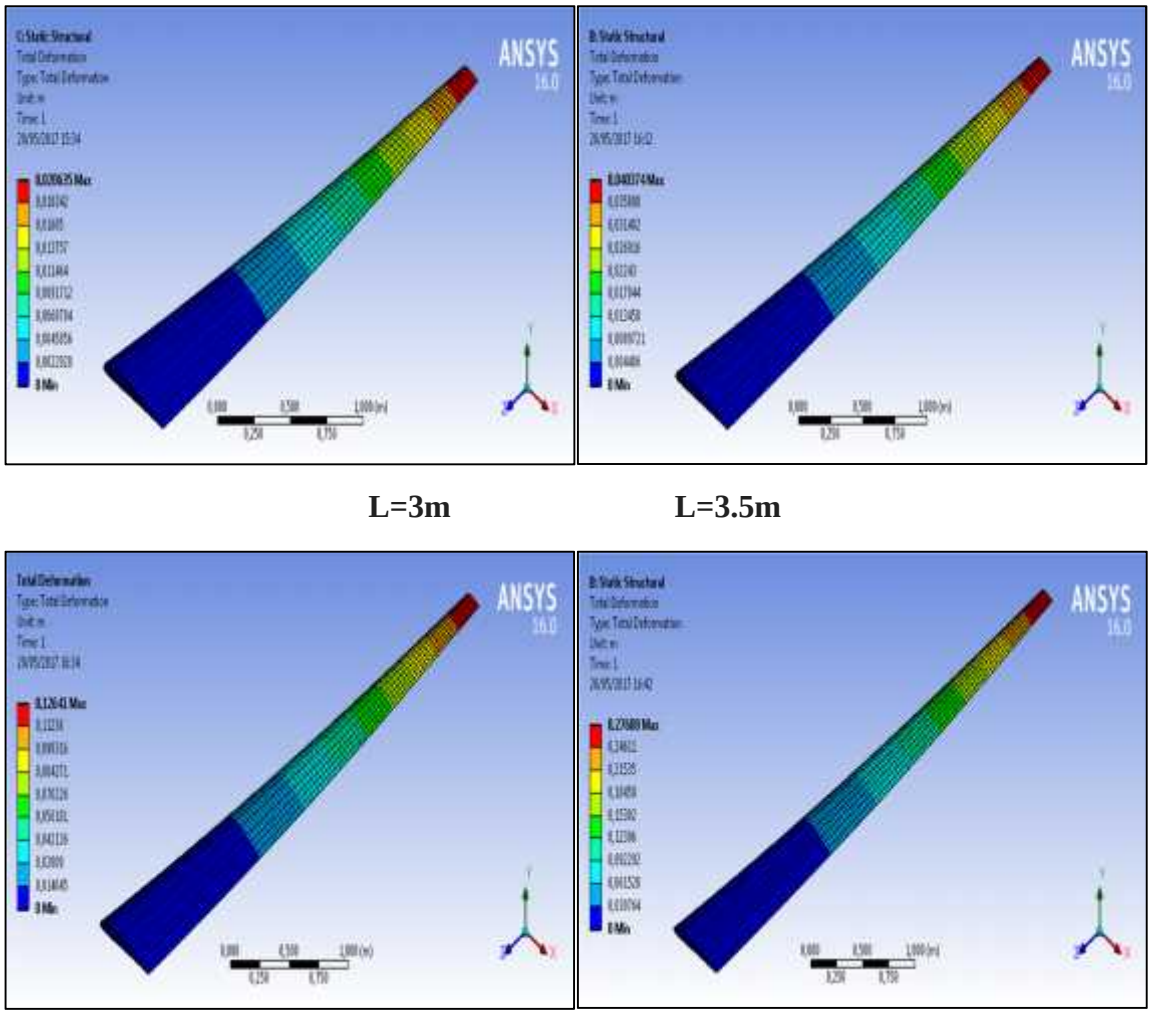

L=3m **L=3.5m**

L=3.9m **L=4.5m**

Figure 24: Total deformation for different wing lengths

- The **figure 24** shows the total deformation according to the wing length for NACA 4412 profile. We observe from this figure that the maximal deformation is located on the free end (red color) for the different wing lengths. We also observe that for the fixed end its deformation is zero (blue color).

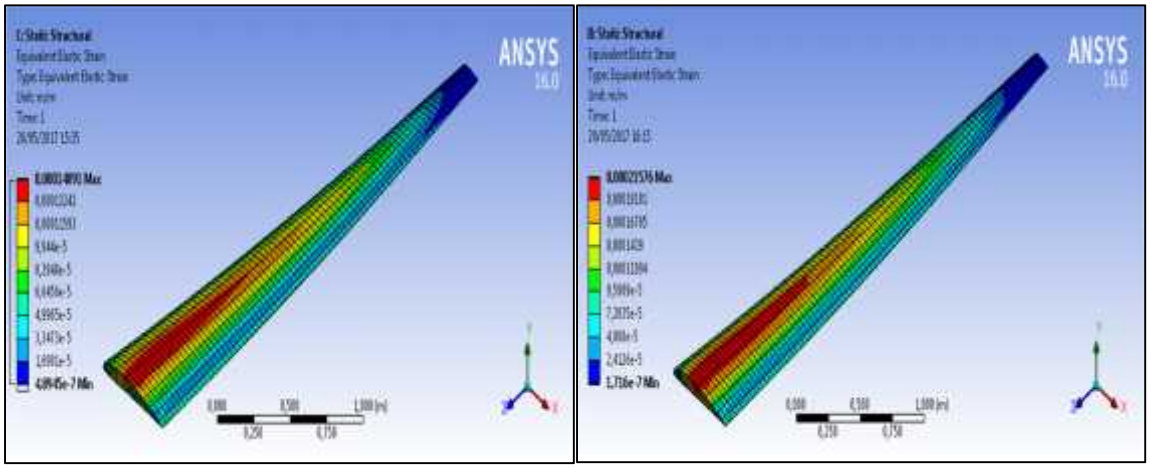

L=3m **L=3.5m**

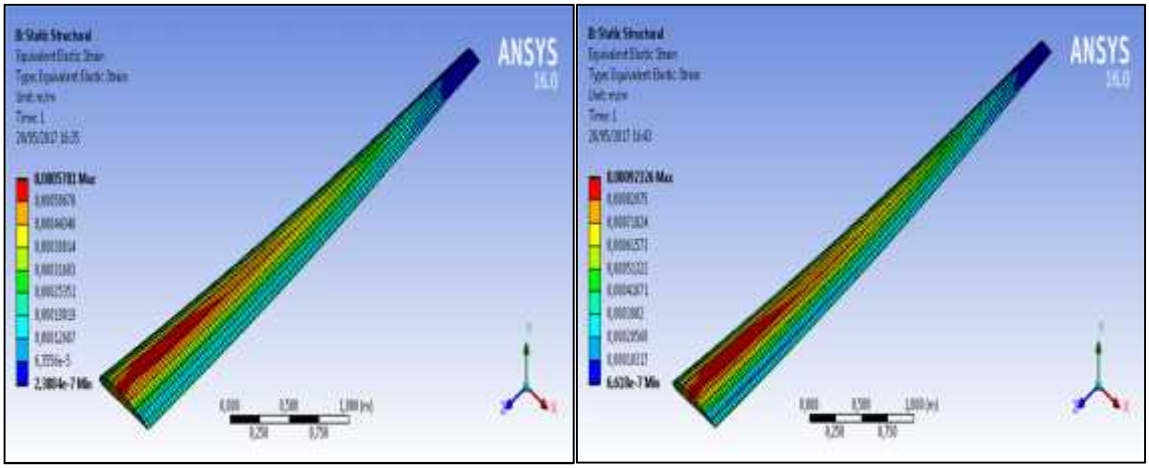

L=3.9m **L=4.5m**

Figure25: Equivalent elastic strain for different wing lengths

- The**figure 25**shows the equivalent elastic strain for different wing lengths of the NACA 4412. We observe from this figure that the maximal elastic strain is located on the fixed end (red color) and for the free end it is zero (blue color).

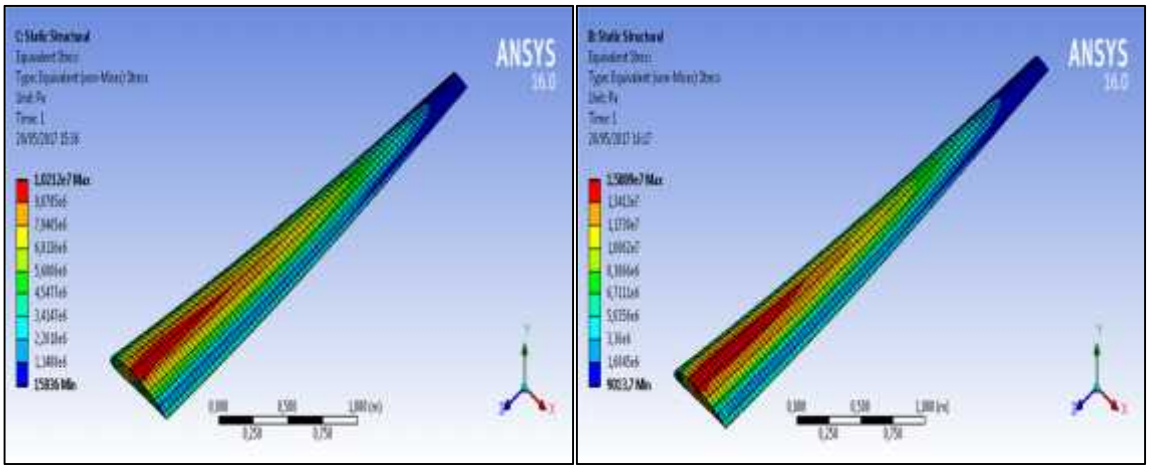

L=3m **L=3.5m**

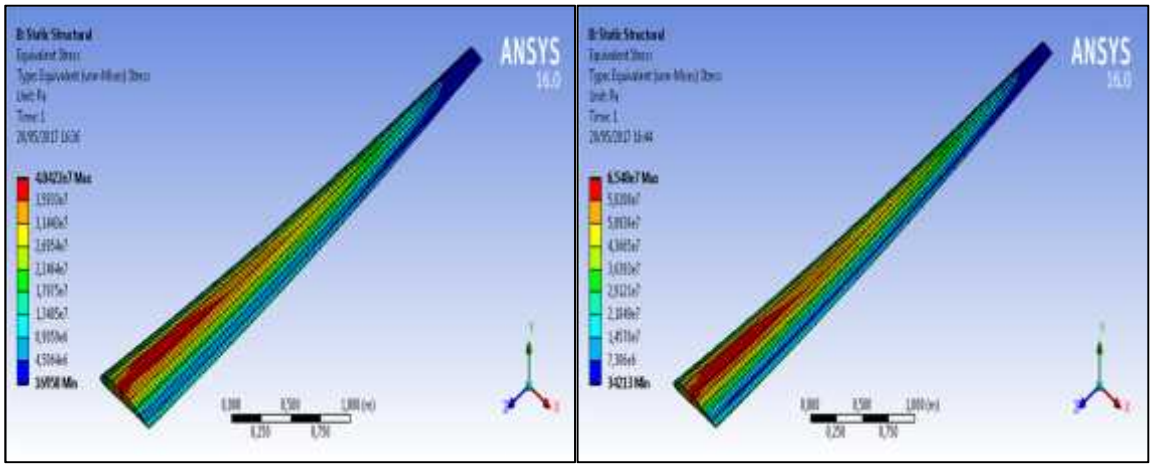

L=3.9m **L=4.5m**

Figure 26: Equivalent von-Mises stressfor different wing lengths

- The **figure 26**shows the equivalent Von-Mises for different wing lengths with NACA 4412. We observe from this figure that the maximal Von-Mises centralized in the fixed extremity (red color) and for the free extremity is null (blue color)

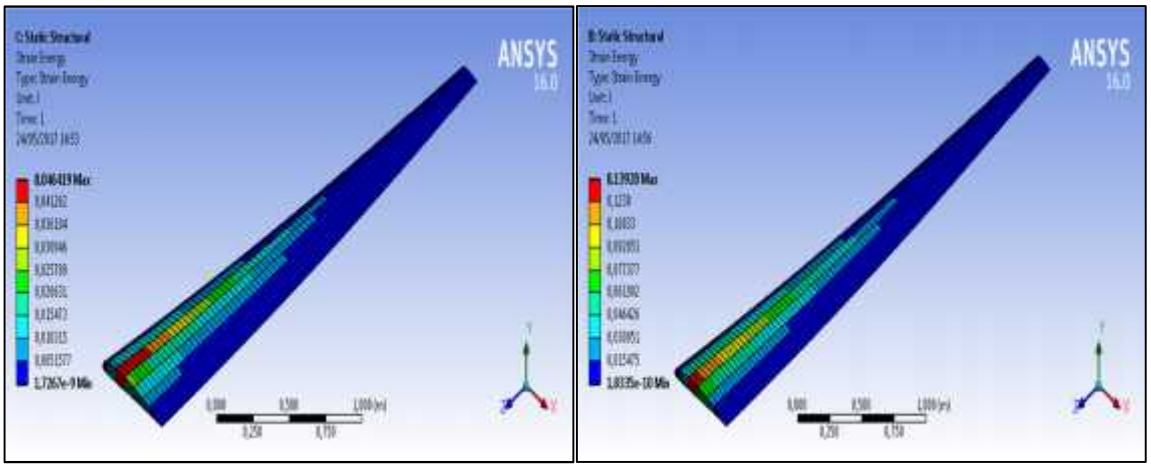

L=3m **L=3.5m**

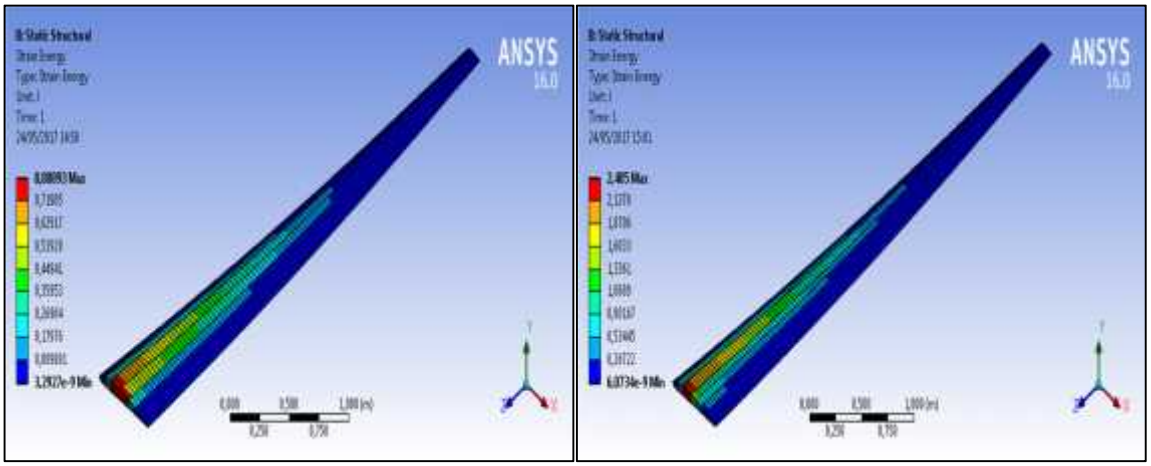

L=3m **L=3.5m**

Figure 27: Strain energy for different wing lengths

- The **figure 27**shows the strain energy for different wing lengths of the NACA 4412. We observe from this figure that the maximal strain energy is located on the fixed end (red color) and for the free end it is zero (blue color)

From these results, we note that the high lift and the low drag are obtained for different length value. The lift is maximal for a span of 4.5m but the drag is minimal for a span of 3.5m.

Concerning the total deformation and the Von-Mises stress we note that they achieved their minimum value for a span of 3m.

We conclude that there is note an only value which satisfies the two constraints then we must make a compromise to have the best characteristics.

II.2. Effect of the chord root length

The table below shows the results of aerodynamic coefficients for the same wing profile and different chord root lengths and with constant wing length.

L (m)	3,9			
C_r (m)	0.3	0.4	0.5	0.582
C_L	0.348	0.362	0.445	0.675
C_D	0.014	0.019	0.023	0.028
C_m	0.046	0.031	0.040	0.068

Table 10: Aerodynamic coefficients with different chord root lengths (profile NACA4412)

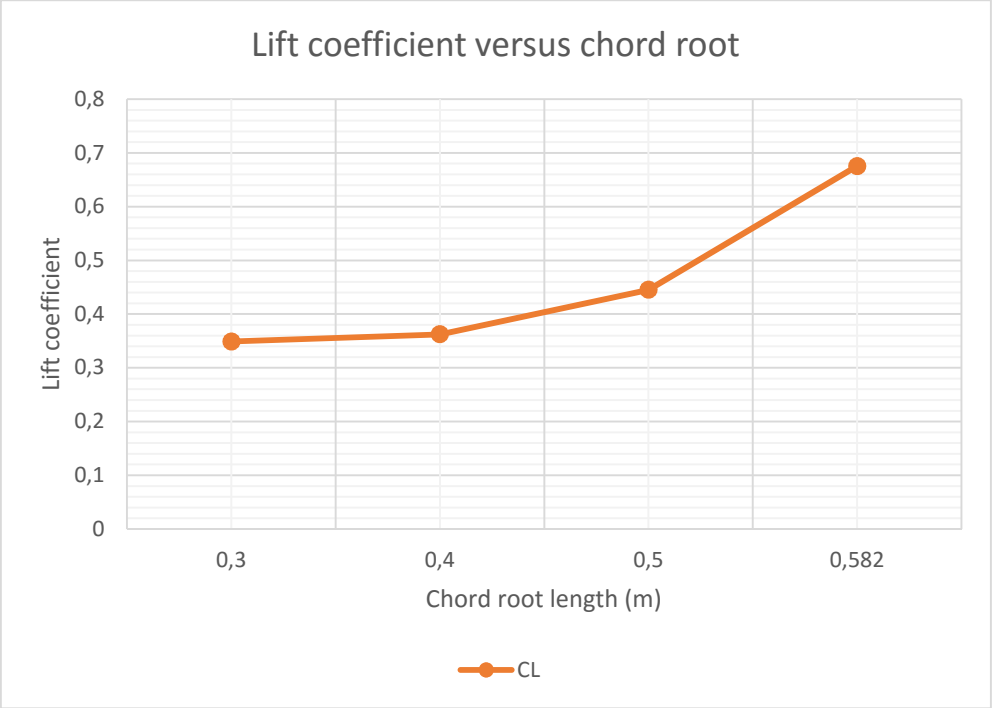

Figure 28: Lift coefficient versus chord root lengths

- The **figure 28**shows that the lift coefficient varies increasingly in function of the chord root length, where it goes up from the minimum value of 0.348 at the chord root of 0.3m to reach the maximal value for 0.675 at the chord root of 0.582m.

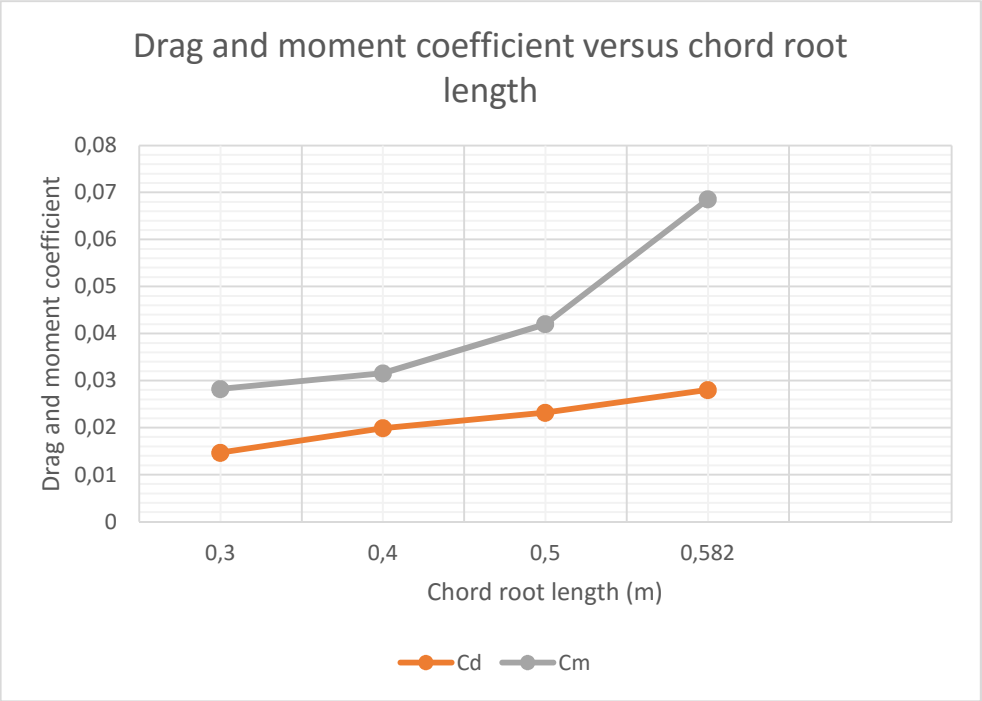

Figure 29: Drag and moment coefficients versus chord root

- The **figure 29**illustrates the curves of drag and moment coefficients according to the chord root length. We notice from this figurethat the drag coefficient varies also in function of the chord root length, where it goes up from $C_r = 0.3m$ for value 0.014 of lift coefficient to reach the maximal value of 0.028 at the chord root of 0,582m
- The moment coefficient varies also in function of the chord root length, so when the chord root length increases the moment coefficient increase, where it goes up from $C_r = 0{,}3m$ for value 0.028 of moment coefficient to reach the maximal value of 0.068 at

$$C_r = 0.45m$$

After the different simulations for different chord root length, we have got a static pressure contours and velocity vectors which are depicted below.

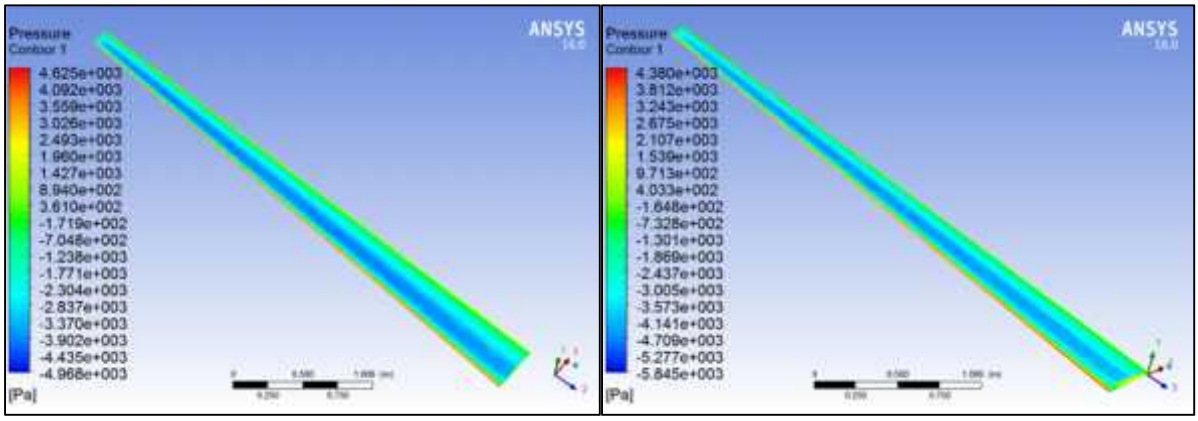

C_r =0.3m C_r =0.4m

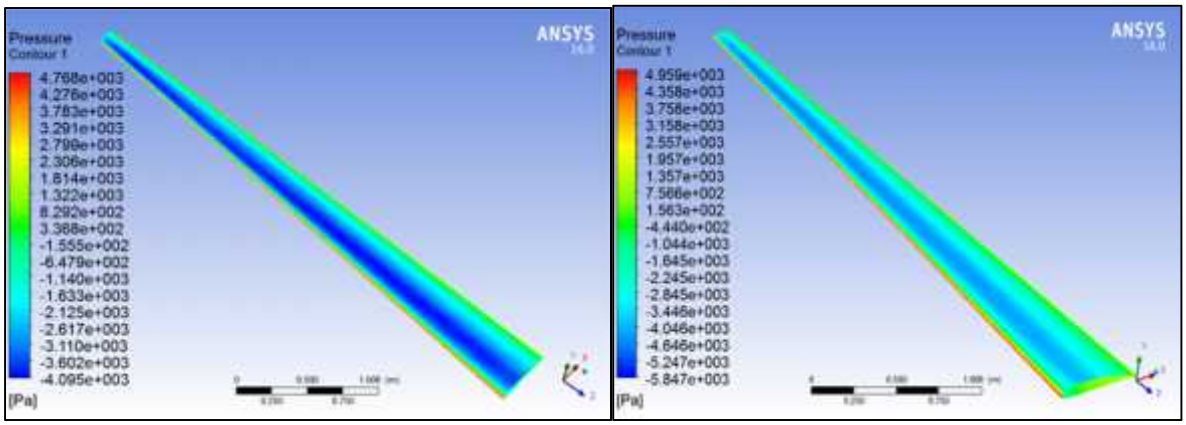

C_r =0.5mC_r =0.582m

Figure 30: Contour of static pressure for different chord root lengths

- The **figure 30** shows contours of static pressure for different chord root lengths.We can see from this figure that we almost have the same pressure evolution for the differentchord root lengths.

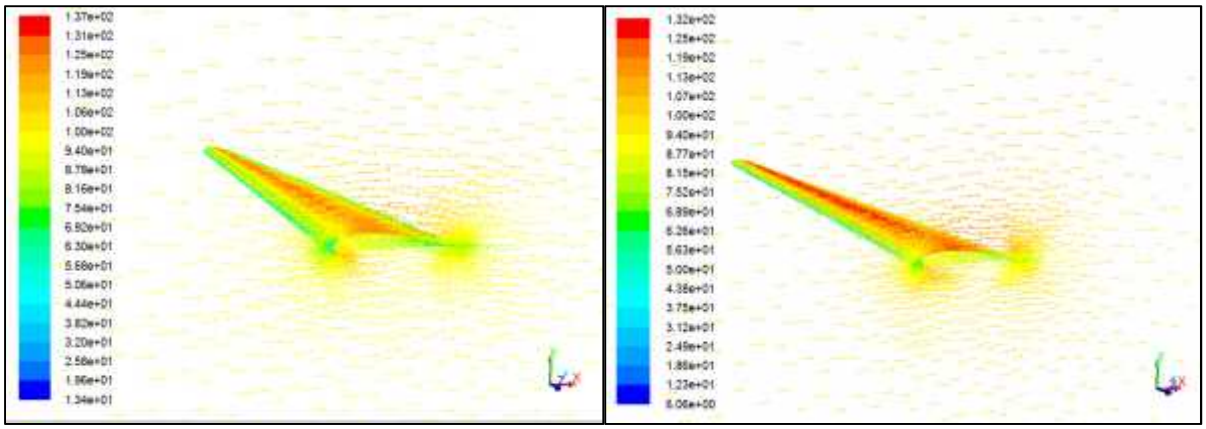

C_r =0.3m C_r =0.4m

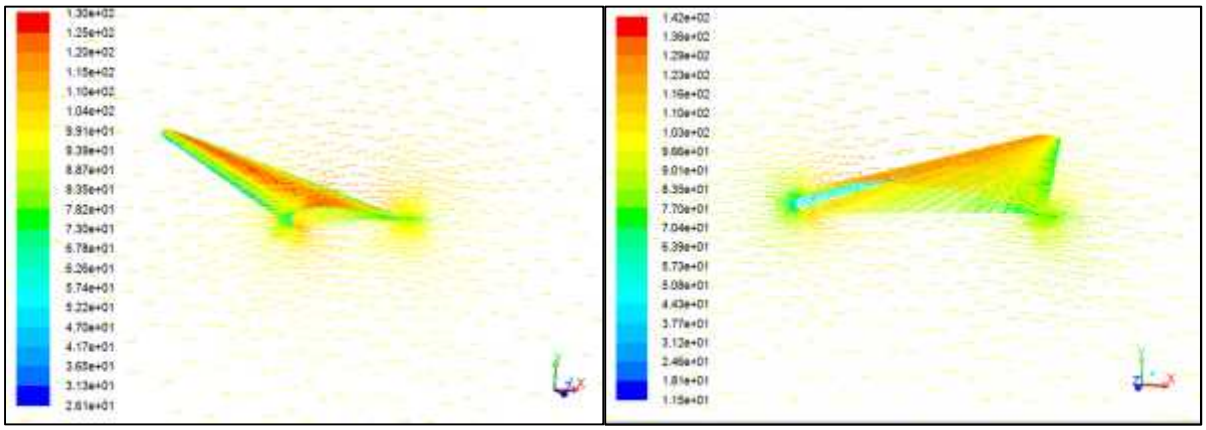

C_r =0.5m C_r =0.582m

Figure31: Velocity vectors for different chord root lengths

- We can see from**figures 31**we have the same velocity evolution for chord root as the case of variation of wing length. So, wehave a sharp decrease in the speed at the leading edge and we observe also that the flow follows the shape of the profile, there is no separation or reversed flow.

II.2.1Calculation of drag and lift forces

- ρ = 1,225 kg/m^3
- V = 100 m/s

C_n (m)	0.3	0.4	0.5	0.582
F_y (N)	1786.78	2336.24	3402.72	5823.02
F_x (N)	77.13	128.21	177.11	241.64
R(N)	1788.44	2339.75	3173.5	5828.03

Table 11: Values of lift and drag forces and their resultant

Figure 32: Resultant force according to the chord root

- The **figure 32**illustrates the curve resultant force according to the chord root length. We observe that we have proportional relationship between these two parameters.When the chord root length increasesthe resultant force also increases.

II.2.2Modal analysis

The **table12** show the results of modal analysis fordifferent profiles, differentchord root length and with constant wing length ($L = 3.9m$).

The modal analysis is characterized by the frequencies and the maximal amplitudes.

		Profile NACA 4318		**Profile NACA 4415**		**Profile NACA 4412**	
Chord root length (m)	Mode shape	Frequency Hz	Maximum amplitude	Frequency Hz	Maximum amplitude	Frequency Hz	Maximum amplitude
C_r =0.3	1	3.283	0.349	2.7732	0.383	2.260	0.427
	2	13.417	0.407	11.333	0.447	9.253	0.499
	3	17.52	0.349	17.355	0.383	17.437	0.427
	4	32.947	0.429	27.832	0,.470	22.733	0.525
C_r =0.4	1	4.838	0.326	4.097	0.358	3.337	0.402
	2	17.382	0.408	14.73	0.449	12.016	0.504
	3	25.899	0.325	25.641	0.357	25.667	0.401
	4	40.803	0.438	34.577	0.481	28.23	0.540
C_r =0.5	1	6.514	0.305	5.5135	0.335	4.4613	0.373
	2	21.482	0.406	18.187	0.447	14.935	0.488
	3	34.814	0.303	34.454	0.333	34.351	0.521
	4	48.742	0.444	41.267	0.4889	34.552	0.379
C_r =0.582	1	7.947	0.290	6.7197	0.318	5.508	0.353
	2	24.886	0.403	21.051	0.443	17.5	0.482
	3	42.374	0.287	41.971	0.316	39.343	0.524
	4	55.207	0.448	46.703	0.492	42.172	0.355

Table12: Results of modal analysis with different chord root length

The first four mode shapes are depicted below.

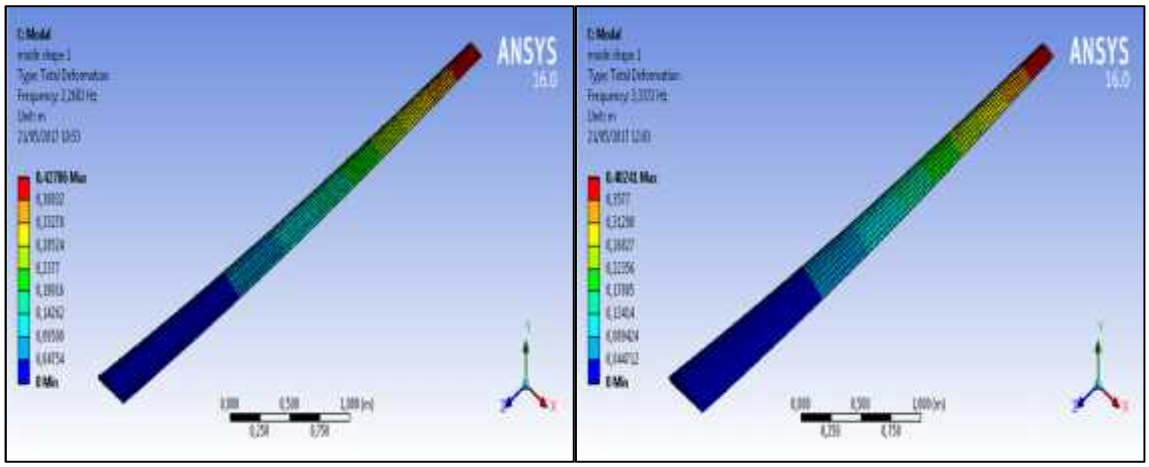

C_r =0.3m **C_r =0.4m**

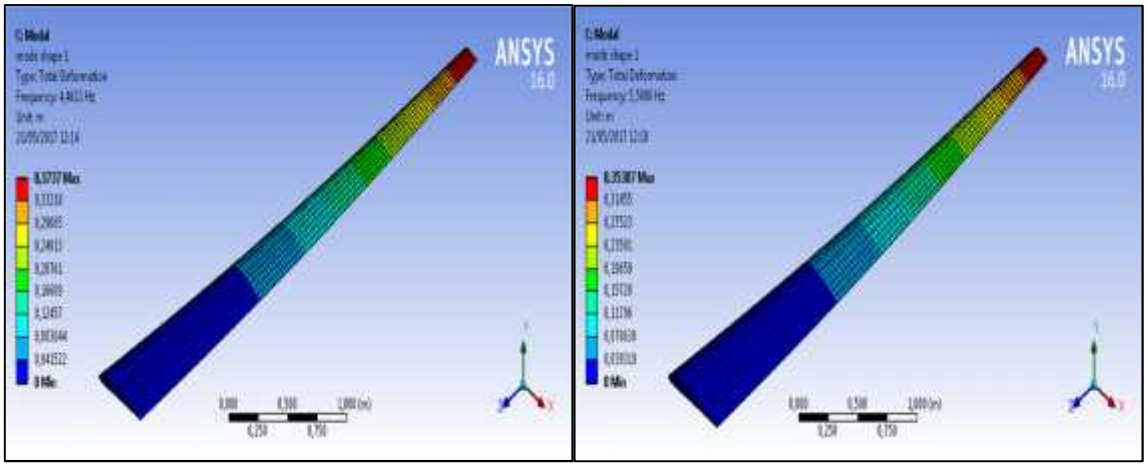

C_r =0.5m **C_r =0.582m**

Figure 33: First mode shape for different chord root lengths(NACA4412)

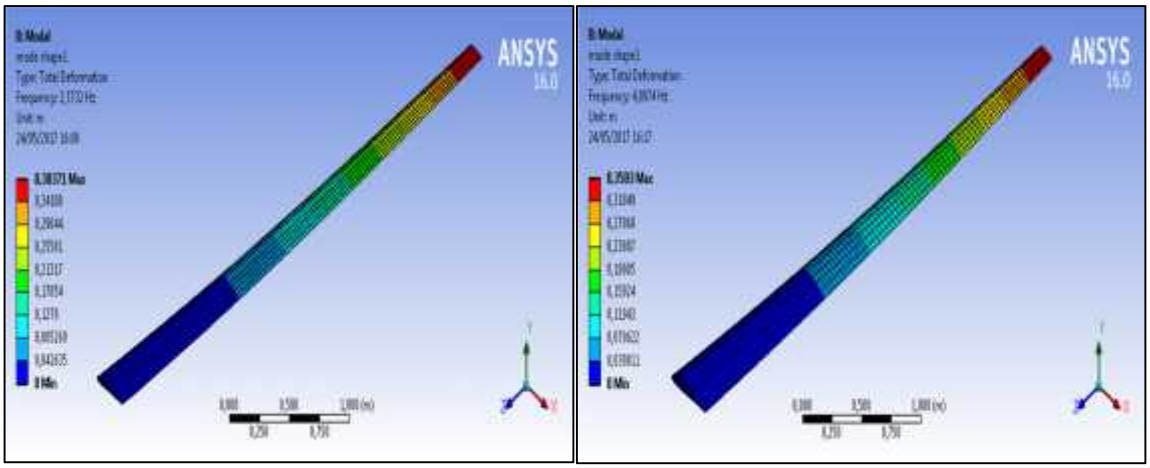

C_r =0.3m C_r =0.4m

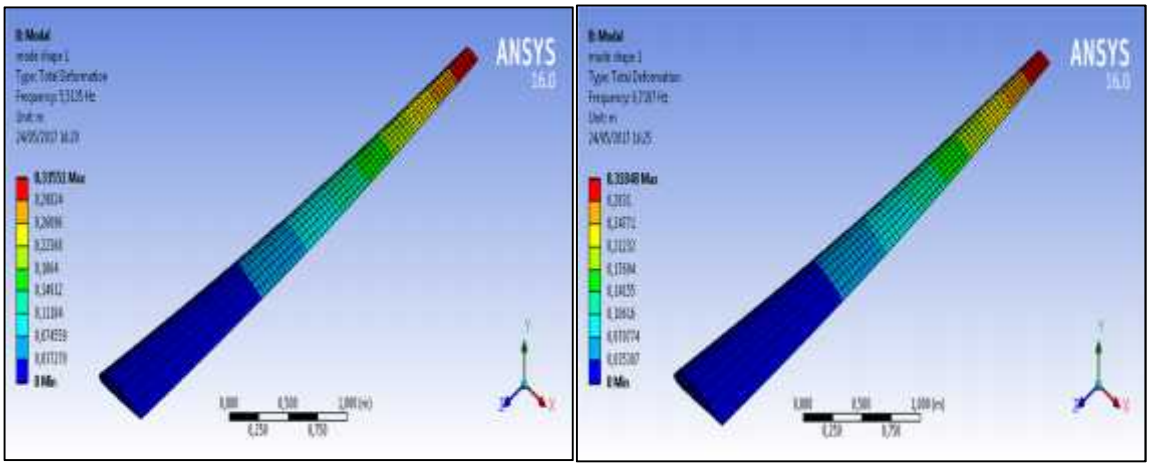

C_r =0.5m C_r =0.582m

Figure 34: First mode shape for different chord root lengths (NACA4415)

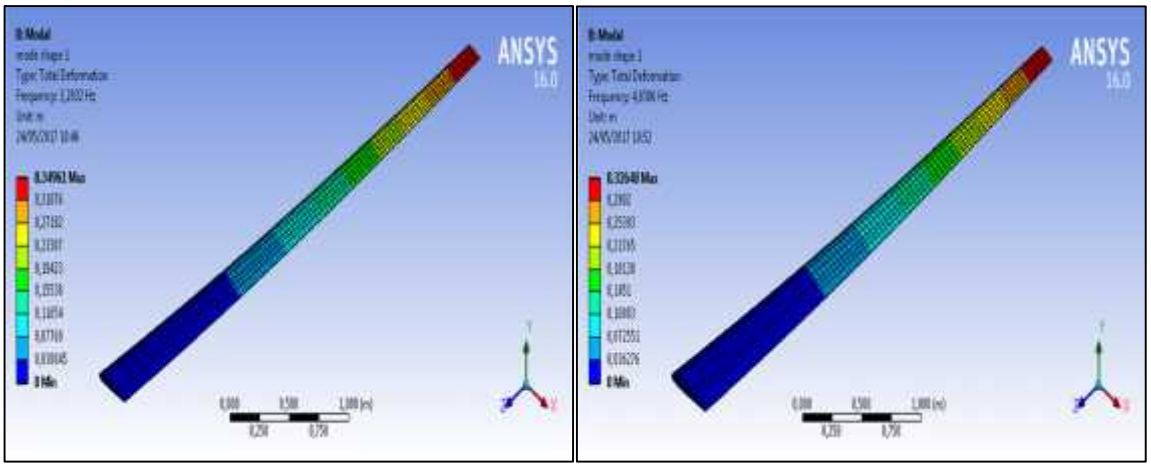

C_r =0.3m C_r =0.4m

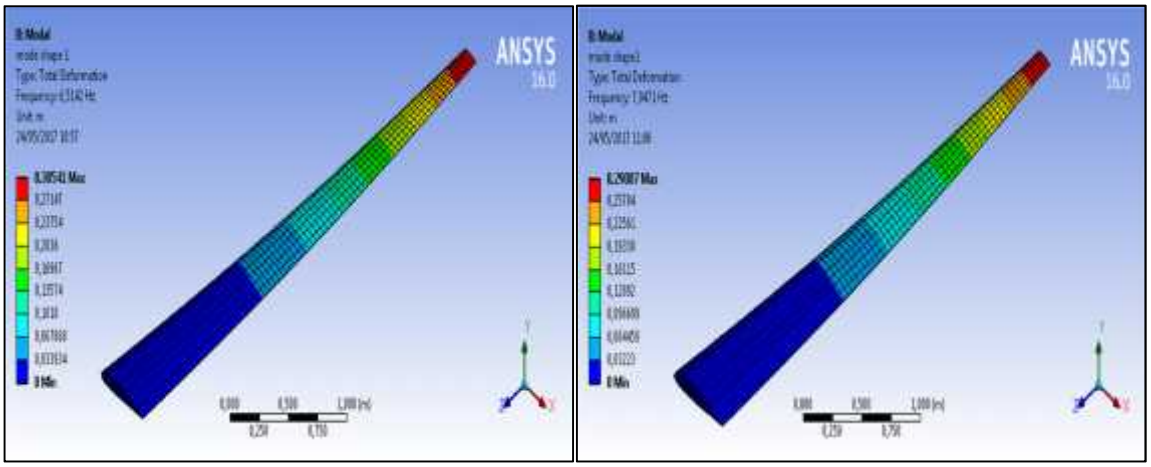

C_r =0.5m C_r =0.582m

Figure 35: First mode shape for different wing lengths (NACA4318)

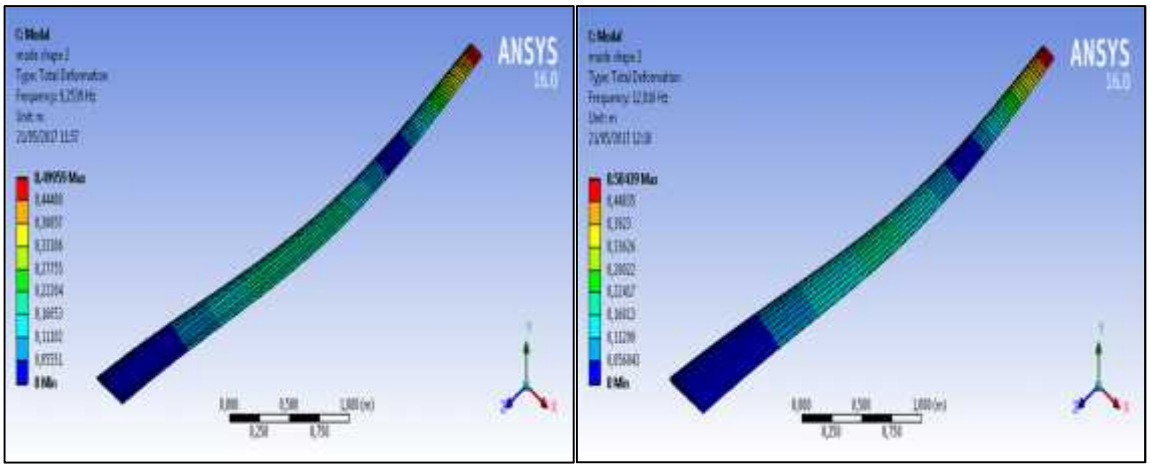

C_r =0.3m C_r =0.4m

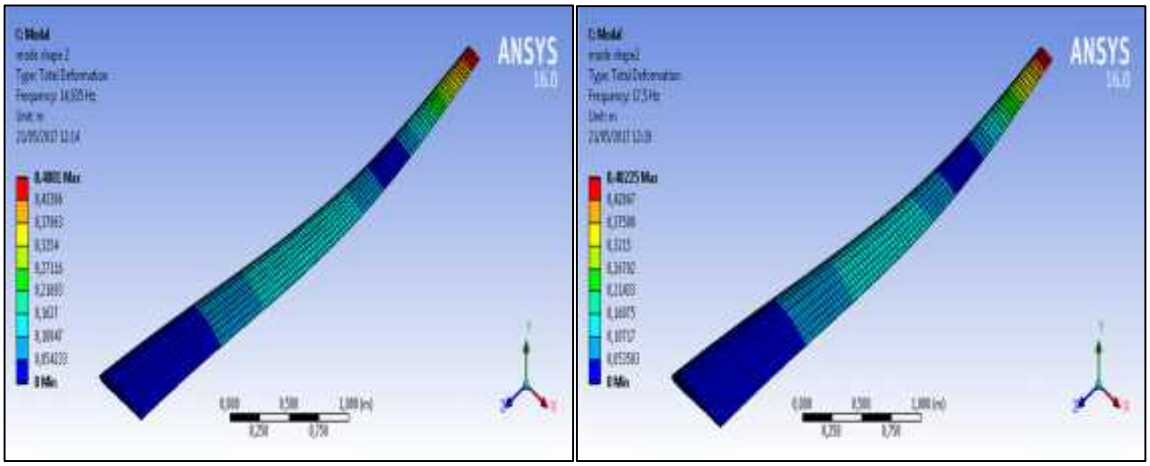

C_r =0.5m C_r =0.582m

Figure 36: Second mode shape for different wing lengths (NACA4412)

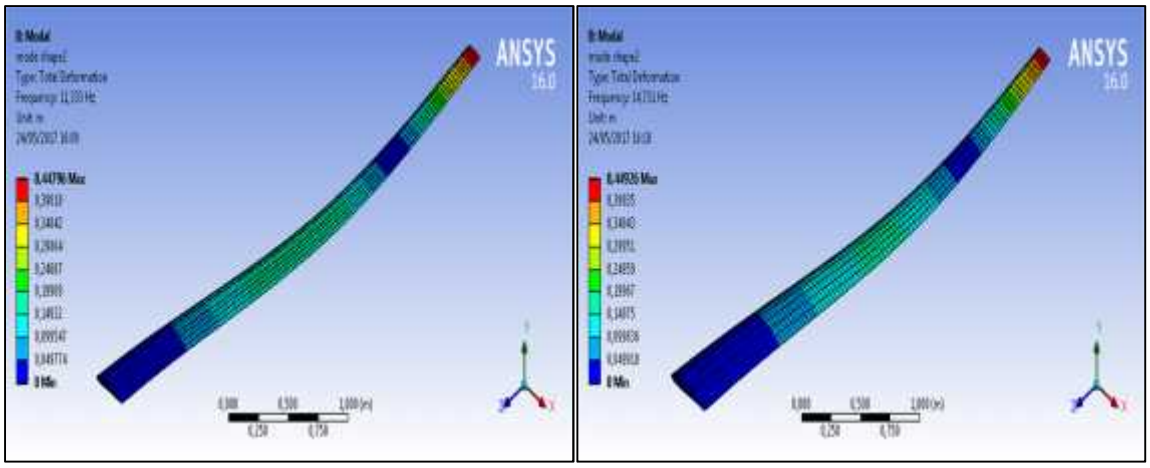

C_r =0.3m C_r =0.4m

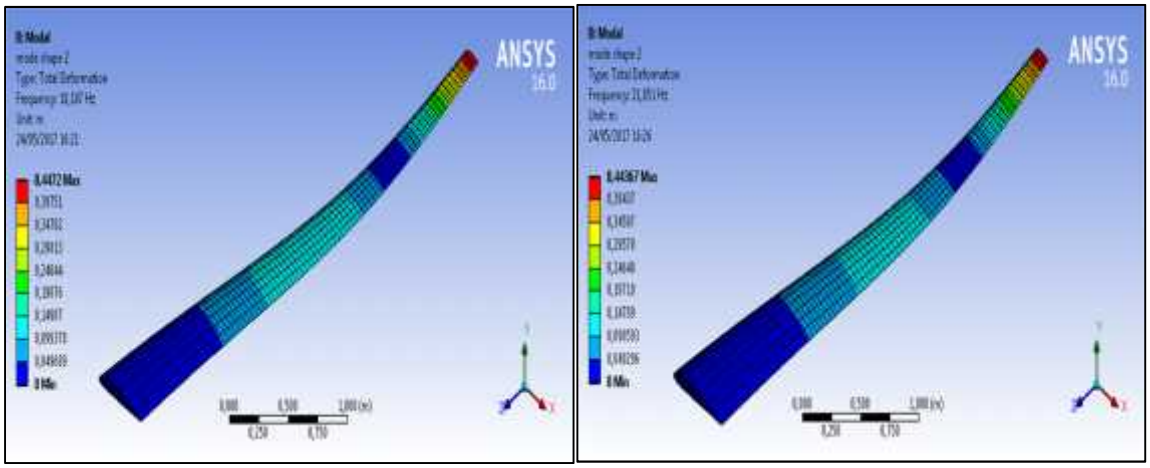

C_r =0.5m C_r =0.582m

Figure 37: Second mode shape for different wing lengths (NACA4415)

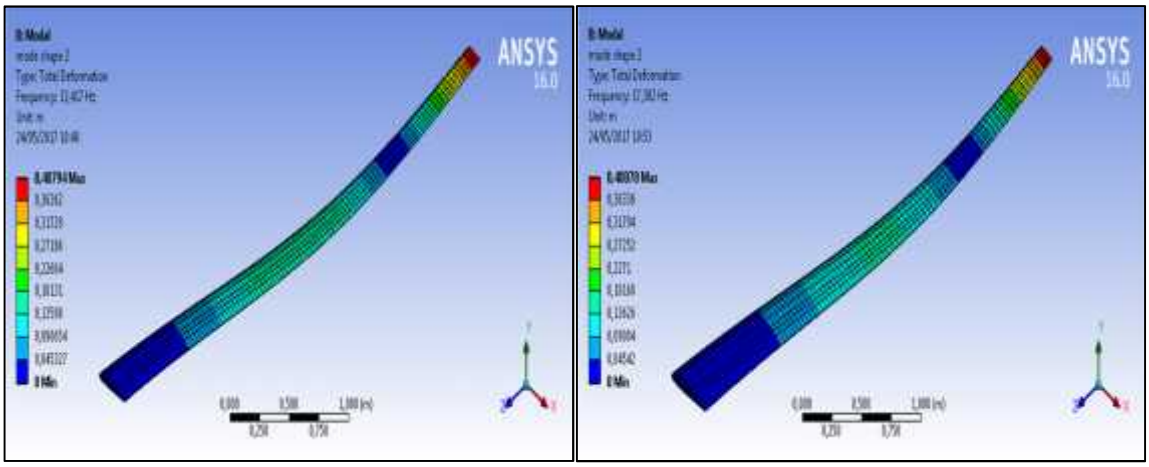

C_r =0.3m **C_r =0.4m**

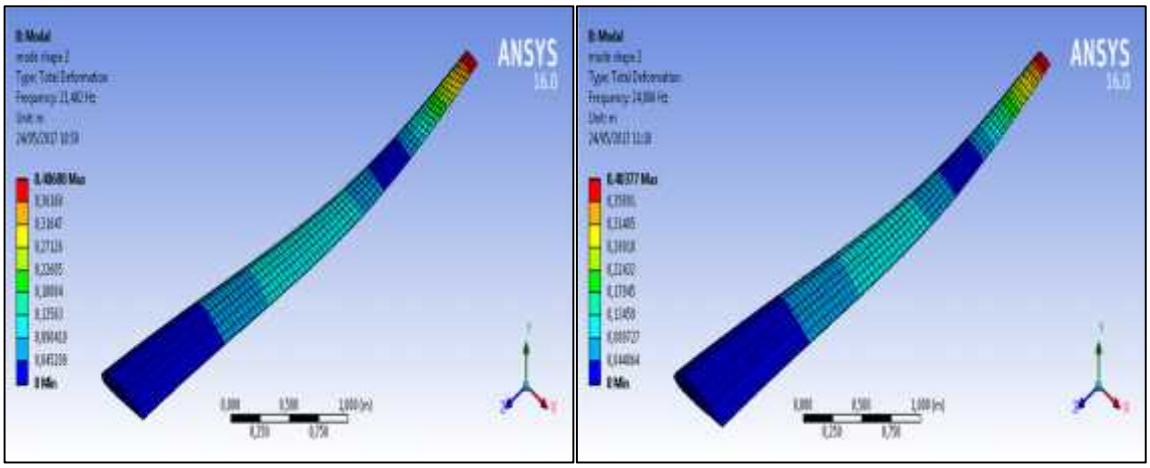

C_r =0.5m **C_r =0.582m**

Figure 38: Second mode shape for different wing lengths (NACA4318)

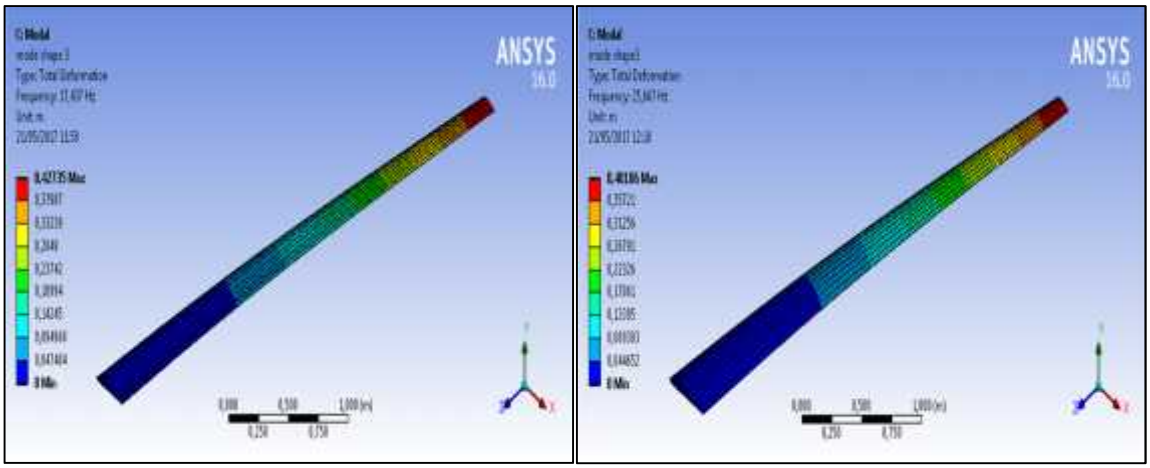

C_r =0.3m **C_r =0.4m**

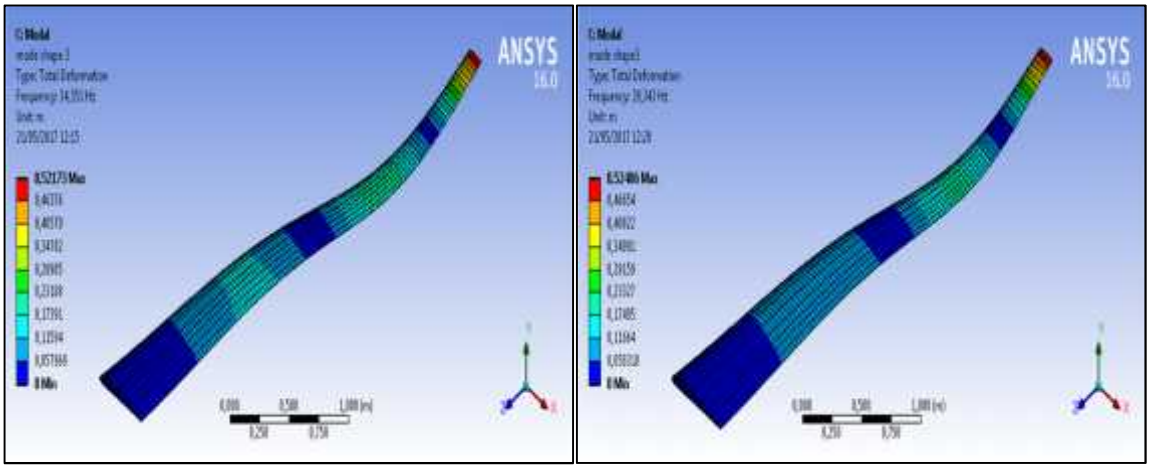

C_r =0.5m **C_r =0.582m**

Figure 39: Third mode shape for different wing length (NACA4412)

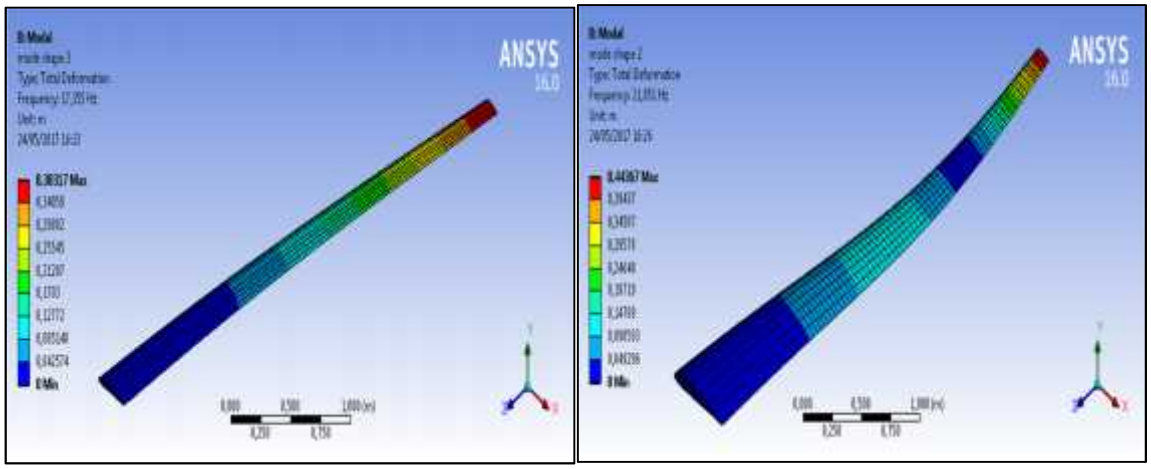

C_r =0.3m C_r =0.4m

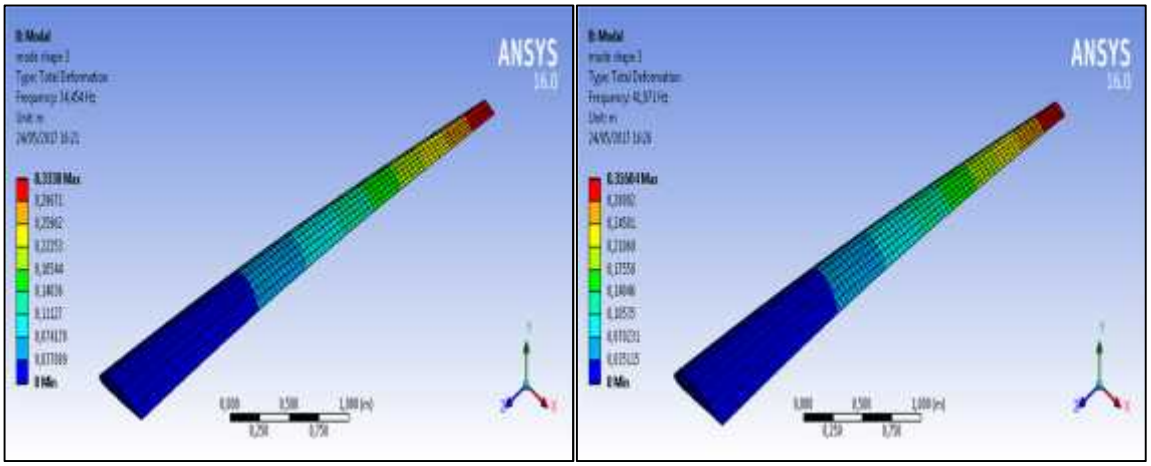

C_r =0.5m C_r =0.582m

Figure 40: Third mode shape for different wing lengths (NACA4415)

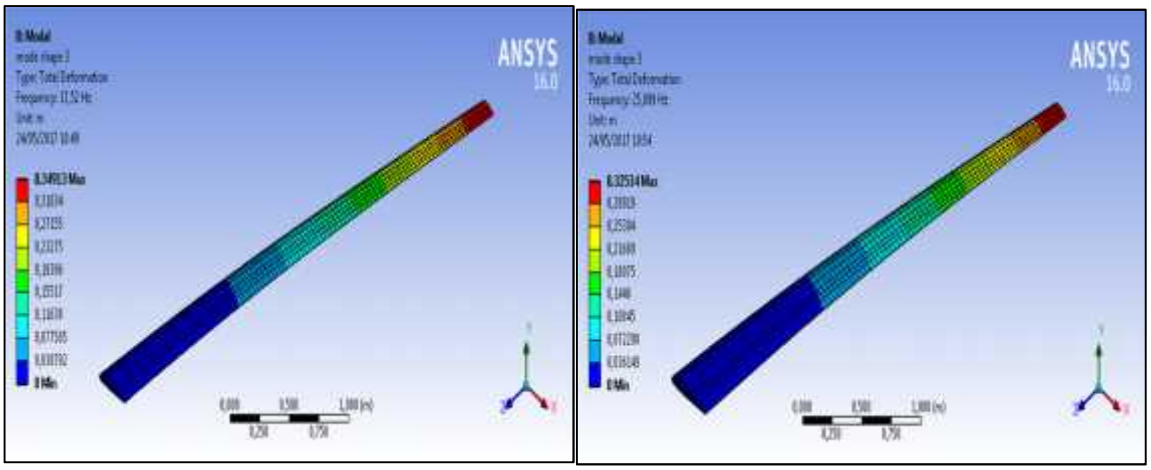

C_r =0.3m C_r =0.4m

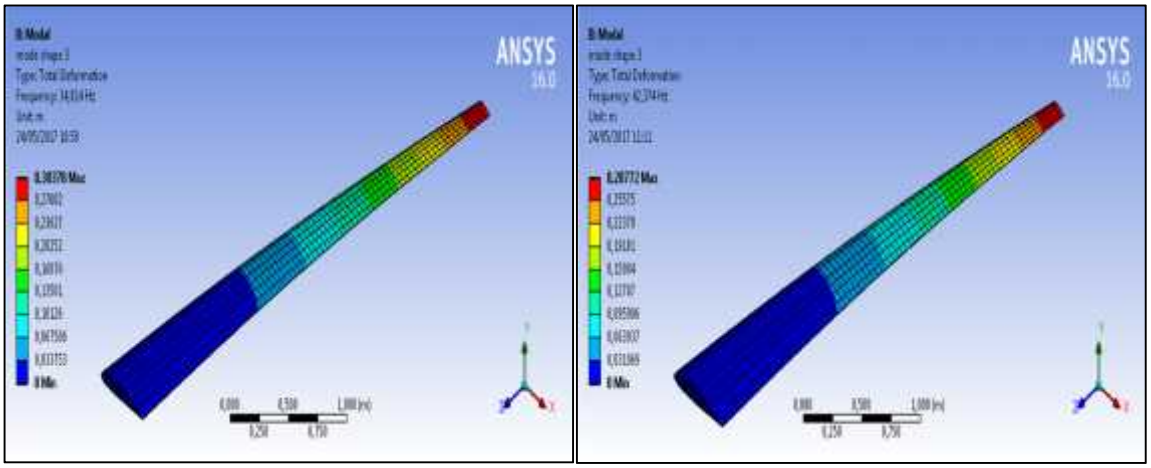

C_r =0.5m C_r =0.582m

Figure 41: Third mode shape for different wing lengths (NACA4318)

The results obtained in table 12 are plotted in **figure 42** and **43.**

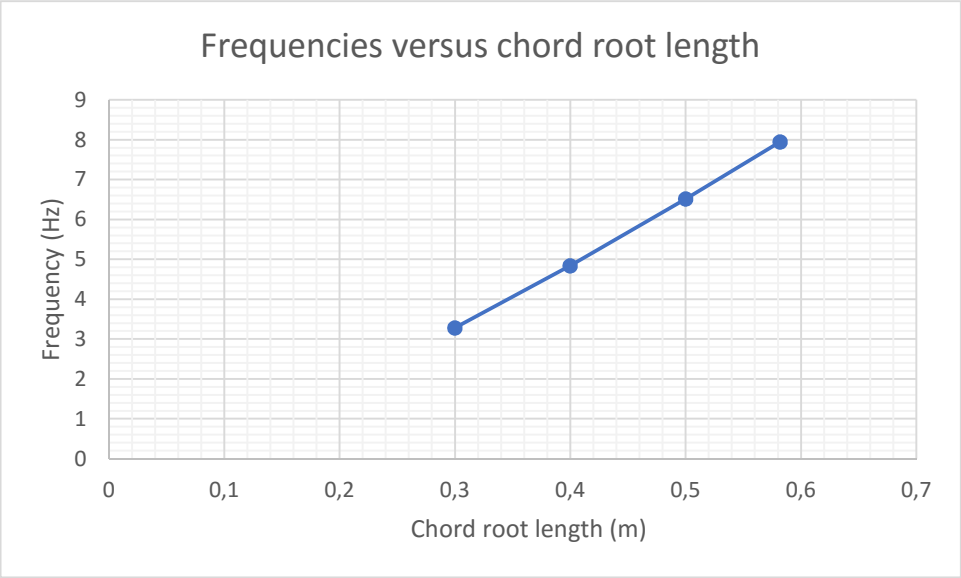

Figure 42: Variation of frequency according to the chord root length (NACA 4318) for the first mode shape

- The **figure 42** illustrates the curve of frequency according to the chord root length (NACA 4318) for the first mode shape. We observe from this figure that the frequency varies increasingly in function of the chord root length.

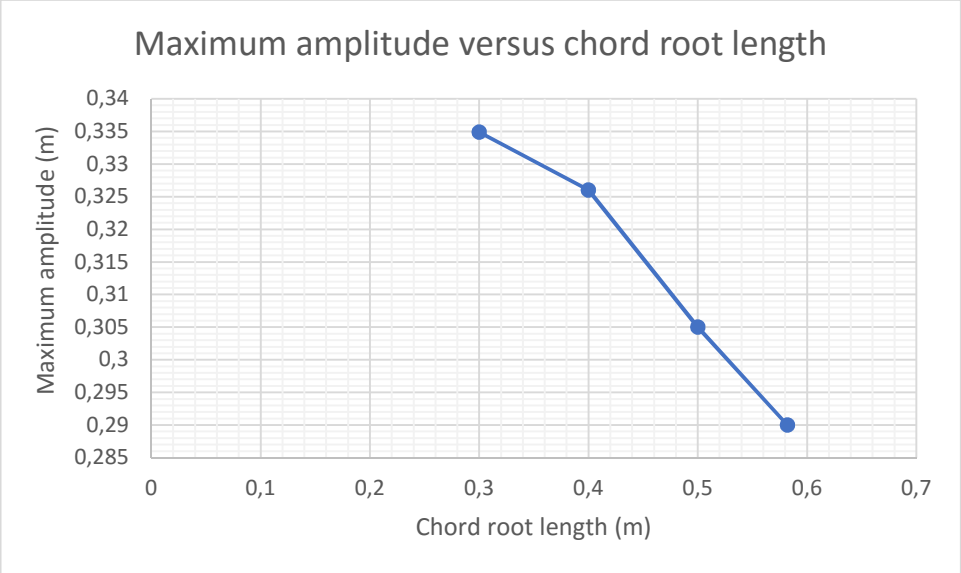

Figure 43: Maximum amplitude according to the chord root length (NACA 4318) for the first mode shape

- The **figure 43** illustrates the curve of maximum amplitude according to the chord root length (NACA 4318) for the first mode shape. We observe from this figure that the maximum amplitude varies decreasingly in function of the chord root length.

II.2.3 static structure analysis

The **tables 13, 14, 15** shows the results of static structural analysis for differentchord root lengths and for different profiles.

Chord root (m)	Maximal von-Mises Stress (Pa)	Maximal Elastic Strain	Maximal deformation (m)	Maximal Strain Energy (J)
0,3	1.008 □ 10^{8}	1.410□ 10^{-3}	0.457	0.650
0,4	5.297□ 10^{7}	7.466 □ 10^{-4}	0,209	0.397
0,5	3.902□ 10^{7}	5.502 □ 10^{-4}	0.134	0.543
0,582	4.053□ 10^{7}	5.717 □ 10^{-4}	0.126	0.813

Table 13: Results of maximalstress, strain, deformation and strain energy with different chord root lengths (NACA 4412)

Chord Root (m)	Maximal von-Mises Stress (Pa)	Maximal Elastic Strain	Maximal deformation (m)	Maximal Strain Energy (J)
0,3	4.5204□ 10^{7}	6.3668□ 10^{-4}	0.142	0.414
0,4	2.487□ 10^{7}	3.504□ 10^{-4}	0.065	0.205
0,5	1.880□ 10^{7}	2.649□ 10^{-4}	0.041	0.218
0,582	1.971□ 10^{7}	2.777□ 10^{-4}	0.040	0.476

Table14: Results of maximal stress, strain, deformation and strain energy with different chord root lengths (NACA 4318)

Chord Root (m)	Forces (N)	Maximal Elastic Strain	Maximal StrainEnergy (J)	Maximal deformation (m)	Maximal von-Mises Stress (Pa)
0,3	F_x =77.13 F_y =1786.785	9.77□ 10^{-4}	0.597	0.239	6.928□ 10^{7}
0,4	F_x =128.21 F_y =2336.24	5.355□ 10^{-4}	0.364	0.109	3.802□ 10^{7}
0,5	F_x =177.11 F_y =3402.726	3.733□ 10^{-4}	0.301	0.069	2.650□ 10^{7}
0,582	F_x =241.64 F_y =5823.02	4.113□ 10^{-4}	0.437	0.067	2.902□ 10^{7}

Table15: Result of stress, strain, maximal deformation and strain energy with different chord root lengths(NACA4415)

The results of maximal deformation for the three profiles and for different chord rootlengths shown in **tables 13, 14, 15** areplotted in **figure 44.**

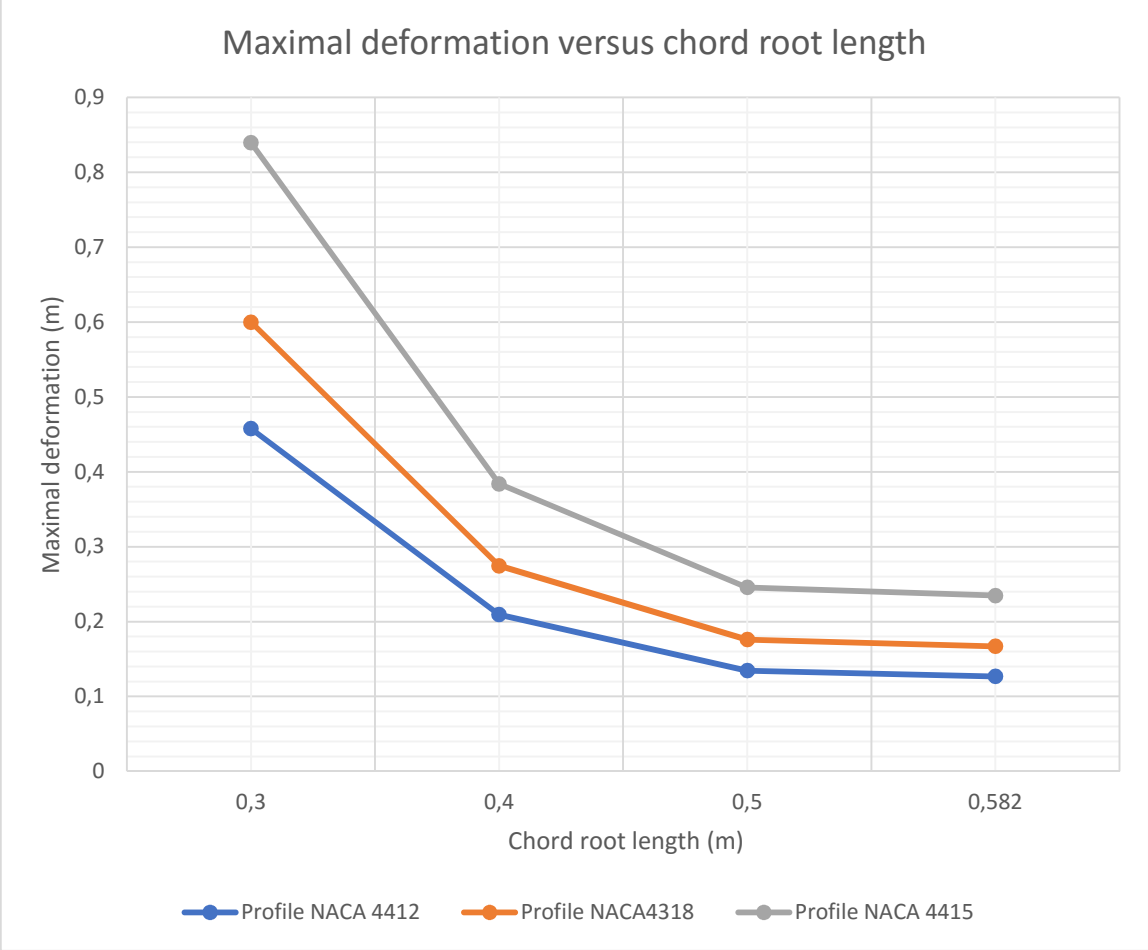

Figure 44: Maximal deformation according to the chord root length.

- The **figure 44**represents the curves of maximal deformation according to the chord root length, we observe that there is an inverse relationship between the maximal deformation and the chord root length.
  We observe also that when the chord root length increases the maximal deformation decreases.

After the different simulations, we have got the maximal deformation, equivalent elastic strain,Von-Mises stressand the strain energy for different chord root lengths, which are depicted below.

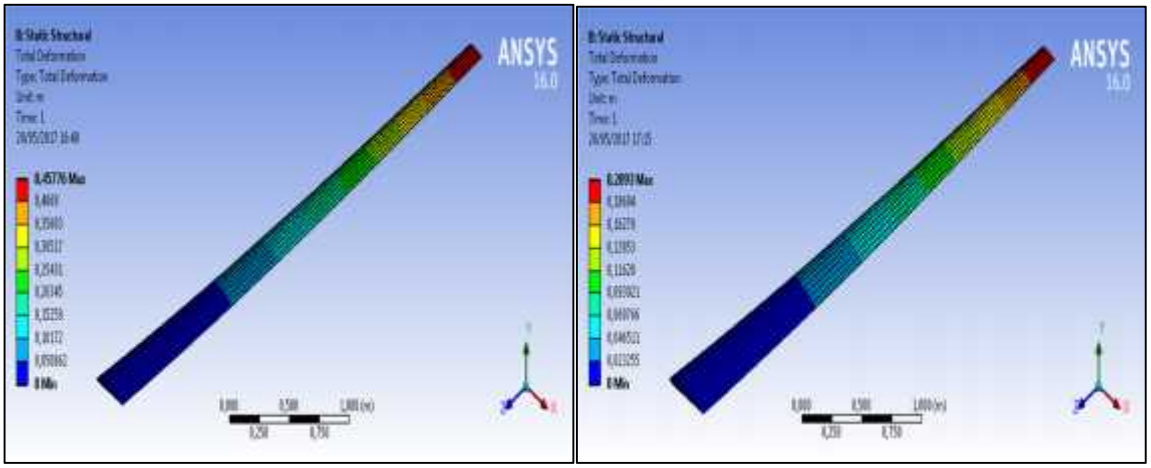

$C_r = 0.3$ $C_r = 0.4$

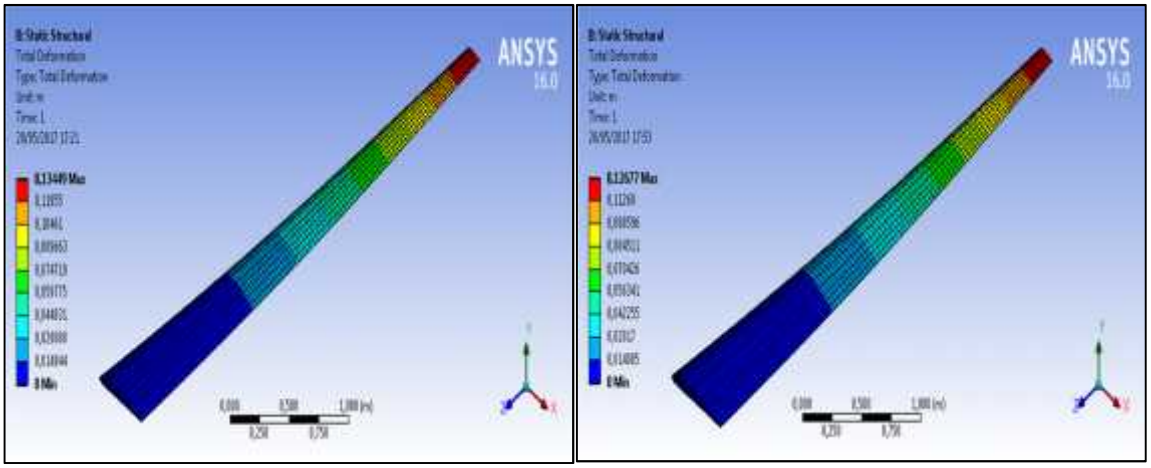

$C_r = 0.5$ $C_r = 0.5$

Figure 45: Total deformationfor different chord root lengths (NACA4412)

- The **figure 43** shows the total deformation for different chord root lengths of the NACA 4412 profile. We observe from this figure that the maximal deformation is located on the free end (red color). We also observe that for the fixed end its deformation is zero (blue color).

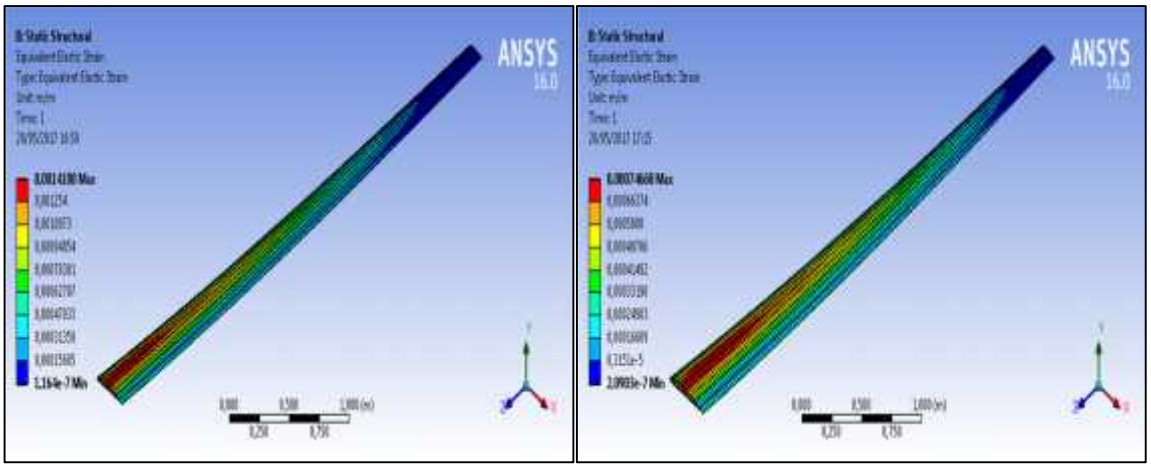

$C_r = 0.3$ $C_r = 0.4$

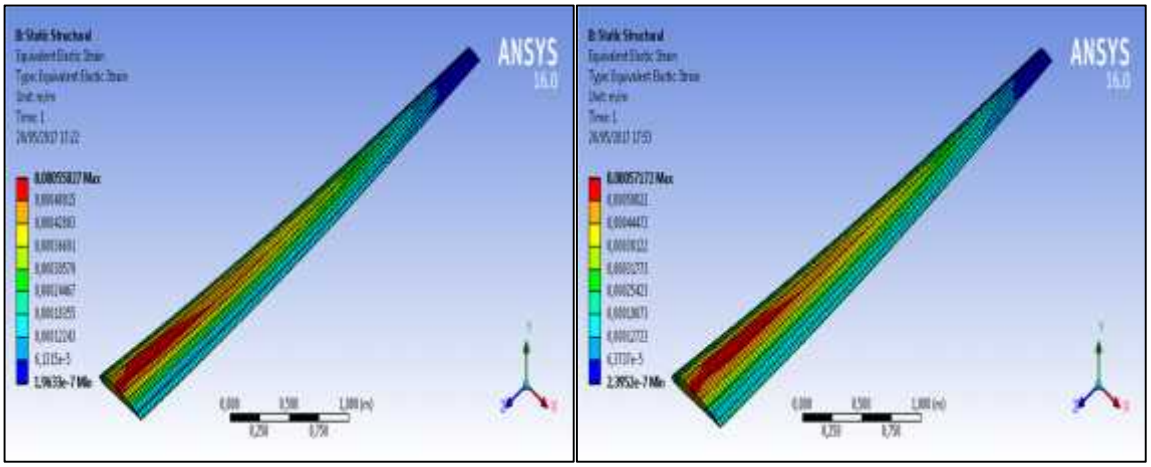

$C_r = 0.3$ $C_r = 0.4$

Figure 46: Equivalent elastic strain for different chord root lengths (NACA4412)

- The **figure 46** shows the equivalent elastic strain for different chord root lengths of the NACA 4412 profile. We observe from this figure that the elastic strain is located on the fixed end (red color) for the different wing lengths. We also observe that for the free end its elastic strain is zero (blue color).

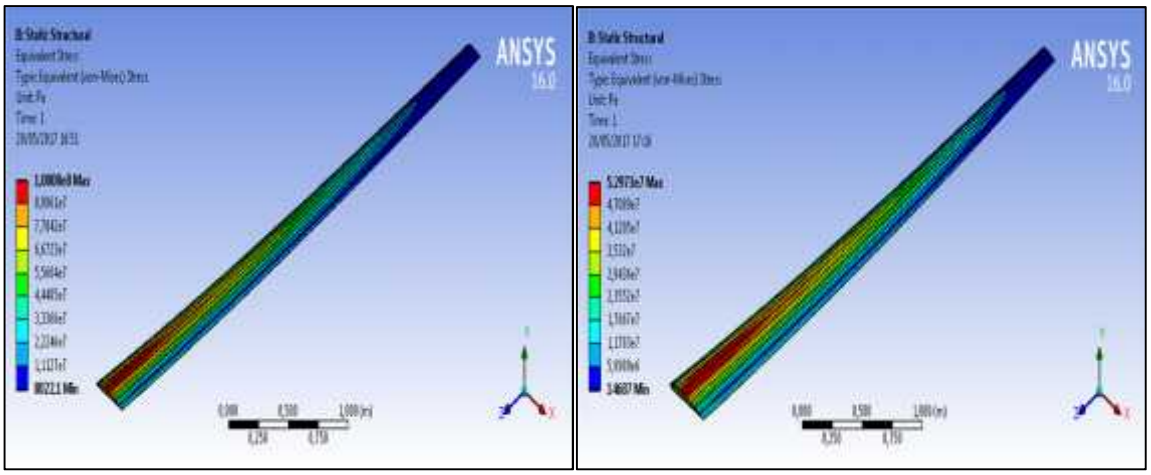

$C_r = 0.3$ $C_r = 0.4$

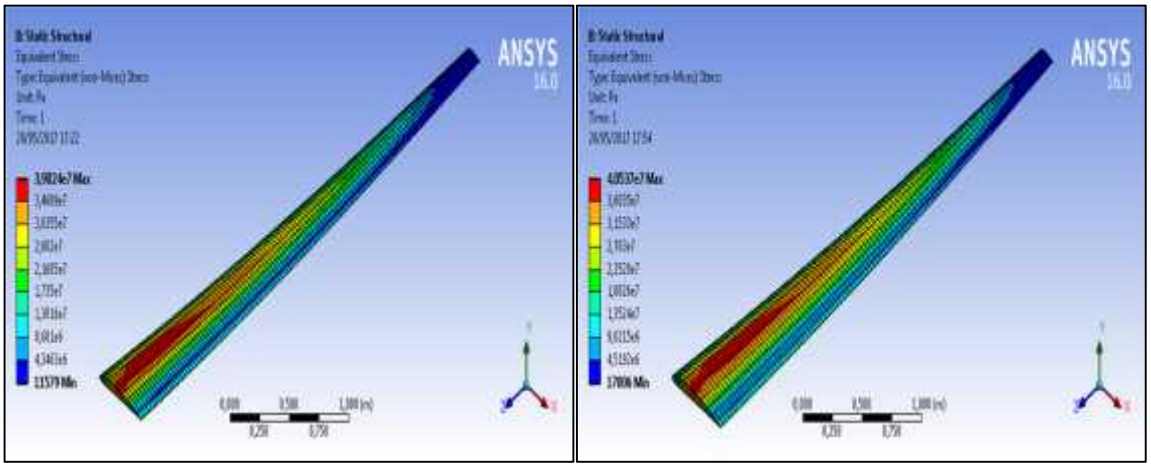

$C_r = 0.3$ $C_r = 0.4$

Figure 47: Equivalent Von-Mises stressfor different chord root lengths (NACA4412)

- The **figure 47** shows the equivalent Von-Mises stress for different chord root lengths with NACA 4412 profile. We observe from this figure that the maximal Von-Mises stress located on the fixed extremity (red color) for different chord root lengths. We also observe that for the free surface its Von-Mises stress is null (blue color).

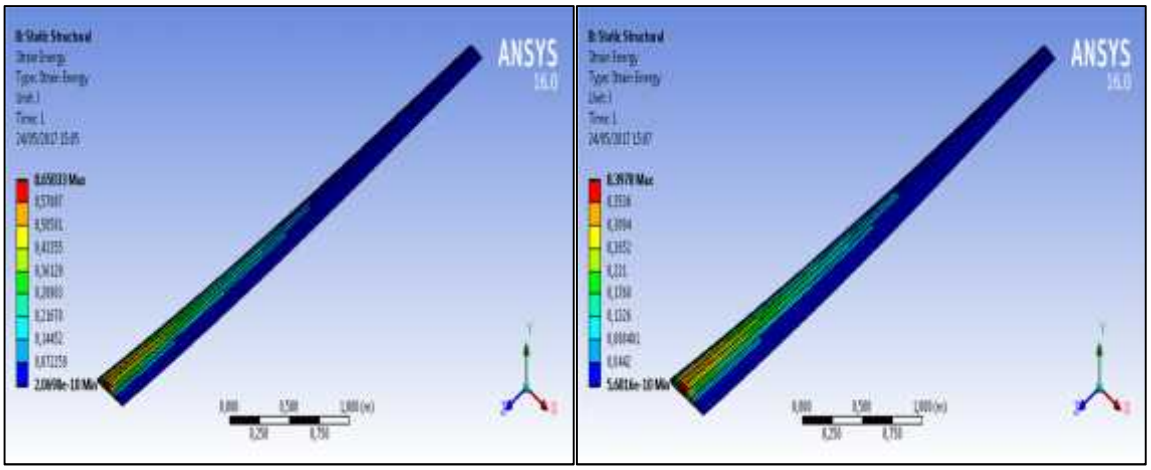

$C_r = 0.3$ $C_r = 0.4$

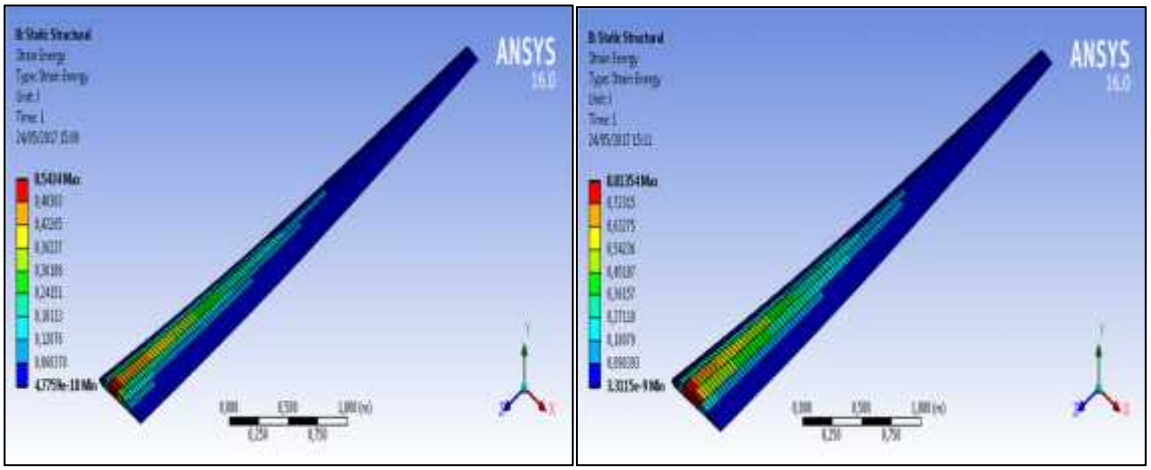

$C_r = 0.3$. $C_r = 0.5$

Figure 48: Strain energyfor different chord root lengths (NACA4412)

- The **figure 48**shows the strain energy for different chord root lengths of the NACA 4412. We observe from this figure that the maximal strain energy is located on the fixed end (red color) and for the free end it is zero (blue color)

From these results, we note that the high lift and the low drag are obtained for different length value. The lift is maximal for chord root of 0.582m. But the drag is minimal for a chord root of 0.3m.

Concerning the total deformation, it's minimal value achieved for chord root of 0.582m and for the minimal Von-Mises stress is achieved for chord root of 0.5m.

We conclude that there is note an only value which satisfies the two constraints then we must make a compromise to have the best characteristics.

II.3Effect of the camber

In this step, we will see theeffect of the camber for three different profiles used in our study which are the NACA 4412, NACA 4318 and NACA 4415 with the same wing length (L=3m) and the same chord (C_r = 0.582m and C_t = 0.14m)

According to the results we have found in the preceding steps, we drawgraph of the frequencies, maximum amplitude, maximum deformation, Von-Mises stress and strain in function of the different profiles used in our study for constant wing length in the first step and with constant chord root in the second step

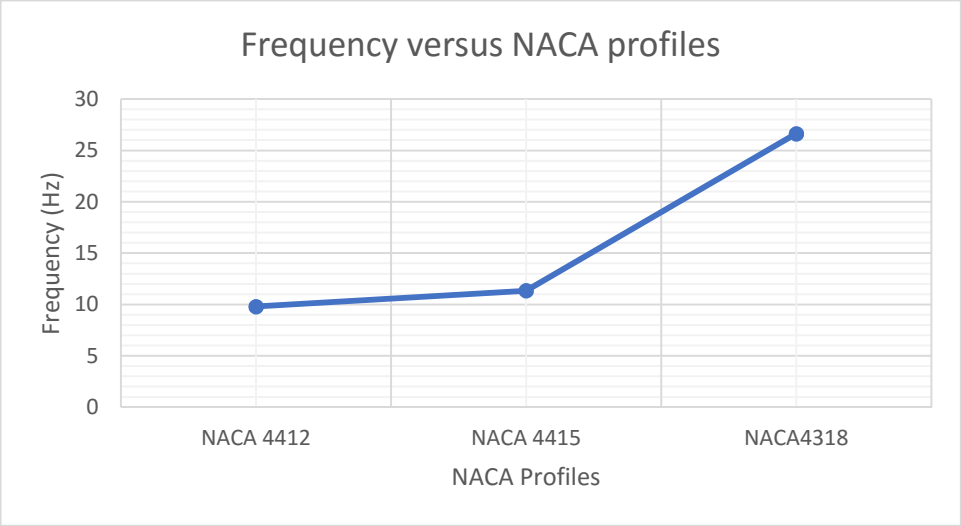

Figure 49: Variation of frequency of the first mode shape according to different profiles(L=3m)

- The **figure 49** illustrates the curve of variation of frequency according to different profile for the same wing length (L=3m). We observe from this figure that the frequency varies increasingly in function of the NACA profiles.

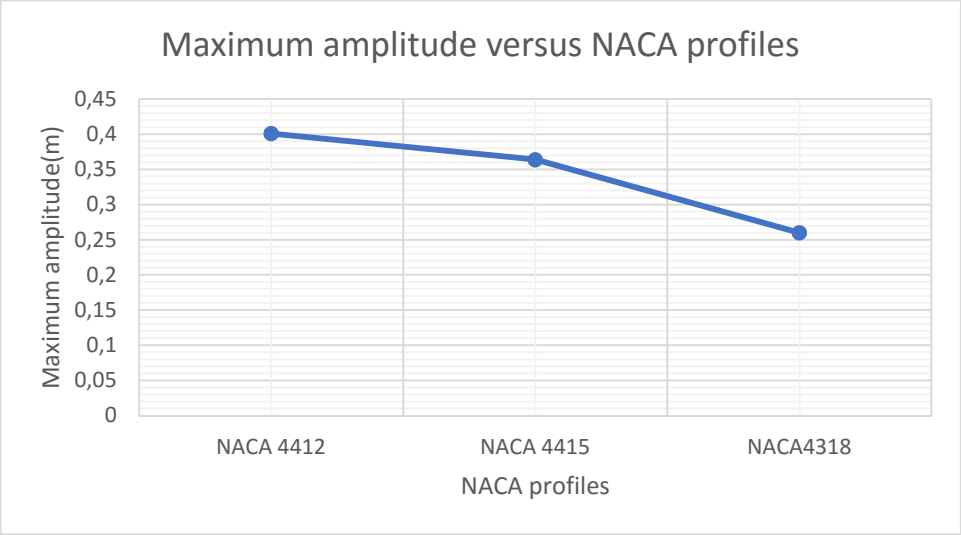

Figure 50: Maximum amplitude of the first mode shape according to different profiles(L=3m)

- The **figure 50** illustrates the curve of maximum amplitude according to NACA profilesfor the same wing length (L=3m). We can see from this figure that the maximum amplitude varies

decreasingly in function of the NACA profiles, we also see that the maximum amplitude of the first mode shape for NACA 4318 is less than the other profiles

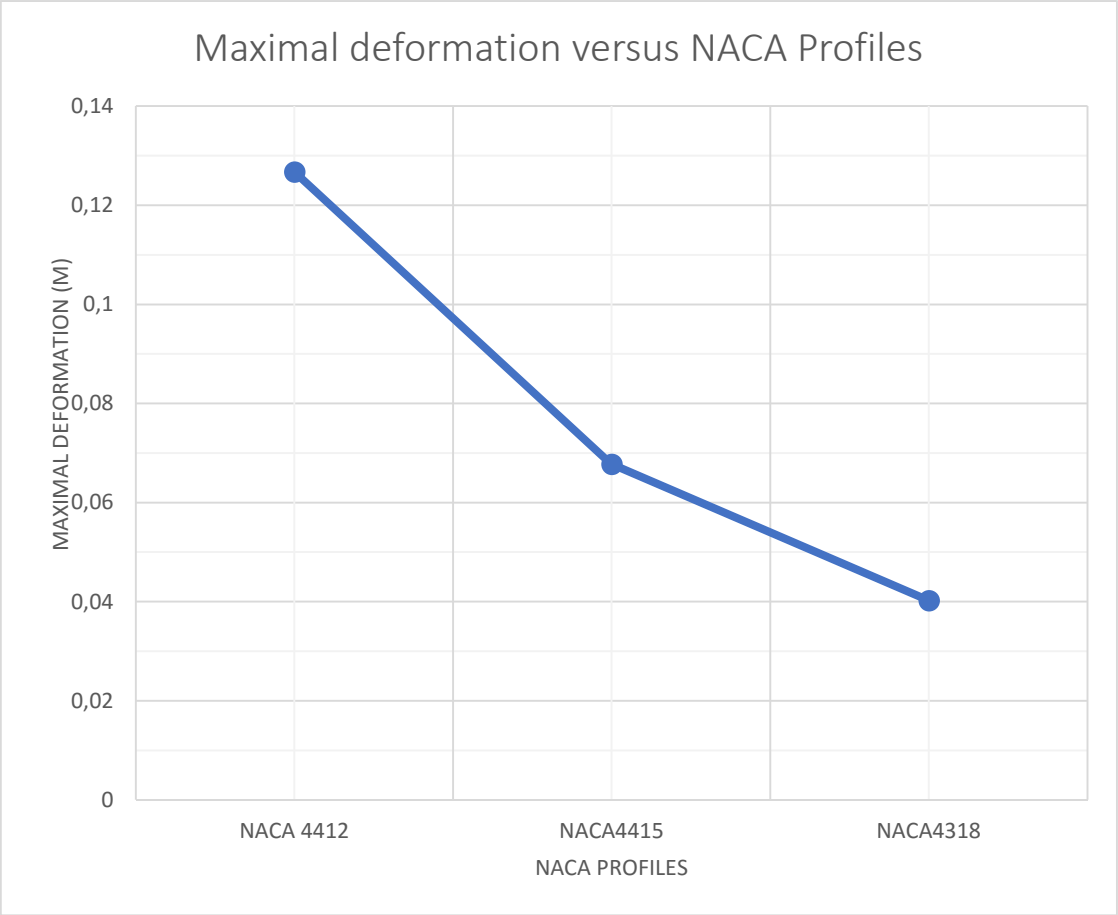

Figure 51: Maximal deformation according to the different profiles

- The **figure 51** illustrates the curve of maximal deformation according to the NACA profiles for the same wing length (L=3m). We observe that the maximal deformation of the wing with profile NACA 4318 is lesser than the NACA 4415 and NACA4412.

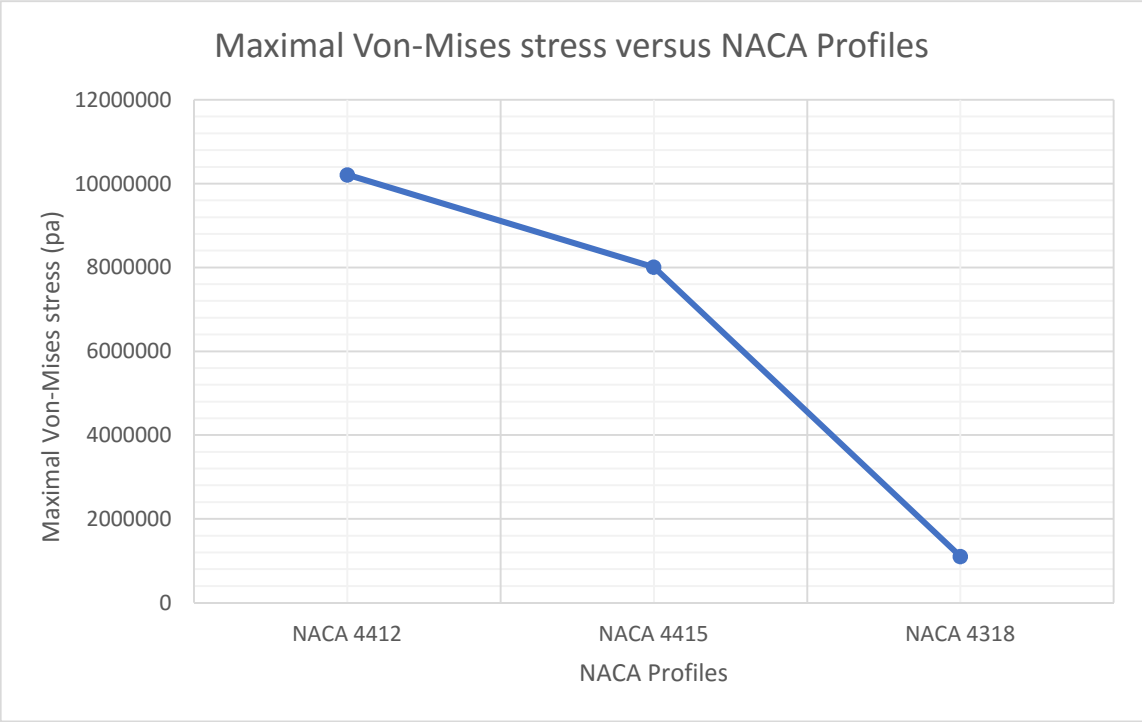

Figure 52: Maximal von-Mises stressaccording to the different profiles

- The **figure 52** illustratethe curve of maximal Von-Mises stress according to different NACA profiles which are used in our simulation and for constant wing length (L=3m).
  We observe from this curve that the maximal stress Von-Mises varies decreasingly in function of the profile shape and that the maximal Von-Mises stress of NACA 4412is higherthan the other profiles.

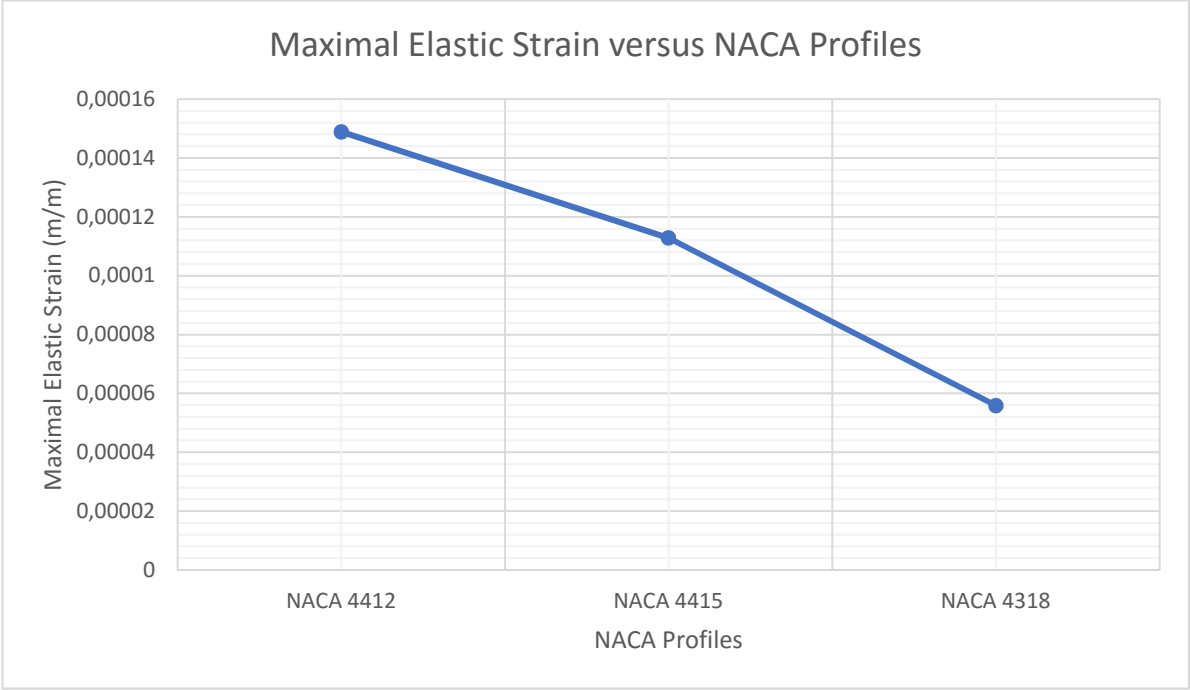

Figure 53: Maximal elastic strain according to different profiles

- The **figure 53** illustrates the curve of maximal elastic strain according to different profiles for constant wing length (L=3m). We notice that the maximal elastic strain varies also decreasingly in function of the profile shape and that the maximal elastic strain for NACA 4412 is higher than the other profiles.

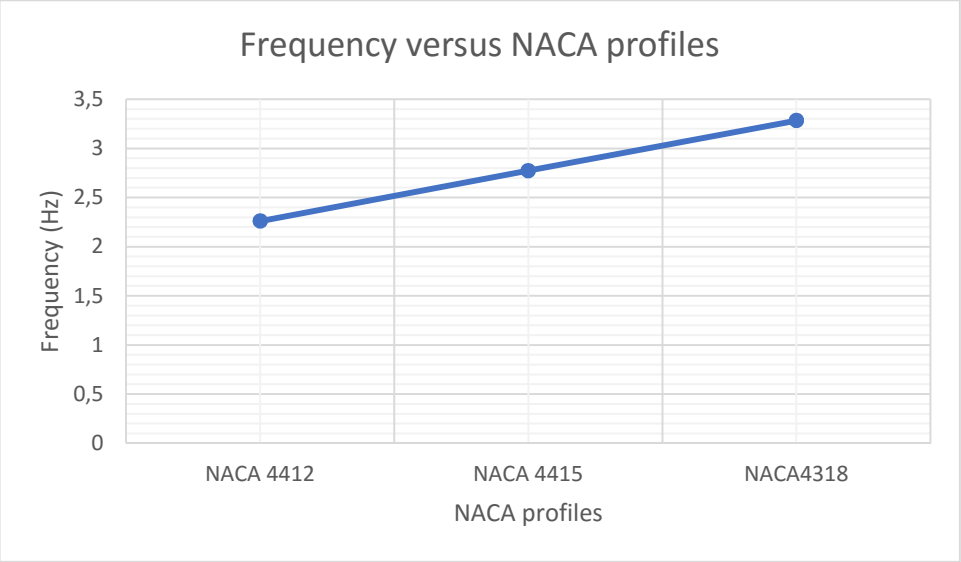

Figure 54: Variation of frequency of the first mode shape according to the NACA profiles (C_{root}=0.3m).

- The **figure 54** illustrates the curve of frequency of first mode shape according to the NACA profiles for (C_{root}=0.3m). We observe from this figure that the frequency of the first mode shape vary increasingly in function of the NACA profiles.

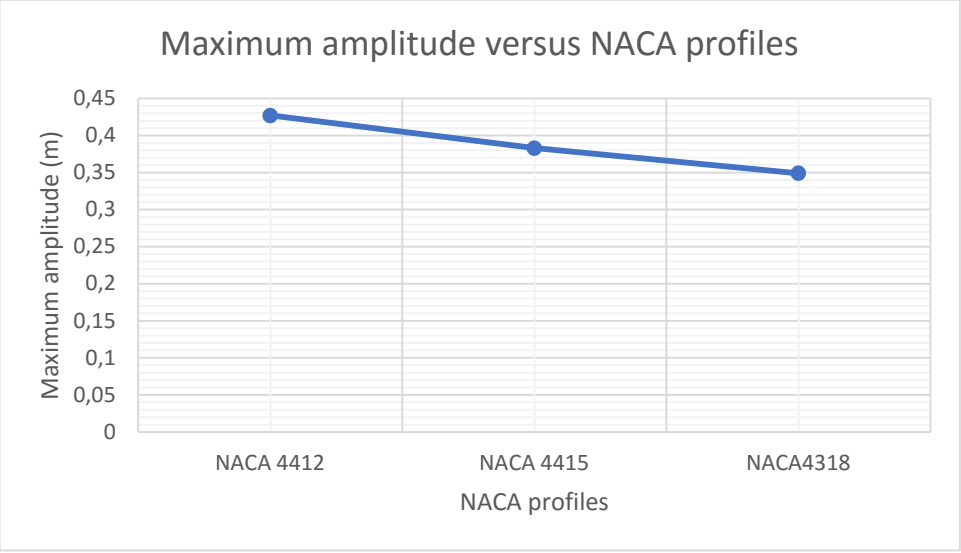

Figure 55: Maximum amplitude of the first mode shape according to the NACA profiles (C_{root}=0.3m).

- The**figure 55**illustrates the curve of maximum amplitude of the first mode shape according to the NACA profiles for constant chord root length (C_{root}=0.3m). We observe from this figure that the maximum amplitude varies decreasingly in function of the NACA profiles. We observe also that the maximum amplitude for the NACA 4318 is lesser than the other profiles

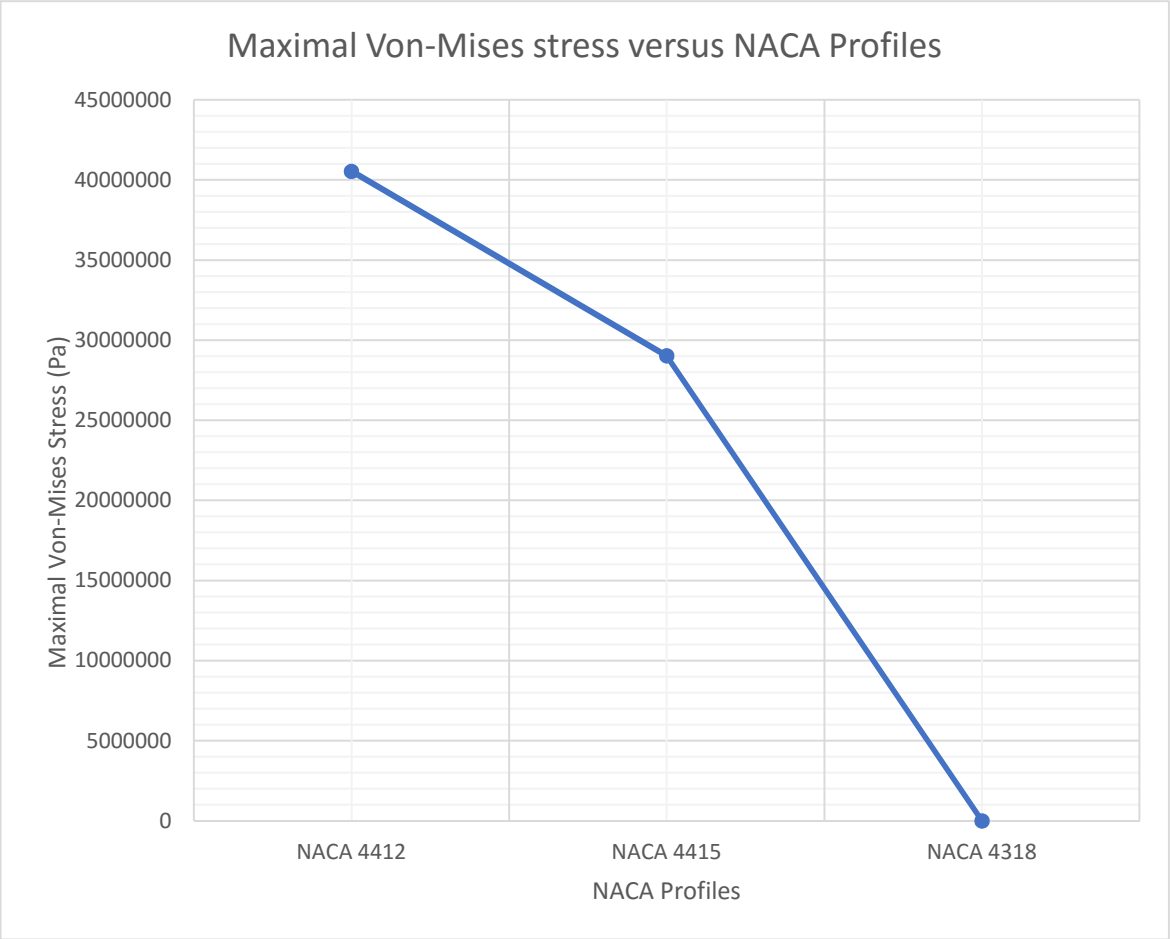

Figure 56: Maximal Von-Mises stress according to the different profiles

- The**figure 56**represents the curve ofmaximal Von-Mises stress according to the different NACA profiles for constant chord root length (C_{root}=0.3m). We can see from this curve that Von-Mises stress varies also decreasingly in function of the profile shape and that the maximal Von-Mises stress for NACA 4412 is higher than the other profiles.

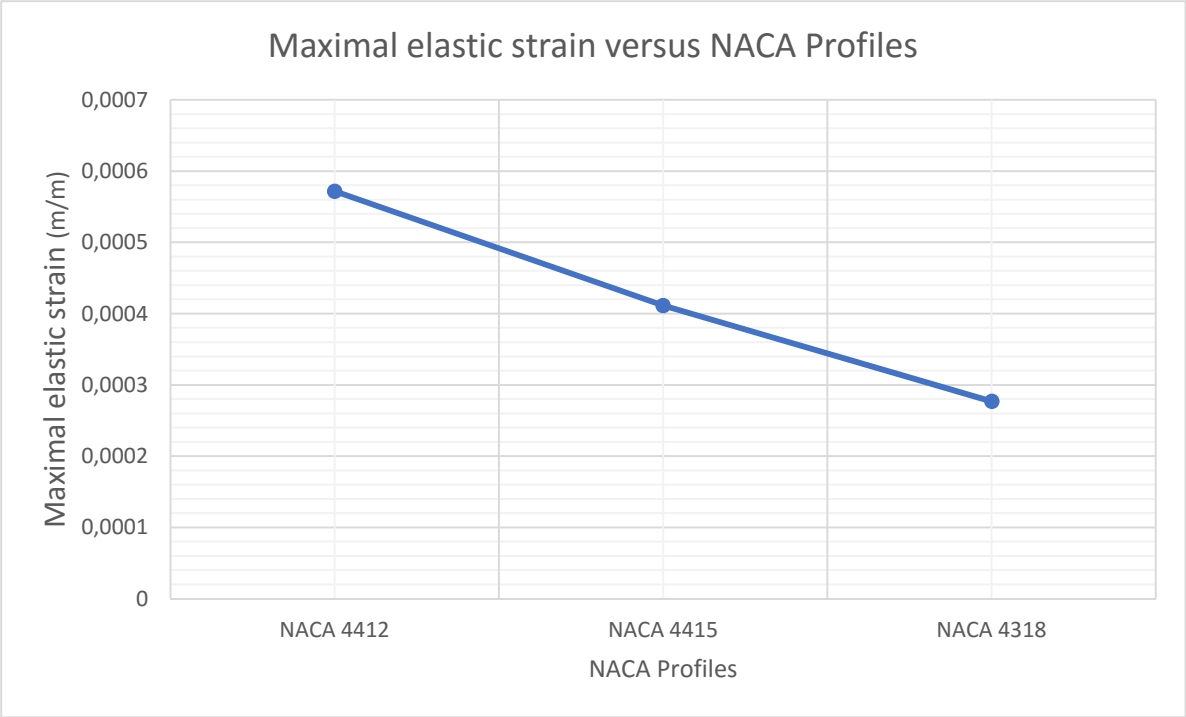

Figure 57: Maximal elastic strain according to the different profiles

- The **figure 57**illustrates the curve of maximal elastic strain according to the different profiles for constant chord length (C_{root}=0.3m). We can see that the elastic strain varies decreasingly in function of the profile shape. So, when the camber of the profile increases the elastic strain decrease and the absolute value of maximal elastic strain for NACA 4412 is higher than the other profiles.

After the different simulations, we have got the total deformation, equivalent elastic strain, equivalent Von-Mises stress and strain Energy for the profiles NACA 4412, NACA4415and NACA 4318 which are depicted below.

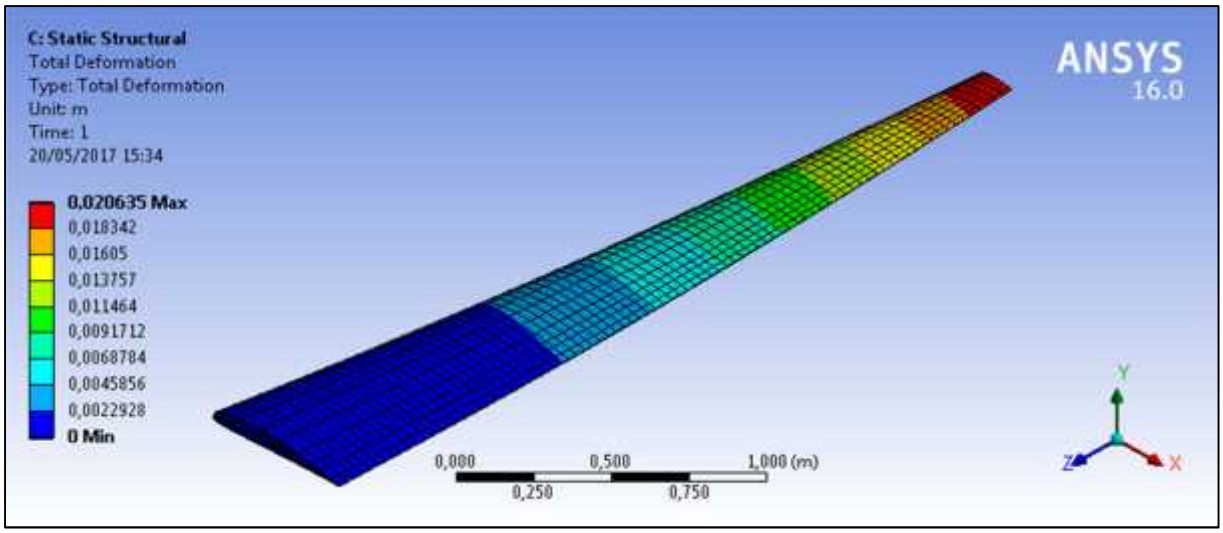

Figure 58: Total deformation L=3 (NACA 4412)

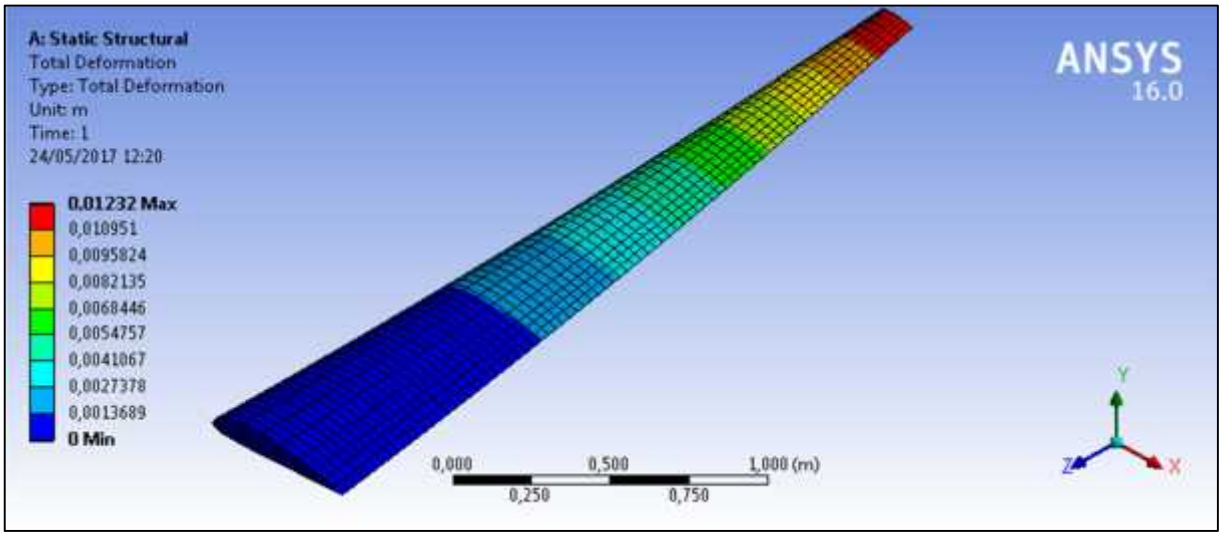

Figure 59: Total deformation for L=3m (NACA 4415)

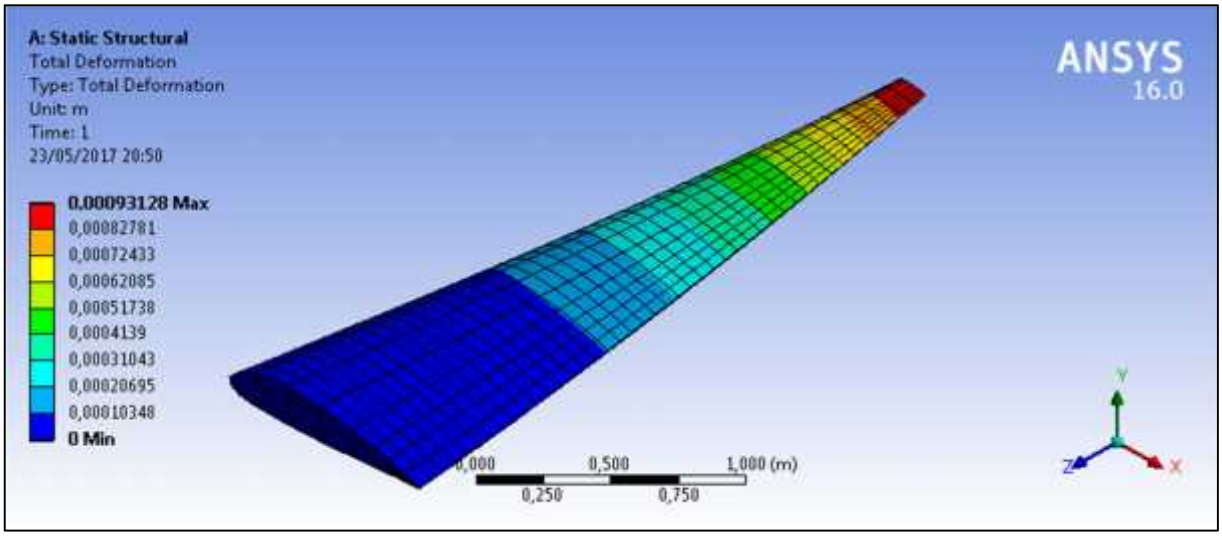

Figure 60: Total deformation for L=3m(NACA 4318)

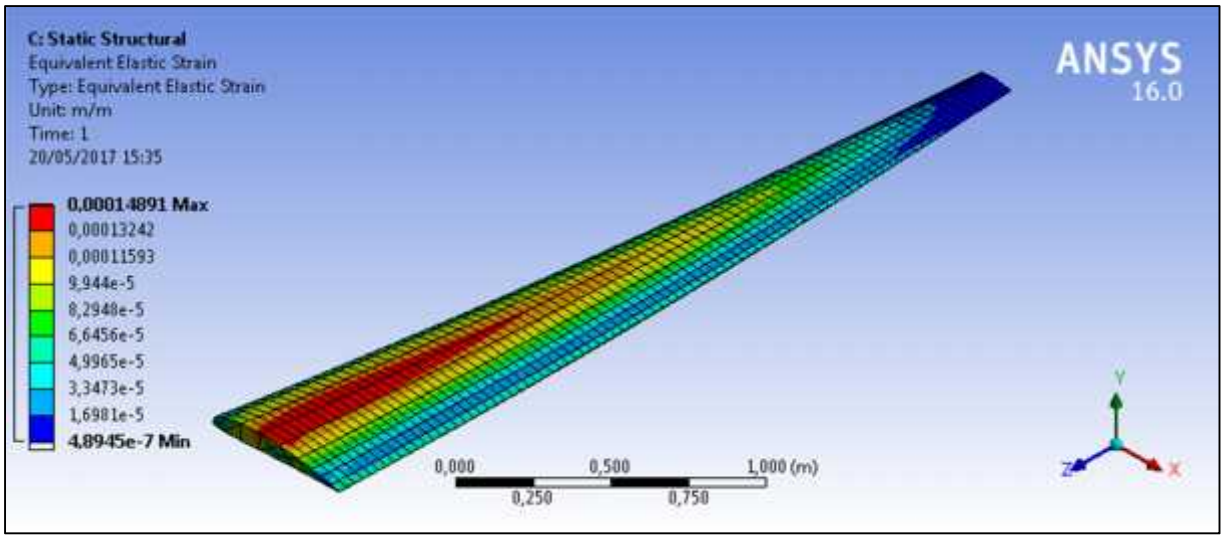

Figure61: Equivalent elastic strain L=3m(NACA 4412)

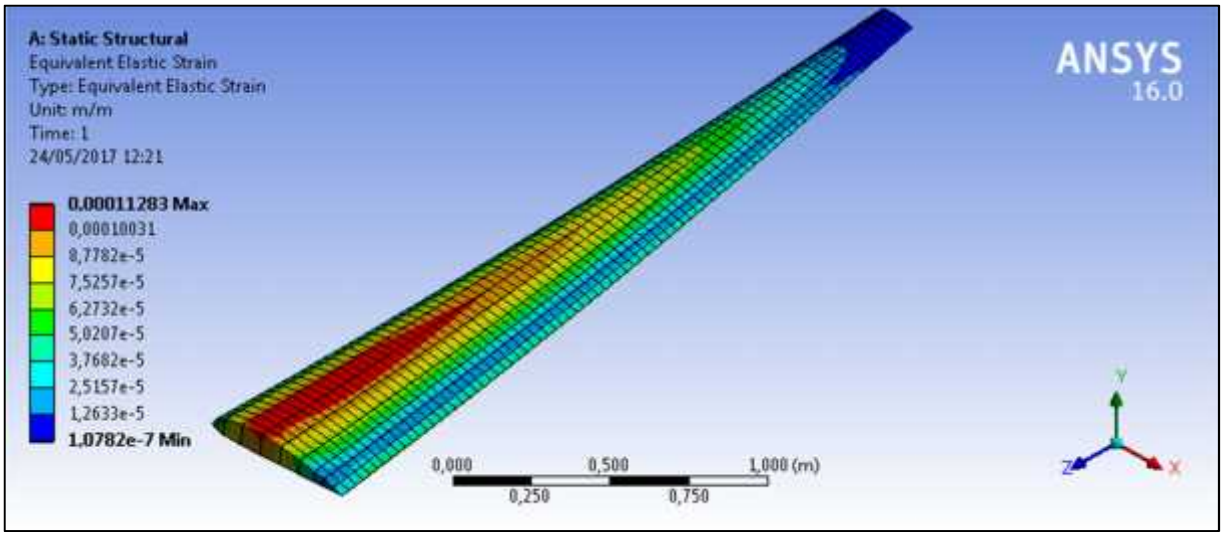

Figure 62: Equivalent elastic strain for L=3m (NACA 4415)

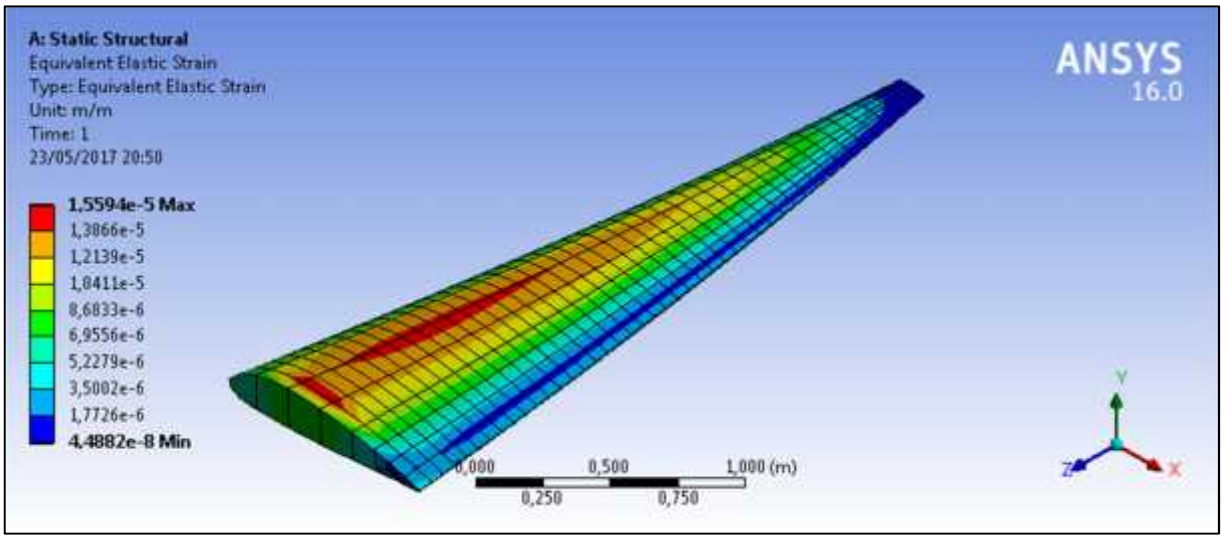

Figure63: Equivalent elastic strain for L=3m (NACA 4318)

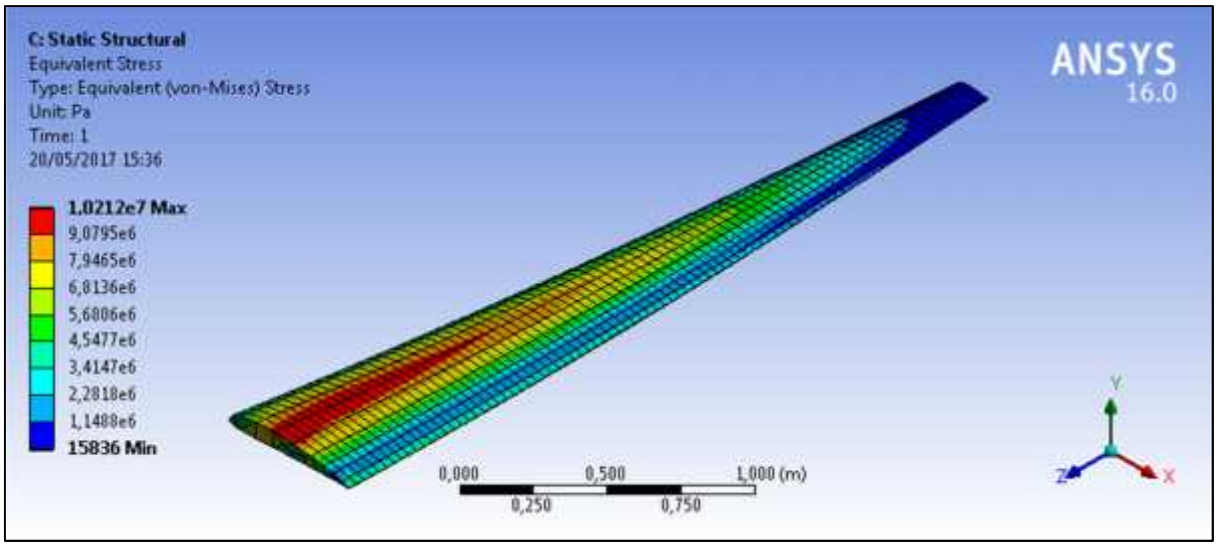

Figure 64: Equivalent von-Mises stress for L=3m (NACA 4412)

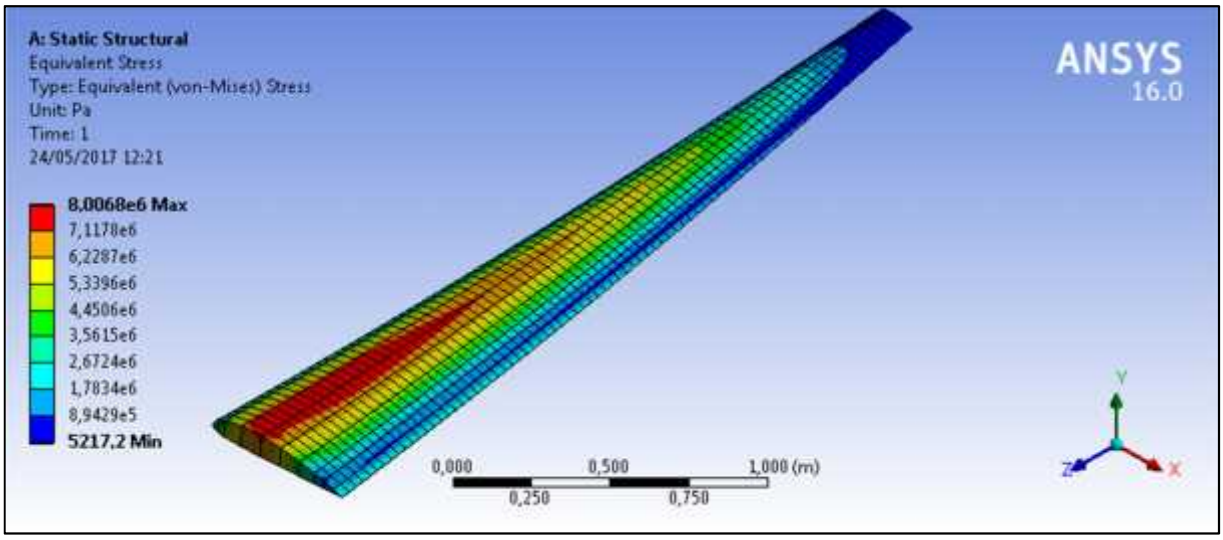

Figure 65: Equivalent von-Mises stress for L=3m (NACA 4415)

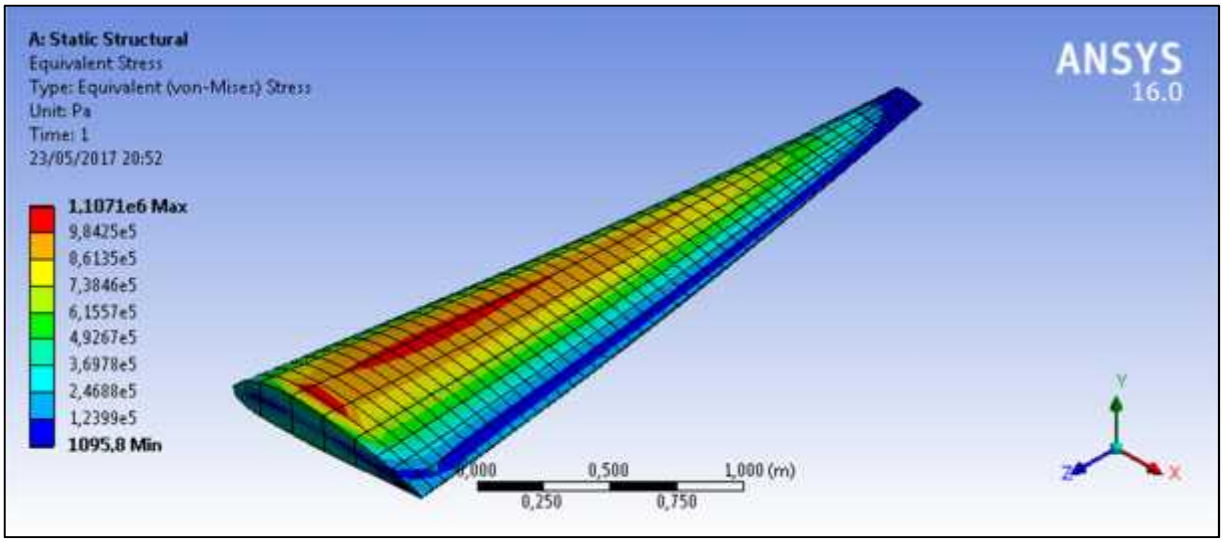

Figure 66: Equivalent von-Mises stress for L=3m (NACA 4318)

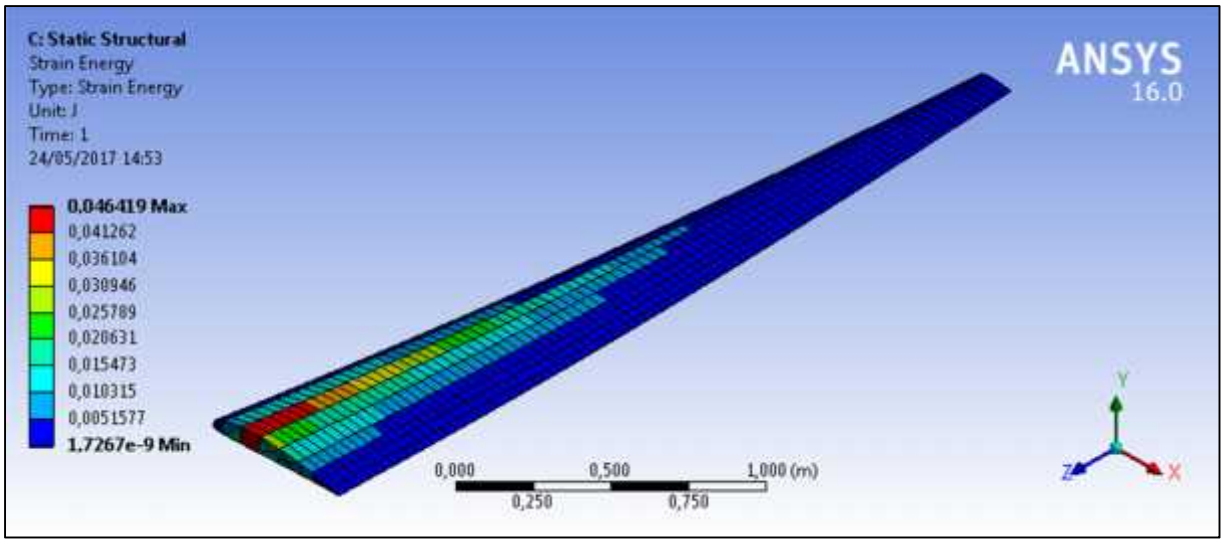

Figure 67: Strain energy for L=3m (NACA 4412)

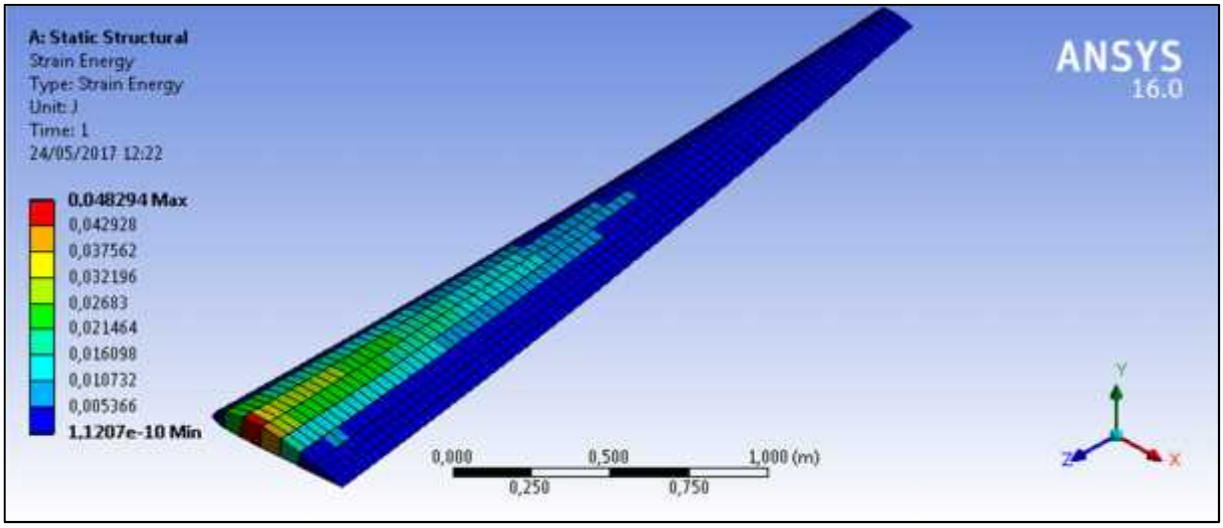

Figure 68: Strain energy for L=3m (NACA 4415)

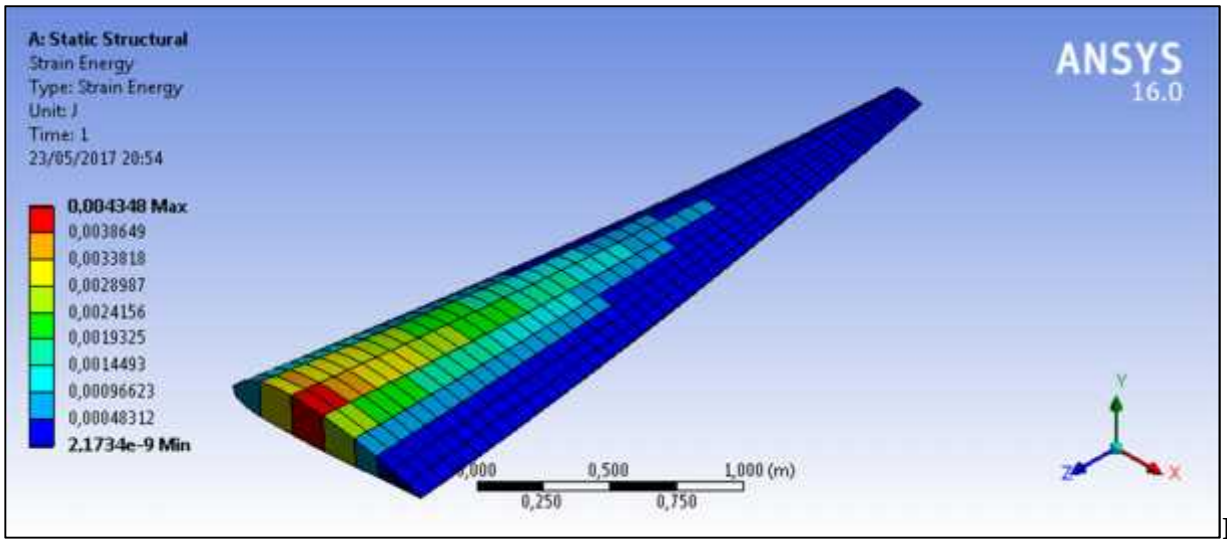

Figure 69: Strain energy for L=3m(NACA 4318)

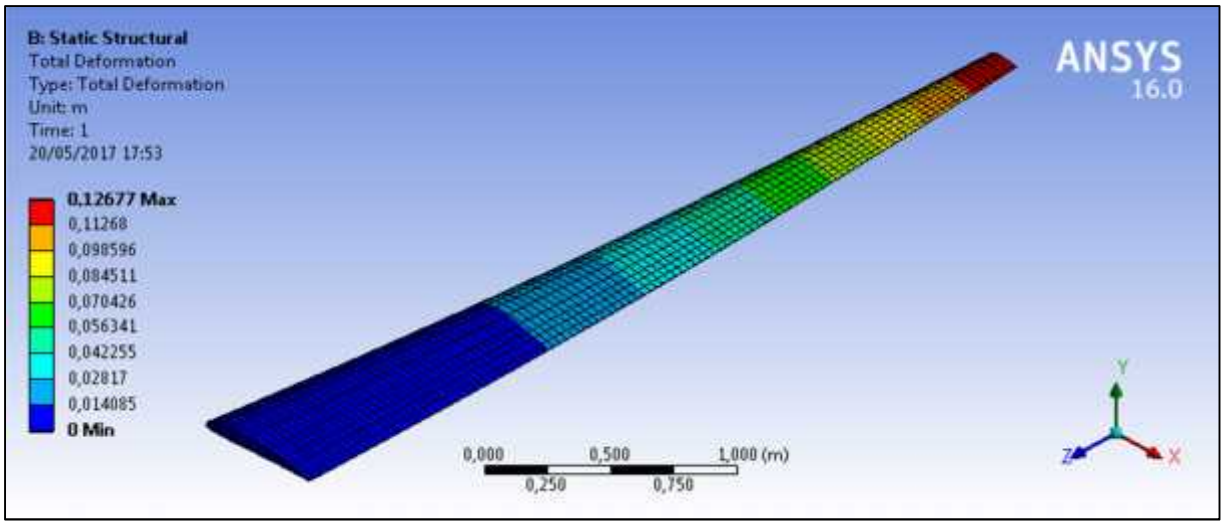

Figure 70: Total deformation forC_r = 0.582m(NACA 4412)

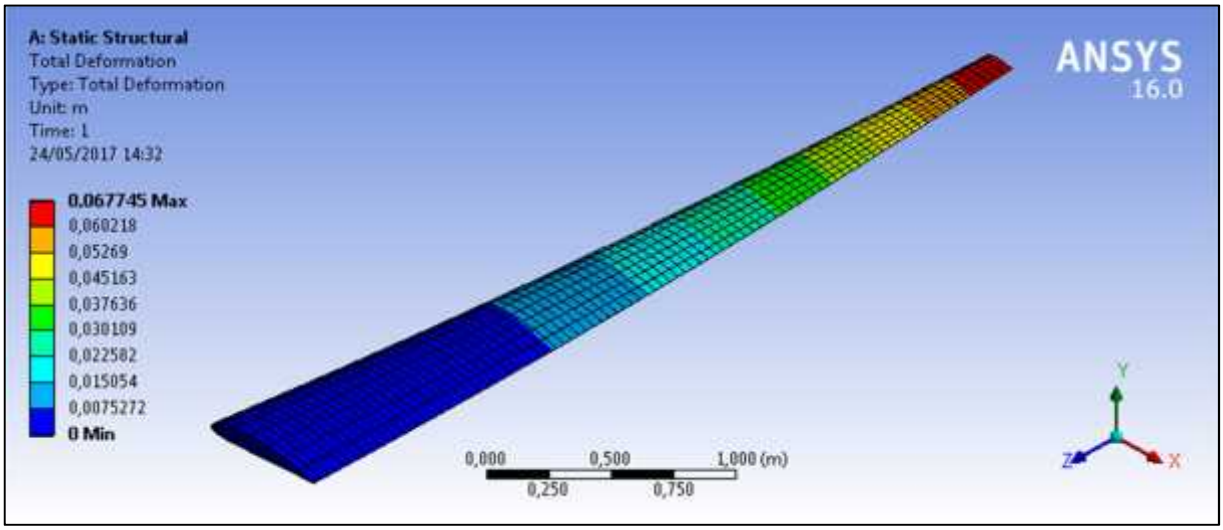

Figure 71: Total deformation for C_r =0.582m(NACA 4415)

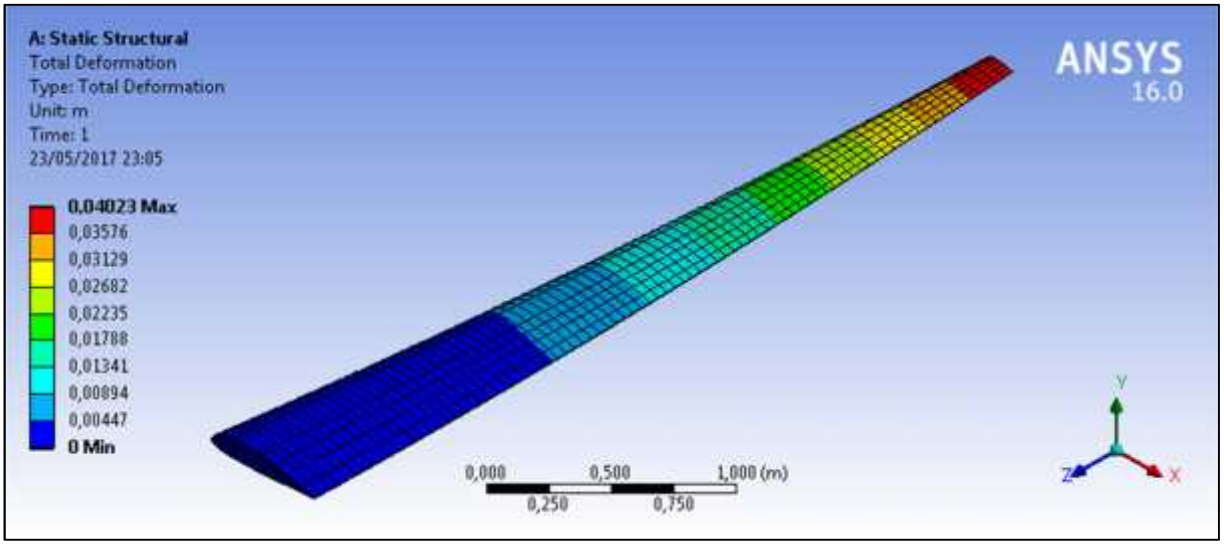

Figure 72: Total deformation forC_r = 0.582m(NACA 4318)

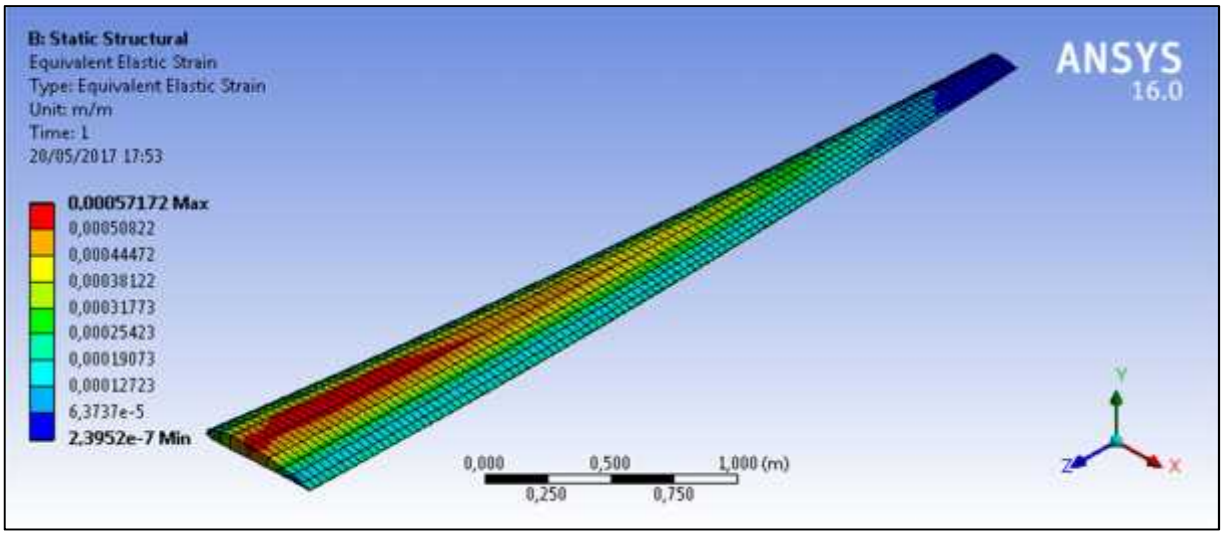

Figure 73: Equivalent elastic strain forC_r = 0.582m(NACA 4412)

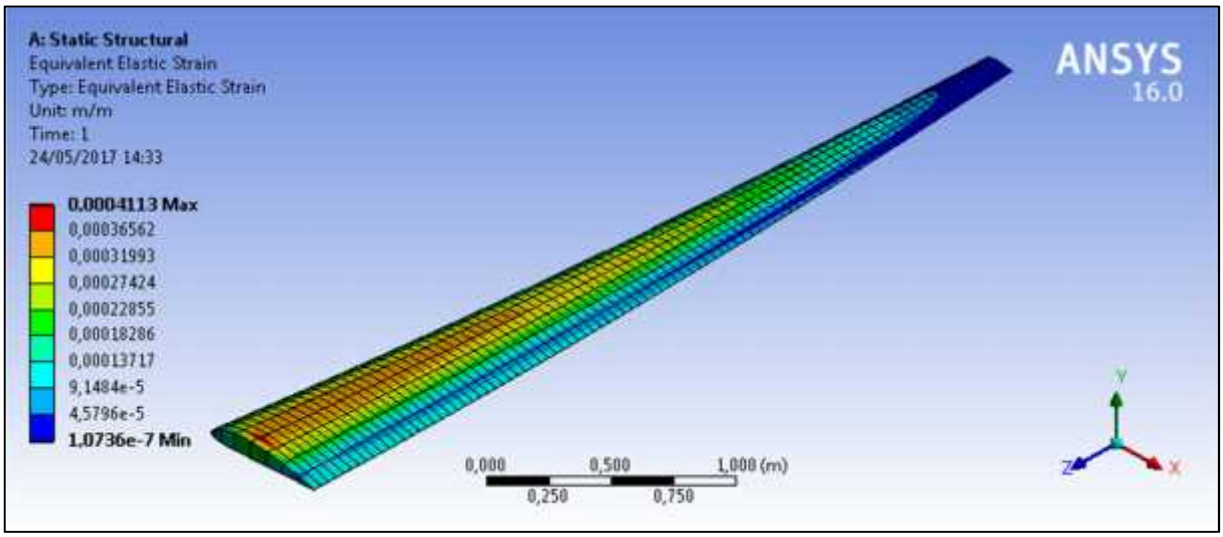

Figure 74: Equivalent elastic strain for C_r =0.582m(NACA 4415)

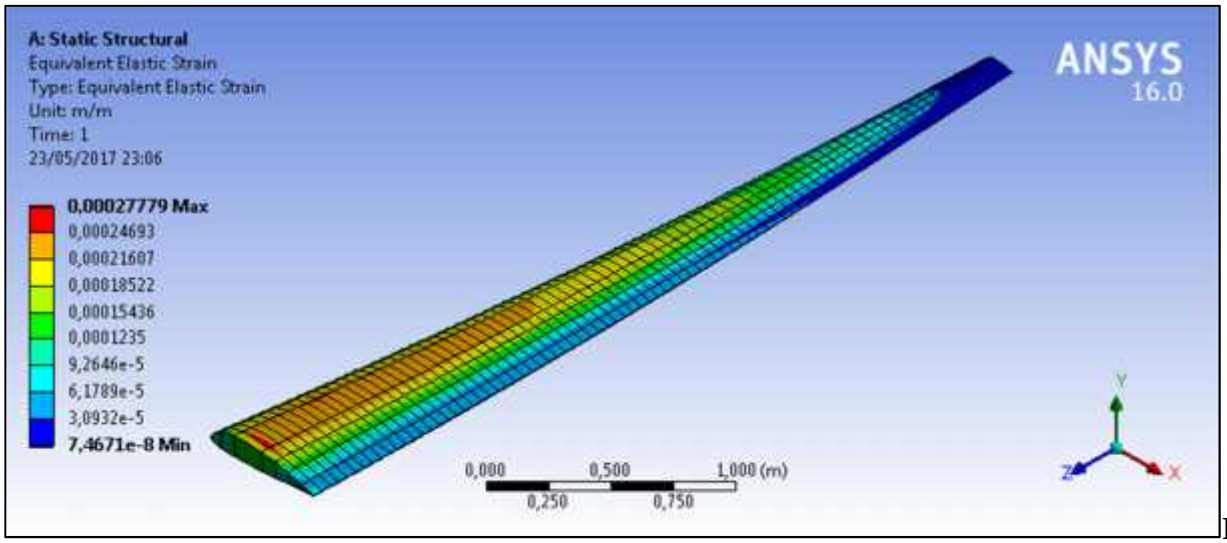

Figure 75: Equivalent elastic strain for C_r = 0.582m(NACA 4318)

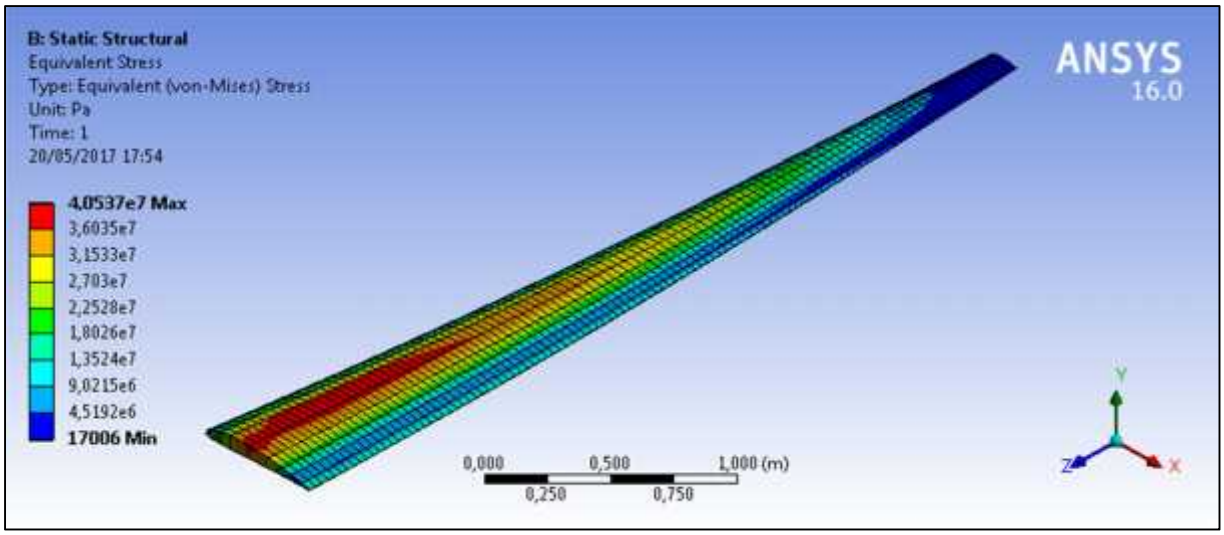

Figure 76: Equivalent von-Mises stress forC_r = 0.582m(NACA 4412)

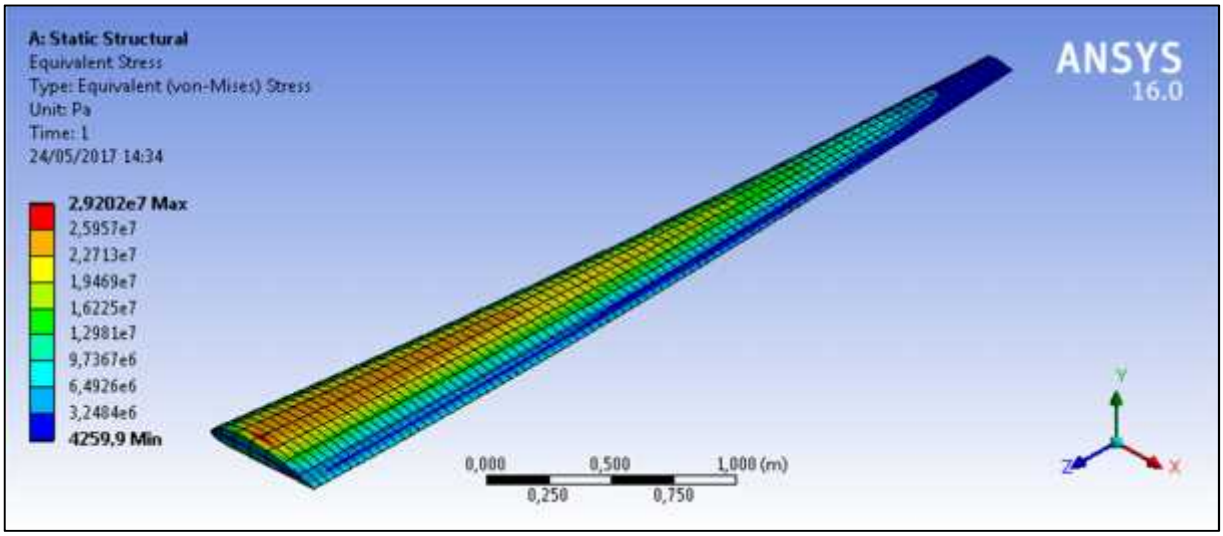

Figure 77: Equivalent von-Mises stress C_r =0.582m (NACA 4415)

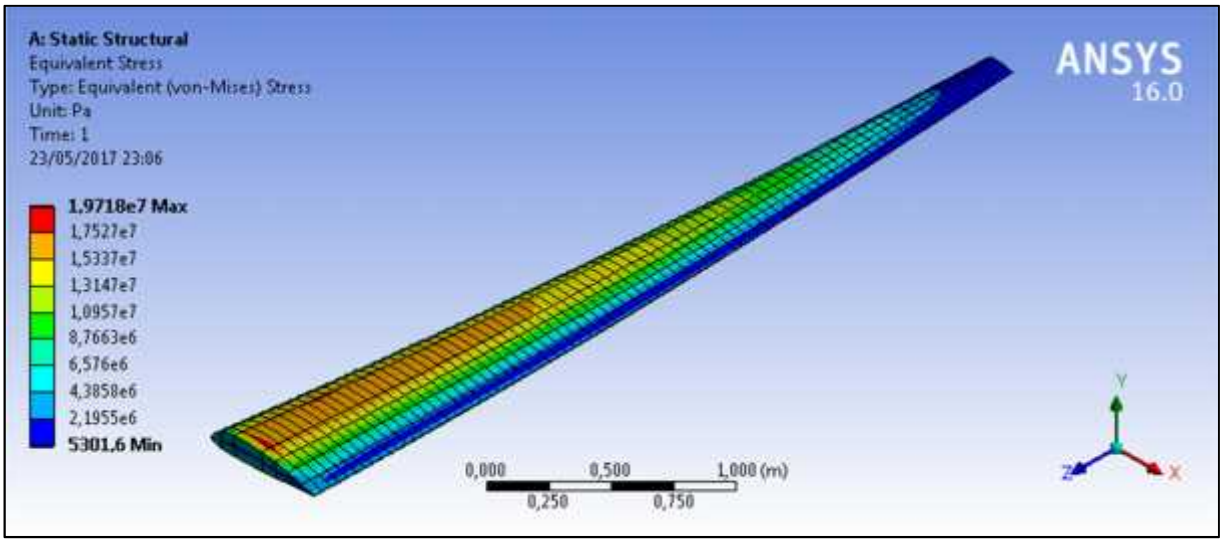

Figure 78: Equivalent von-Mises stress for C_r = 0.582m (NACA 4318)

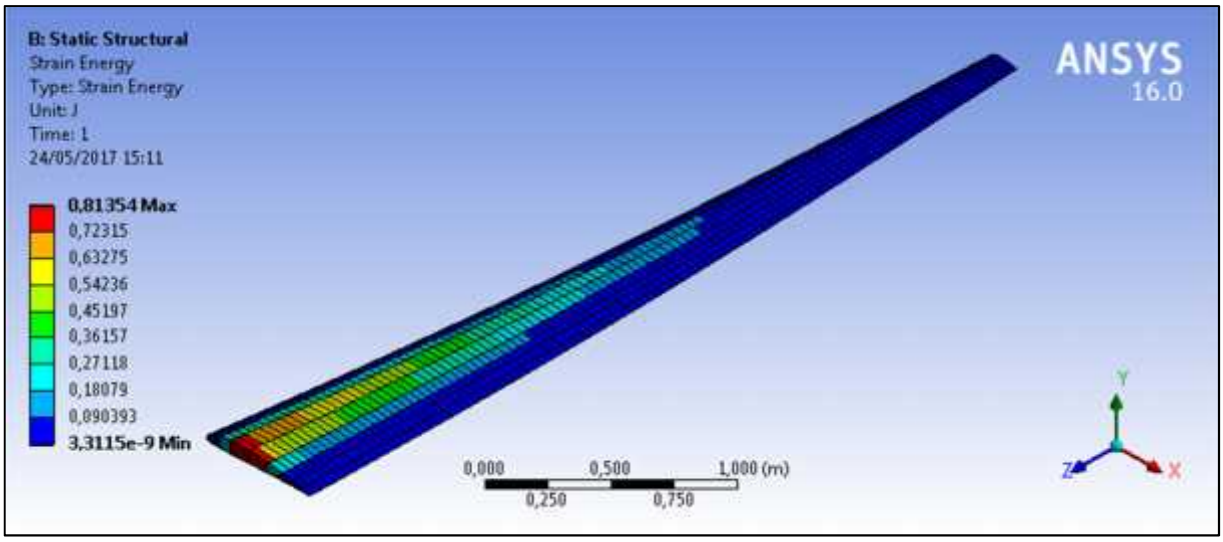

Figure 79: Strain energy for C_r = 0.582m(NACA 4412)

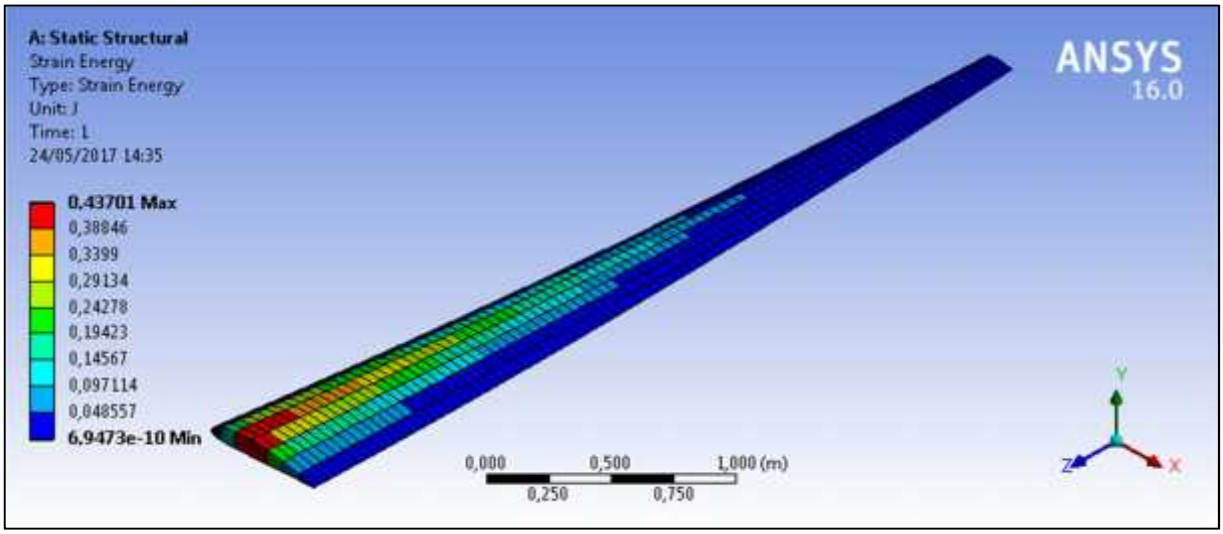

Figure 80: Strain energy for C_r =0.582m(NACA 4415)

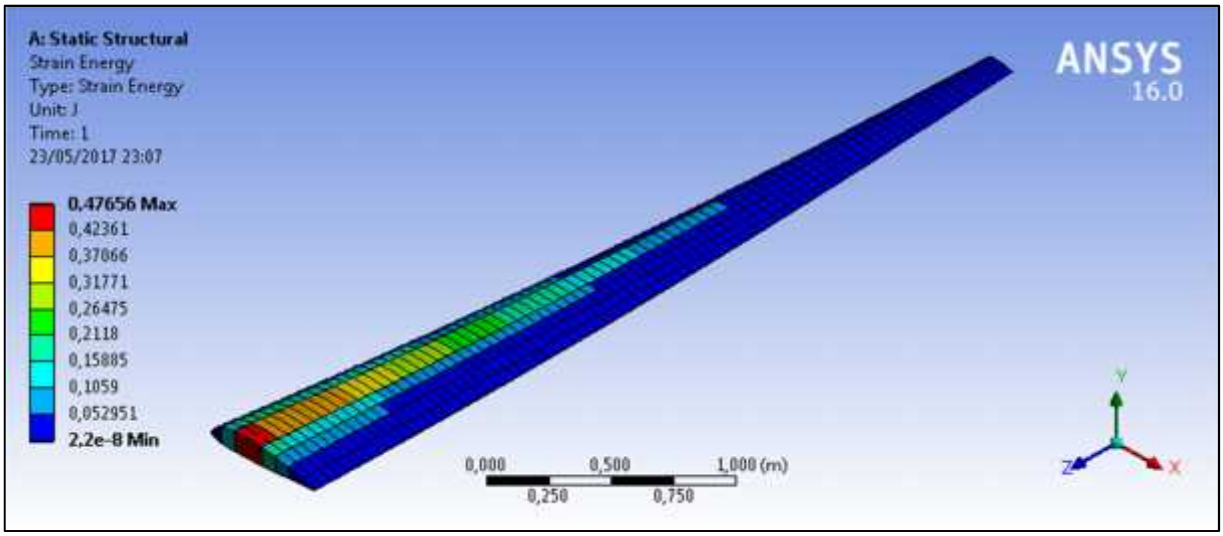

Figure 81: Strain Energy for C_r = 0.582m (NACA 4318)

From these results, we note that the minimal deformation and the Von-Mises stress that they achieved their minimum value for the NACA 4318.

Conclusion:

In this chapter, we have carried out a numerical simulation of the air flow over an aircraft wing in order to evaluate the aerodynamic forces, represented by the aerodynamic coefficients (lift and drag), which are exerted on the wing and thereafter to analyze the structure behavior under these forces.

The main aim of this work was toshow the effect of the geometrical parameters as the wing span, the profile cord and the camber on the variation of the aerodynamic forces and on the response of the structure to these forces. For this, an analyzewas performed, with different wing spans, cord lengths and with different cambers (different profiles). The simulation was done by the ANSYS 16.0 software.

At the end of this work we conclude that the wings surface proprieties (span, cord and camber)are factors on which depend the flow behavior characterized by the aerodynamic coefficients and the structure response represented by the Von-Mises stress, elastic strain, strain energy and the total deformation.

GENREAL CONCLUSION

It is clear from this work that the ANSYS software is a good tool for the numerical simulation of unsteady phenomena, which is the air flow over an airplane wing. This will provideto make the right choices in terms of the wing geometry.

The study was performed in terms of different profiles which are NACA 4412, NACA 4415 and NACA4318, with different spans and chord lengths. For the fluid part we wereinterested to see the influence of the geometric parameters of the forces exerted by the fluid on the wing. These forces are characterised by the aerodynamic coefficients and the repartition of the flow over the wing.

In the solid part we have seen the response of the wing to the aerodynamic forces.At first a modal analysis was performed to determine the first four modes with their frequencies and their maximal amplitudes.this analysis was followed by a static structural analysis through what we have obtained the maximal deformation, Von-Mises stress, strain energy and the equivalent elastic strain.

The fine analysis of the results gave access to some important informations.

We found that:

- The wing surface properties which are the span ,the chord root length and the camber are important factors on which depend on the aerodynamic forces.
- The frequencies and the maximum amplitudes of mode shapes are effected by the variation of the wing geometrical parameters.
- The variation of the wing length, chord root and the camberinfluencesthe disturbition of the Von-Mises stress, elastic strain, strain energy and the maximal deformation.
- The best wing is that which has thehigh lift, small drag, minimal Von-Mises stress, minimal strain energy, minimal elastic strain and minimal deformation.

But these caracteristics can't be achieved simultaniously for the same geometric parameters ,then a comprimise will be make in order to have the optimal caracteristics.

Finally, we can say that we have achieved the work objective. But it stillsa lot to do in the field of aeronautic and airplane wings.

REFERENCES

[1]: Taylor, John W.R.The lore of Flight, London: Universal Books LTD.,1990.

[2]: Anyi, M.J.; G. Bhuyana , M.T. Iqbal, J.E. Quaicoe (2009).”Hydrokinetic engergy energy conversation systems and assessment of horizontal and vertical axis turbins for river and tidal applications: A technology status review”. Applied Energy 86: 1823-1835.Doi: 10.1016/j.apenergy .2009.02.017.

[3]: National Aeronoutics and Space Administration, grc.nasa.gov.

[4]: Kermode, A.C. (1972); Mechanics of Flight, Chapter 3 (Eighth (metric) edition). Sir Isaac Pitman and sons LTD, London.

[5]: The NACA airfoil series.pdf, page (142_156).

[6]: the online encyclopedia BRITANICA article: Titanium processing written by: Star R. Seagle**.**

[7]: Fluids Mechanics and Thermodynamics of Turbomachinery By Sydeny Lawernce Dixon

[8]: S. Toll and M .Ekh. Mechanics of solids &fluids. Part I: Fundamentals. Report Div. of Material and computional Mechanics, Dept. of Applied Mechanics, Chalmers University of technology, G oteborg, Sweden, 2011.

[9]: The artical Equation of Mechanical Energy and Bernoulli form the website engineeringtoolbox.com

[10]: AA(Von Karman Inst. For Fluid Dynamics, Rhode-Saint-Gense (Belgium).), AB (Von Karman Inst. For fluid Dynamics, Rhode-Saint-Gense (Belgium).), AC(Von Karman Inst.

[11]: A numerical fluid dynamics calculation method for all flow speeds. Journal of compulational physics 1971, pp. 197-2013.

[12]: Bhaskar Kumar LAMINAR, TRANSITIONAL AND TURBULENT FLOWS.

[13]: Glenn research center- National aeronoutics and space of sound, Mach Number & Sound Barrier written by: Greg Alexander,1 june 2003.Giverning Equations of fluid Dynamics chapter 2- by J.D. Anderson,Jr.

[14]: Introdcution to compressible Flows- Thermodynamics Concepts Lecture 11by: Anderson. Fluid dynamics lecture-types of fluid flow.

[15]: Anderson, John David (1997). *A History of Aerodynamics and its Impact on Flying Machines*. New York, NY: Cambridge University Press.

[16]: Stokes, G. (1845). "On the Theories of the Internal Friction of Fluids in Motion". *Transaction of the Cambridge Philosophical Society*. **8**: 287–305.

[17]: Abu-Ghannam B.J, Show R 1980 Natural transition of boundary layers—the effect of turblance, paressure grandient and flow history. J. Mech. Eng. Sci. 22, 213-228.

REFERENCES

[18]: Fluids—Lecture 3MIT By Anderson.

[19]: SP-367 Introduction to the Aerodynamics of Flight- IV.SUBSONIC FLOW EFFECTS—chapter 4—nasa history.Glenn research center—National aerauntics and space Administration – lift coefficient-written by Nancy Hall 05/05/2015.

[20]: The Aviationist journal run by David Cenciotti- article wing in the worst case scenario 22/10/2009.

[21]: turbomachinery aerodynamics lec-12 prof.bhaskarroy, prof.AMPradeep, departement of Aerospace,IIT Bombay.

[22]: J.D. MacDougall, R.S. McKelive. Journal of Applied Physiology Published 1 October 1992 VOL. 73 no.4, 1590-1597DOI. Aerodynamic of flight [NASA SP- 367] By theoedore A. Talay Langley Center.

[23]: Aerodynamics for engineering students, Houghton and Carpenter Fundamentals of Aerodynamics, John D. Anderson.

[24]: National Aeronoutics and Space Administration. Nancy Hall May 05 2015. The Journal of Hand Surgery Volume 24, Issue 2, March 1999, Pages 345–351.

[25]: Livre mécanique vibratoire l'auteur MICHEL DEL PEDRO page (5et7) troisième édition ISBN 2-88074-243-9 presses polytechnique et universitaire romandes CH-1015 Lausanne.

[26]: Flight mechanics controls Air defense.Net page 117.

[27]: Aero_student_guide_7_April_2008.pdf.

[28]: P.C. Paris, Gomes, and W.E. Anderson. A rotational analytic theory of fatigue. The Trend in engineering 1961,13;p.9-14.

[29]: P.C. Paris, Gomes, and W.E. Anderson. A rotational analytic theory of fatigue. The Trend in engineering 1961,13;p.9-14.

[30]: Wahab, M.M.A.,I.A. Ashcroft, A.D. Crocombe, and P.A, Smith, Fatigue crack propagation in adhesive bonded joints. Key Engineering Materials, 2003, 251-252: p.229-234.

[31]:T.L.(2005). Fracture mechanics: fundamental and applications.CRC press.

[32]: Stress intensity factor for the tension of an eccentrically cracked strip, transactions of the ASME Applied Mechanics Section, v. 88, p. 94.

[33]: Gross, D. And Seeling, T. (2001). Fracture mechanics: with an introdution to micromechanis. Springer.

APPENDIX

Appendix 01: NACA coordinates system

#x_chord	#y_chord	#x_chord	#y_chord	#x_chord	#y_chord
1.000167	0.001249	0.580092	0.083817	0.024421	0.033434
0.999924	0.001316	0.564422	0.085609	0.019693	0.030193
0.999198	0.001518	0.548679	0.087310	0.015462	0.026976
0.997988	0.001853	0.532880	0.088914	0.011729	0.023789
0.996295	0.002320	0.517040	0.090418	0.008498	0.020639
0.994122	0.002919	0.501176	0.091816	0.005770	0.017531
0.991469	0.003647	0.485304	0.093105	0.003547	0.014471
0.988339	0.004502	0.469440	0.094281	0.001828	0.011461
0.984735	0.005481	0.453601	0.095340	0.000615	0.008507
0.980660	0.006582	0.437802	0.096279	-0.000093	0.005611
0.976117	0.007801	0.422059	0.097095	-0.000298	0.002775
0.971111	0.009135	0.406390	0.097785	0.000000	0.000000
0.965646	0.010579	0.390664	0.098334	0.000791	-0.002676
0.959726	0.012130	0.374939	0.098691	0.002067	-0.005217
0.953357	0.013782	0.359335	0.098850	0.003823	-0.007622
0.946545	0.015531	0.343868	0.098810	0.006057	-0.009892
0.939296	0.017372	0.328558	0.098573	0.008765	-0.012027
0.931615	0.019300	0.313420	0.098140	0.011942	-0.014028
0.923510	0.021309	0.298472	0.097515	0.015585	-0.015895
0.914989	0.023393	0.283730	0.096699	0.019688	-0.017629
0.906059	0.025547	0.269212	0.095696	0.024245	-0.019232
0.896728	0.027764	0.254934	0.094510	0.029250	-0.020704
0.887004	0.030040	0.240912	0.093147	0.034698	-0.022047
0.876897	0.032366	0.227162	0.091611	0.040581	-0.023264
0.866416	0.034738	0.213699	0.089909	0.046893	-0.024355
0.855570	0.037149	0.200538	0.088046	0.053626	-0.025324
0.844370	0.039593	0.187695	0.086030	0.060773	-0.026172
0.832825	0.042062	0.175183	0.083869	0.068325	-0.026902
0.820948	0.044551	0.163016	0.081569	0.076274	-0.027517
0.808749	0.047054	0.151208	0.079140	0.084613	-0.028020
0.796239	0.049564	0.139770	0.076589	0.093332	-0.028415
0.783430	0.052074	0.128716	0.073927	0.102423	-0.028706
0.770335	0.054578	0.118058	0.071162	0.111876	-0.028895
0.756966	0.057070	0.107805	0.068303	0.121682	-0.028988
0.743335	0.059543	0.097969	0.065360	0.131831	-0.028989
0.729457	0.061992	0.088560	0.062343	0.142315	-0.028903
0.715343	0.064411	0.079587	0.059262	0.153123	-0.028734
0.701009	0.066792	0.071059	0.056125	0.164245	-0.028488
0.686467	0.069130	0.062983	0.052944	0.175672	-0.028170
0.671732	0.071420	0.055369	0.049728	0.187393	-0.027786
0.656819	0.073655	0.048221	0.046485	0.199398	-0.027342
0.641742	0.075830	0.041547	0.043226	0.211676	-0.027342
0.626515	0.077939	0.035352	0.039959	0.224218	-0.026297
0.611155	0.079976	0.029642	0.036692	0.237012	-0.025709

APPENDIX

Table: NACA 4412 coordinates system

#x_chord	#y_chord	#x_chord	#y_chord	#x_chord	#y_chord
1.000215	0.001878	0.518447	0.114037	-0.000827	0.004094
0.999974	0.001958	0.502592	0.116103	0.000000	0.000000
0.999251	0.002197	0.486726	0.118047	0.001320	-0.003963
0.998048	0.002594	0.470867	0.119864	0.003114	-0.007741
0.996364	0.003150	0.455030	0.121547	0.005375	-0.011334
0.994202	0.003861	0.439231	0.123093	0.008098	-0.014744
0.991563	0.004726	0.423487	0.124495	0.011275	-0.017973
0.988450	0.005742	0.407814	0.125748	0.014899	-0.021022
0.984865	0.006907	0.392228	0.126848	0.018963	-0.023893
0.980811	0.008218	0.376745	0.127792	0.023458	-0.026589
0.976292	0.009670	0.361382	0.128573	0.028377	-0.029112
0.971311	0.011259	0.346155	0.129191	0.033711	-0.031465
0.965873	0.012982	0.331080	0.129640	0.039451	-0.033653
0.959982	0.014833	0.316172	0.129919	0.045588	-0.035677
0.953644	0.016808	0.301447	0.130025	0.052112	-0.037543
0.946864	0.018901	0.286080	0.129890	0.059015	-0.039255
0.939649	0.021107	0.270851	0.129422	0.066287	-0.040816
0.932003	0.023420	0.255876	0.128627	0.073918	-0.042232
0.923935	0.025833	0.241174	0.127513	0.081899	-0.043507
0.915451	0.028342	0.226766	0.126089	0.090220	-0.044648
0.906558	0.030940	0.212671	0.124365	0.098872	-0.045660
0.897266	0.033619	0.198907	0.122353	0.107846	-0.046548
0.887582	0.036374	0.185494	0.120064	0.117131	-0.047319
0.877515	0.039198	0.172448	0.117512	0.126720	-0.047981
0.867074	0.042083	0.159786	0.114710	0.136602	-0.048538
0.856268	0.045024	0.147525	0.111672	0.146770	-0.049000
0.845108	0.048014	0.135678	0.108414	0.157215	-0.049373
0.833604	0.051044	0.124261	0.104951	0.167928	-0.049665
0.821767	0.054109	0.113287	0.101299	0.178902	-0.049884
0.809607	0.057202	0.102767	0.097474	0.190128	-0.050039
0.797136	0.060315	0.092714	0.093493	0.201599	-0.050137
0.784366	0.063440	0.083137	0.089371	0.213308	-0.050189
0.771309	0.066573	0.074047	0.085127	0.225246	-0.050203
0.757976	0.069704	0.065452	0.080775	0.237407	-0.050189
0.744382	0.072828	0.057359	0.076333	0.249784	-0.050156
0.730538	0.075937	0.049775	0.071817	0.262370	-0.050113
0.716458	0.079024	0.042706	0.067241	0.275158	-0.050070
0.702156	0.082082	0.036158	0.062621	0.288141	-0.050038
0.687646	0.085104	0.030133	0.057972	0.301405	-0.050025
0.672940	0.088084	0.024636	0.053308	0.315704	-0.049960
0.658055	0.091014	0.019668	0.048641	0.330182	-0.049793
0.643004	0.093888	0.015232	0.043985	0.344828	-0.049529
0.627802	0.096698	0.011329	0.039350	0.359627	-0.049171
0.612464	0.099439	0.007959	0.034747	0.374565	-0.048726
0.597006	0.102102	0.005121	0.030186	0.389629	-0.048198

0.581442	0.104683	0.002814	0.025675	0.404805	-0.047593
0.565789	0.107172	0.001037	0.021222	0.420079	-0.046916
0.550061	0.109566	-0.000212	0.016833	0.435436	-0.046172
0.534275	0.111856	-0.000937	0.012513	0.450862	-0.045366
0.481863	-0.043592	0.680479	-0.029187	0.850839	-0.015052
0.497408	-0.042633	0.694992	-0.028018	0.861895	-0.014107
0.512964	-0.041634	0.709321	-0.026857	0.872596	-0.013188
0.528515	-0.040598	0.723452	-0.025704	1.000215	-0.001878
0.544047	-0.039531	0.737372	-0.024562		
0.559544	-0.038437	0.751065	-0.023433		
0.574992	-0.037320	0.764518	-0.022318		
0.590375	-0.036185	0.777717	-0.021220		
0.605679	-0.035035	0.790649	-0.020140		
0.620888	-0.033874	0.803300	-0.019079		
0.635987	-0.032706	0.815657	-0.018038		
0.650962	-0.031533	0.827707	-0.017019		

Table: NACA 4318 coordinates system

#x_chord	#y_chord	#x_chord	#y_chord	#x_chord	#y_chord
1.00000	0.00000	**0.30866**	0.11294	0.14645	-0.04166
0.99893	0.00039	**0.27886**	0.11141	0.17033	-0.04177
0.99572	0.00156	**0.25000**	0.10903	0.19562	-0.04147
0.99039	0.00349	**0.22221**	0.10584	0.22221	-0.04078
0.98296	0.00610	0.19562	0.10190	0.25000	-0.03974
0.97347	0.00932	0.17033	0.09726	0.27886	-0.03845
0.96194	0.01303	0.14645	0.09195	0.30866	-0.03700
0.94844	0.01716	0.12408	0.08607	0.33928	-0.03547
0.93301	0.02166	0.10332	0.07970	**0.37059**	**-0.03390**
0.91573	0.02652	0.08427	0.07283	**0.40245**	-0.03229
0.89668	0.03171	0.06699	0.06541	**0.43474**	-0.03063
0.87592	0.03717	0.05156	0.05753	**0.46730**	-0.02891
0.85355	0.04283	0.03806	0.04937	**0.50000**	-0.02713
0.82967	0.04863	0.02653	0.04118	**0.53270**	-0.02529
0.80438	0.05453	0.01704	0.03303	**0.56526**	-0.02340
0.77779	0.06048	0.00961	0.02489	**0.59755**	-0.02149
0.75000	0.06642	0.00428	0.01654	**0.62941**	-0.01958
0.72114	0.07227	0.00107	0.00825	**0.66072**	-0.01772
0.69134	0.07795	0.00000	0.00075	**0.69134**	-0.01596
0.66072	0.08341	0.00107	-0.00566	**0.72114**	-0.01430
0.62941	0.08858	0.00428	-0.01102	**0.75000**	-0.01277
0.59755	0.09341	0.00961	-0.01590	**0.77779**	-0.01136
0.56526	0.09785	0.01704	-0.02061	**0.80438**	-0.01006
0.53270	0.10185	0.02653	-0.02502	**0.82967**	-0.00886
0.50000	0.10538	0.03806	-0.02915	**0.85355**	-0.00775
0.46730	0.10837	0.05156	-0.03281	**0.87592**	-0.00674
0.43474	0.11076	0.06699	-0.03582	**0.89668**	-0.00583
0.40245	0.11248	0.08427	-0.03817	**0.91573**	-0.00502
0.37059	0.11345	0.10332	-0.03991	**0.93301**	-0.00431

0.33928	0.11361	0.12408	-0.04106	**0.94844**	-0.00364
#x_chord	#y_chord	#x_chord	#y_chord	#x_chord	#y_chord
0.96194	-0.00297	**0.99039**	-0.00092	**1.00000**	0.00000
0.97347	-0.00227	**0.99572**	-0.00042	**0.96194**	-0.00297
0.98296	-0.00156	**0.99893**	-0.00011		

Table: NACA 4415 coordinates system

Appendix 02: 3D geometry creation

Generate data points that define the airfoil:

- Open an internet browser and go the NACA 4 Digits Series Profile Generator at **http://airfoiltools.com/airfoil/naca4digit**
- Create the NACA 4412 airfoil

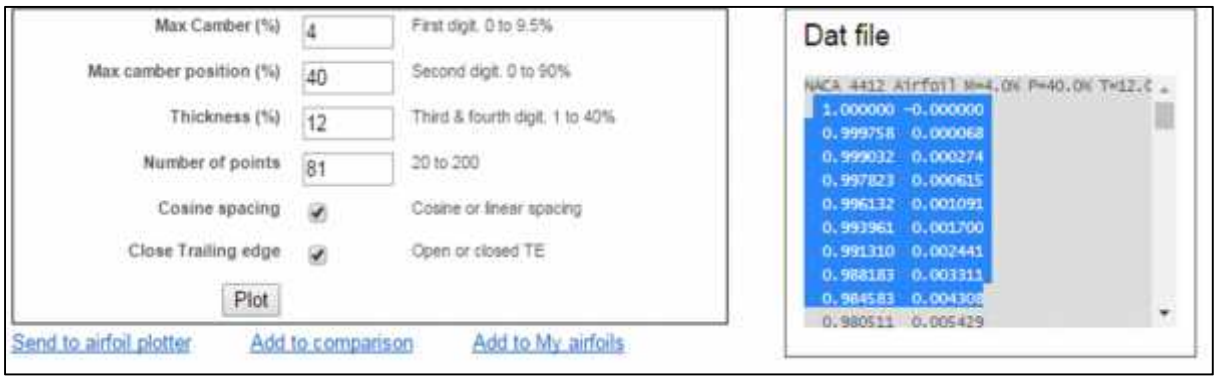

- Show Points, then highlight everything that appears in the window to the right of the sliders and copy it to the clipboard.
- Open Microsoft Excel and create table of NACA 4412 coordinates like this:

	A	B	C	D	E
1			#NACA 4412		
2	#group	#point	#x_cord	#y_cord	#z_cord
3	1	1	1.000167	0.001249	0
4	1	2	0.998653	0.001668	0
5	1	3	0.994122	0.002919	0
6	1	4	0.986596	0.004976	0
7	1	5	0.976117	0.007801	0
8	1	6	0.962742	0.011341	0

- Save as type “Text “and Close Excel.

ANSYS Workbench software

ANSYS software presentation:

The Workbench allows to manage the files and the launch of the different Software from a single window.

- Launch ANSYS Workbench from the Windows Start menu.

The Workbench main window appears.

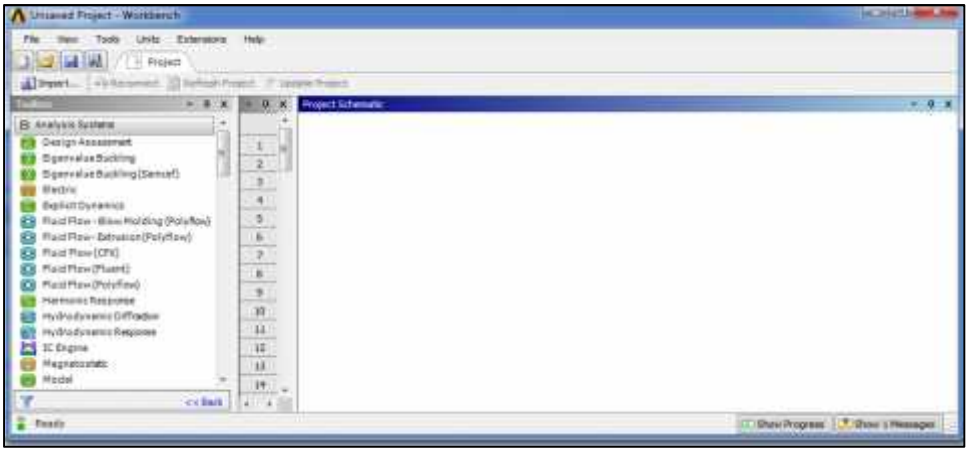

This is where the files will be created, Launched the software and managed the interactions between Various software used for geometry, meshing, simulation itself and post-processing.

Create a 3d Fluid Flow analysis system:

To create an "Analysis System" That is to say a calculation chain for a Fluent simulation

- Select with the mouse Fluid Flow (FLUENT) in the menu on the left
- Select in the window Project Schematic.
- Rename the analysis system by double clicking on the title Fluid Flow (Fluent) in "wing-A321"

APPENDIX

The different stages:

The system is composed of different things associated with different successive steps, each realized with software from the ANSYS suite.

	CAD - Creating geometry	ANSYS Design Modeler
	Mesh	ANSYS meshing
	Getting data and simulation	ANSYS Fluent
	Result CFD	
	Post- treatment	CFD Post

In our case, we will work in 3d in the XY plane to create the geometry of the problem.

- Double-click on the Geometry box 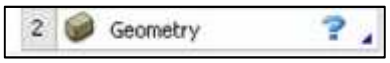 to launch the ANSYS Design Modeler software

- At startup chose Meter for the unit of length
- Concept-3D Curve. In *Details View*, **Not Selected**. Browse to where you saved the airfoil data, select the text file, and Open then Generate  .
- Create a surface:
  - Concept-Surfaces from Edges.
  - Click on the Edges colored box in yellow
  - Click Apply in the Edges box then Generate.
- Look at Face  and chose XY plane 

- Click on XY plane then click on new plane  then modify the details parameters of the new plane as shown in the figure below. Transform the Z axis by longer of 12.5m in reason to have a wing span of 12.5m.

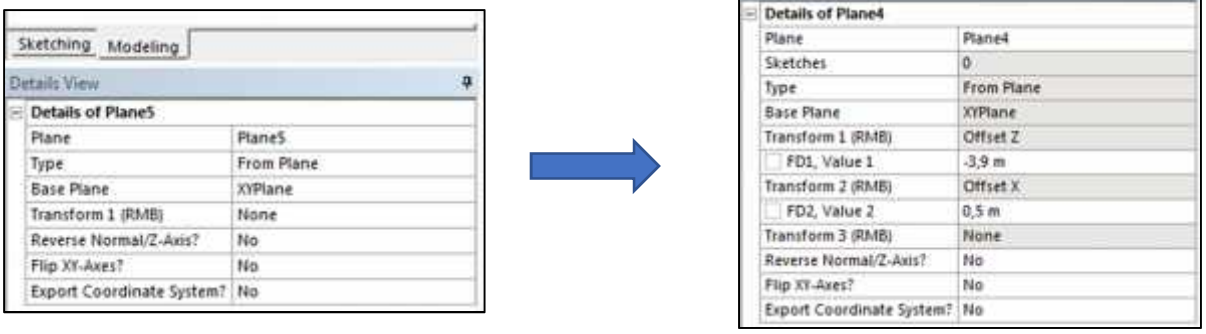

- Concept-3D Curve in the new plane (plane4). In Details View, chose from coordinates file in definition, **Not Selected**. Browse to where you saved the airfoil data, select the text file, and Open Then Generate 
- Create surface: Concept-Surfaces from Edges. LMB on the second curve that was created in the previous step to select it. Apply and  generate.
- Select 

to connect the two curve and generate  .

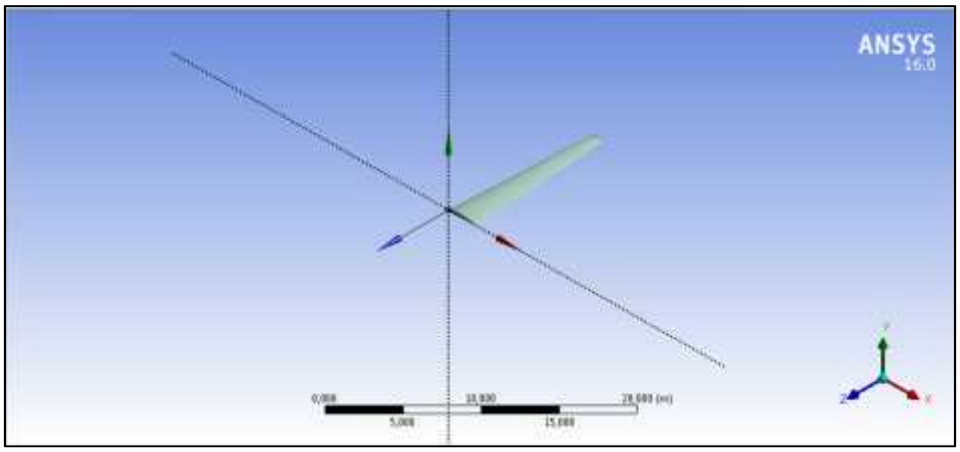

Drawing of the domain:

We will now draw the computational domain around the wing profile.

- Create an arc by center with radius of R=15m

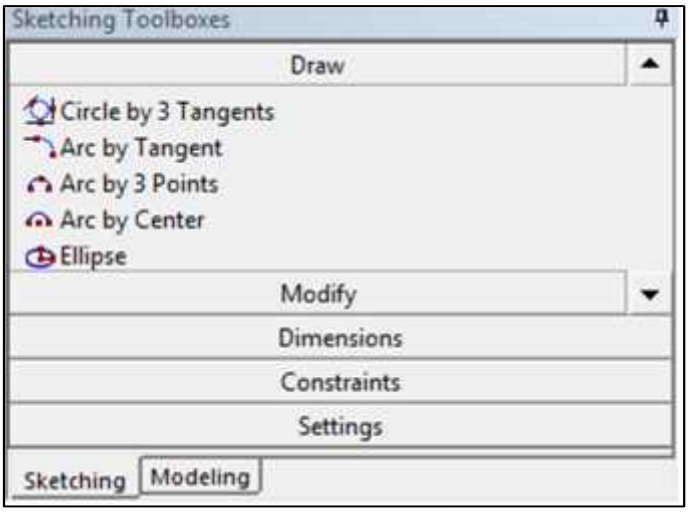

- connect the tow edge of the arc using line after that revolve 

this sketch along Y axis then extrude it by 10m.

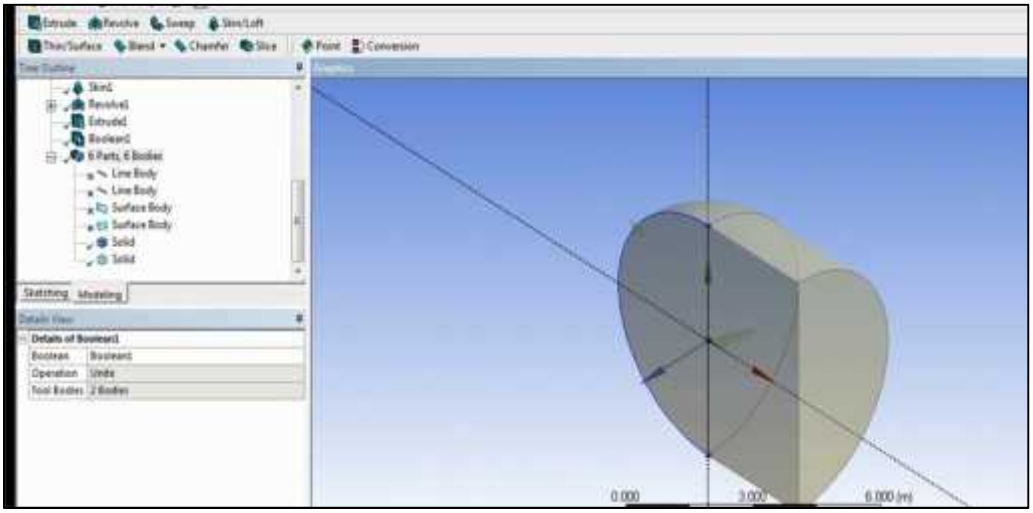

- We intersect the sketch 3 by performing a Boolean operation.
  - Create-Boolean 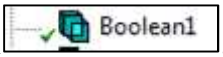

.
  - Change *Operation* from "Unite" to "Subtract".
  - For *Target Bodies*, Not Selected, choose "Solid" and Apply.
  - For *Tool Bodies*, Not Selected, choose "wing", and Apply. Generate

Details of Boolean2	
Boolean	Boolean2
Operation	Subtract
Target Bodies	1 Body
Tool Bodies	1 Body
Preserve Tool Bodies?	No

- Select ZX plane and we draw a trapezoidal in which the wing is inside.

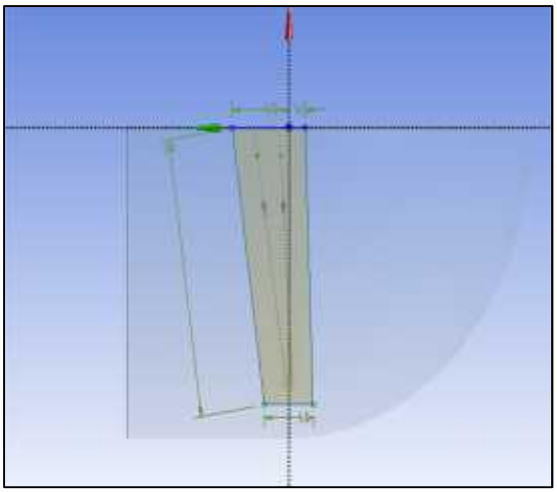

Sketching | Modeling

Details View

Sketch	Sketch2
Sketch Visibility	Show Sketch
Show Constraints?	No
Dimensions: 4	
L4	13,5 m
L5	3 m
V1	1 m
V3	3,5 m
Edges: 4	
Line	Ln19
Line	Ln20
Line	Ln21
Line	Ln22

- Extrude the trapezoidal by symmetry with depth (d=0,3 m).

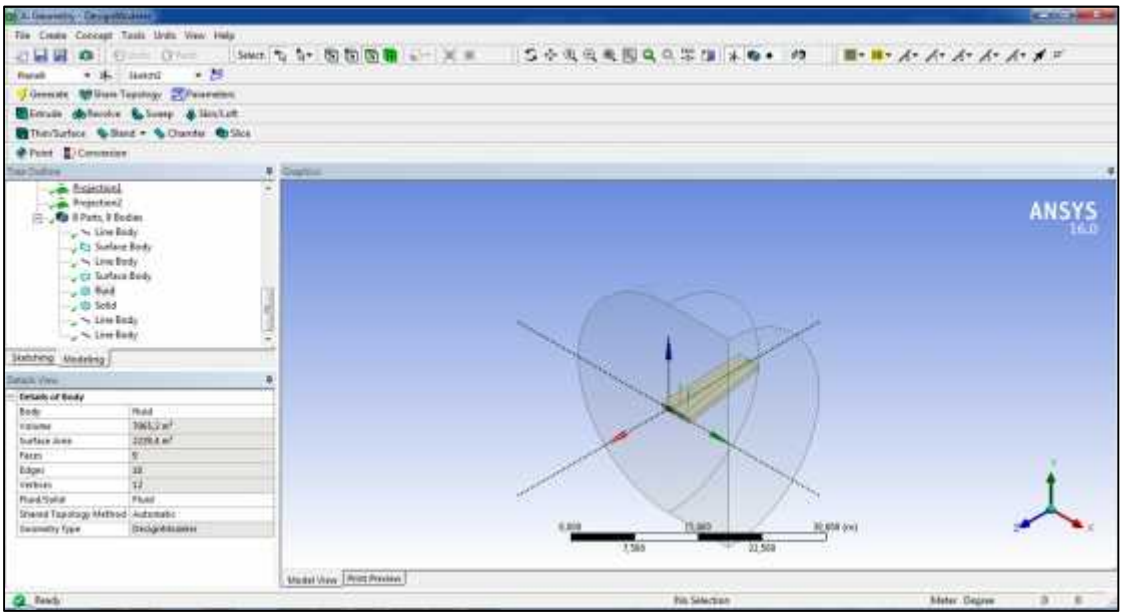

- Suppress all the line in the tree outline, and rename the first solid by fluid.

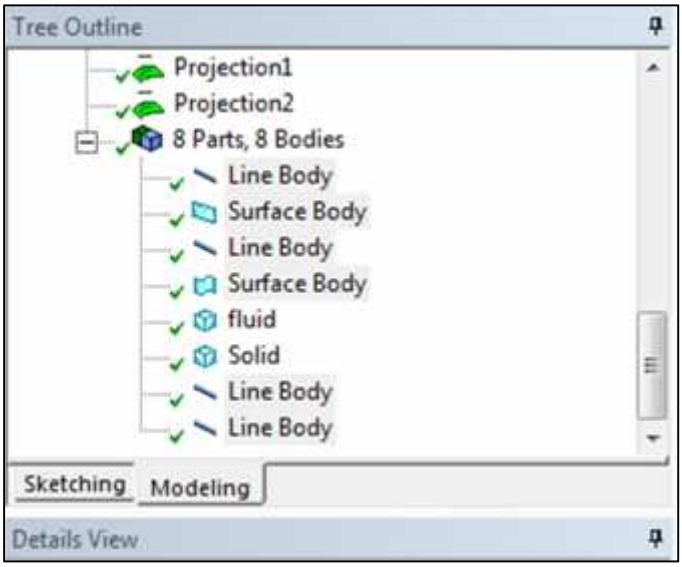

- File-Save Project. After selecting an appropriate folder in which to save the project, and Save as name (**fluid analysis 1**)
- Close DM.

Set the meshing method:

Mesh in the *Fluid Flow (Fluent)* template to open *ANSYS Meshing.*

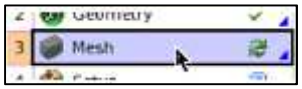

From the *Meshing Options* window that opens, select "Tetrahedrons (Patch Independent)" to set the *Mesh Method*. OK.

Mesh of the fluid domain:

- Launch mesh software from the work bench. As the previous step is validated this opens directly the mesh software ANSYS meshing and loads the geometry created during step one.
- Select mesh in the outline window
- click right and choose mesh geometry mesh with the default options is generated and appears in the visibility window.

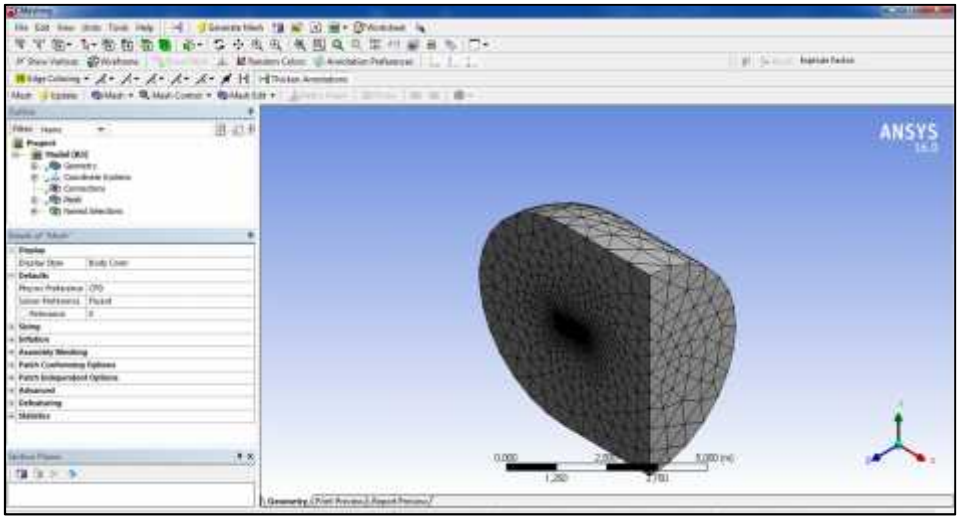

Appendix 04: fluent steps of work

Scale the geometry

General → scale →Mesh was created in "m"

And we chose the view length unit in "m"

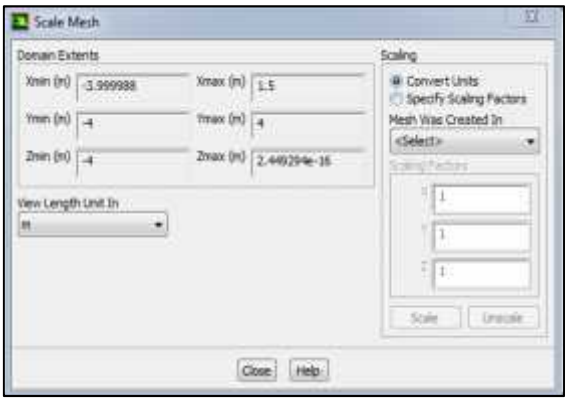

APPENDIX

- **Flow properties:**

➢ **Flow type:**

As it is known that the flow around the wing is a time dependent. But for our study we select the steady form for reason to simplify and fasting the simulation.

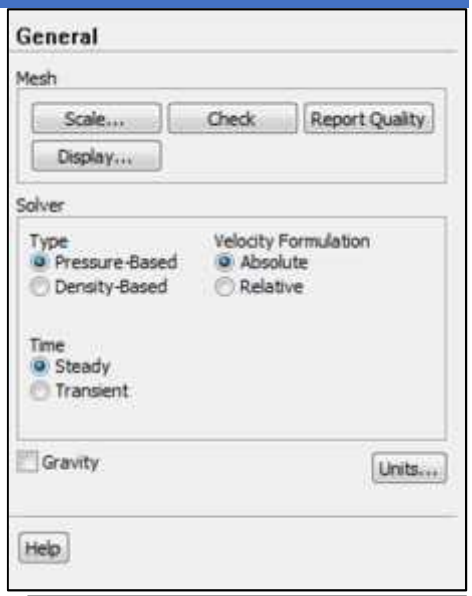

➢ **Flow characteristic:**

In the wing, the environment is viscous

Models → viscous → spamlart-allmaras (1 eqn)

And we set the energy equation ‘’ON’’

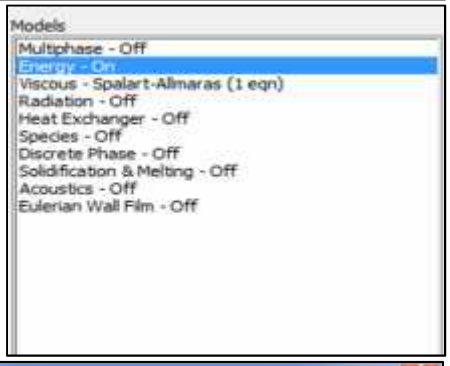

➢ **Flow material property:**

The flow over a wing is air

Materials → fluid → air

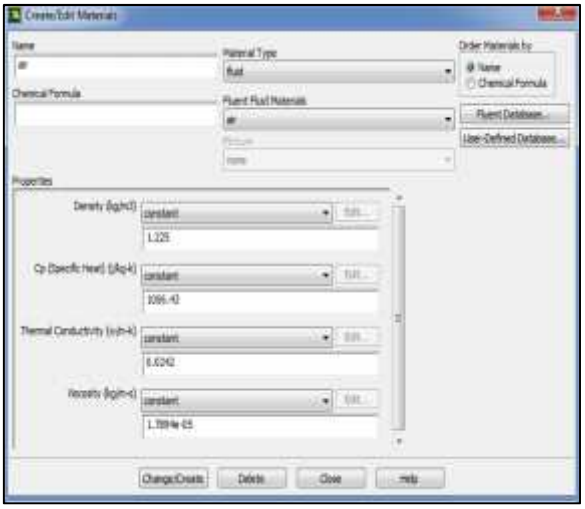

✓ **Boundary conditions:**

- Inlet pressure: Atmospheric pressure 101325 Pa
- Velocity magnitude: 100 m/s
- X component of flow direction: cos (Angle of attack)
- Y component of flow direction: sin (Angle of attack)
- Z component of flow direction: tan (Angle of attack)
- Angle of attack 0°

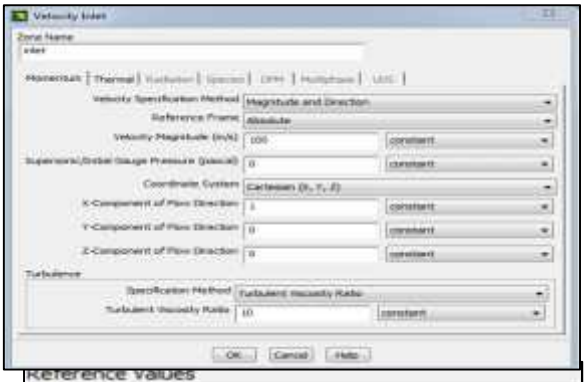

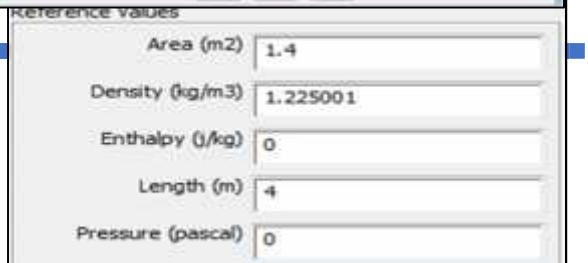

- **Reference values:**

  we input the surface area of wing for

  each geometry.

- **Solution method:**

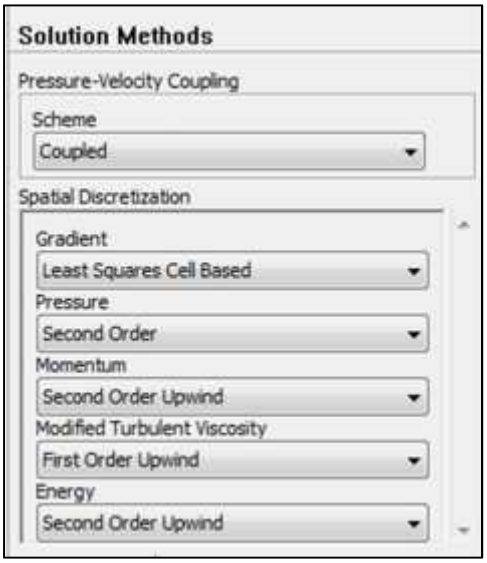

we must specify the solution method for the calculus:

- ✓ Pressure: standard
- ✓ Density: Second order
- ✓ Momentum: second order

- **Monitor:**

  In order to display the lift, drag and moment historic results, we proceed as follow:

  Monitor → c_i → $\begin{cases} L \\ D \\ M \end{cases}$

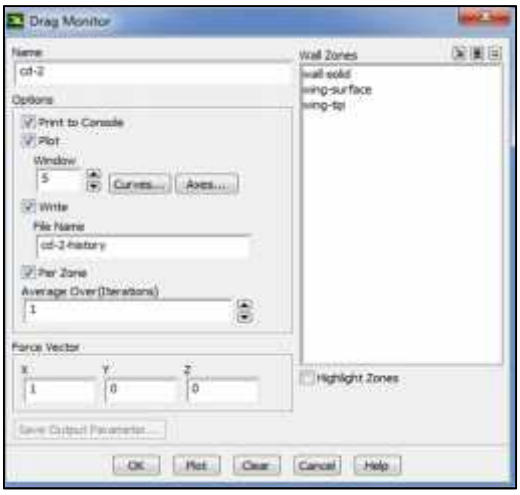

  Then for each one we enable the sub-options:

- ✓ Print to console
- ✓ Plot
- ✓ Write
- ✓ Per zone

- **Solution initialization:**

Before the start of every simulation we must initialize the solution from the inlet conditions:

Solution initialization → standard initialization → compute from → inlet →initialize

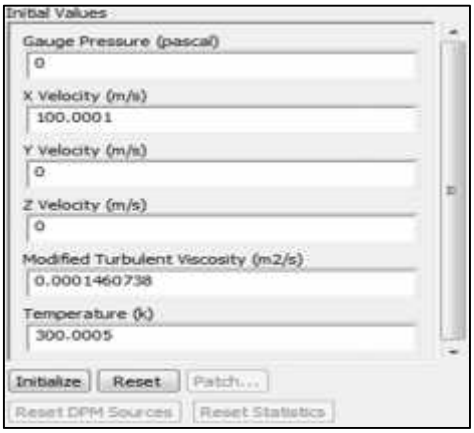

- **Run calculation:**

Finally, we lunch the calculation by clicking on run calculation Options and we set number of iteration 2000.

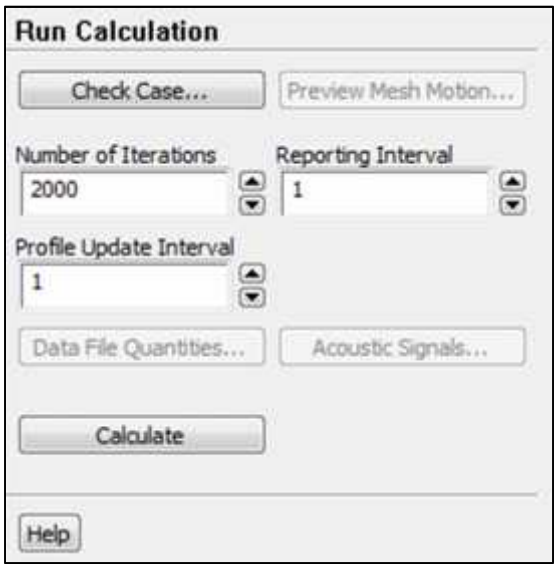

Appendix 05: Modal analysis

- Open ANSYS workbench.
- Go to file → open the last Project of fluide flow fluent (Fluid analysis 1)
- Load the Modal tool box by dragging and dropping it into the project schematic.

➢ **Geometry**

click (and hold) on the geometry how was created in the fluid flow

drag and drop on

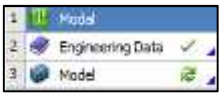

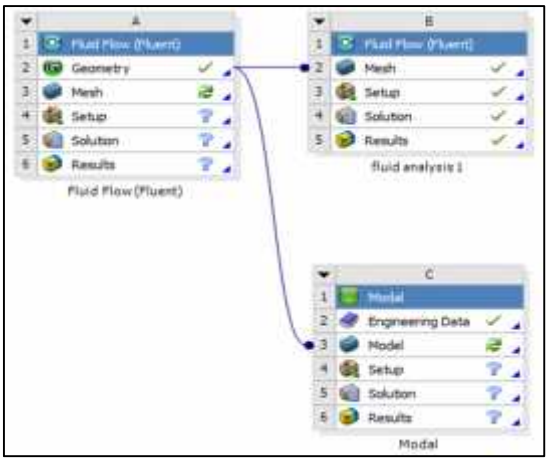

- Engineering data → Engineering data source → general material →add aluminum alloy
- **Model**
  - For the type of material used are aluminum alloy
    Geometry → solide → assignment → aluminum alloy
  - **Mesh**
    after modify the parameters of mesh as shown in the figure, click on generate mesh

Details of "Mesh"	
Relevance	0
Sizing	
Use Advanced Size Function	Off
Relevance Center	Medium
Element Size	Default
Initial Size Seed	Active Assembly
Smoothing	High
Transition	Fast
Span Angle Center	Fine
Minimum Edge Length	0,29460 m
Inflation	
Use Automatic Inflation	None
Inflation Option	Smooth Transition
Transition Ratio	0,272
Maximum Layers	5
Growth Rate	1,2

  - **Modal**
    supports→ fixed supports → select the face with chord root

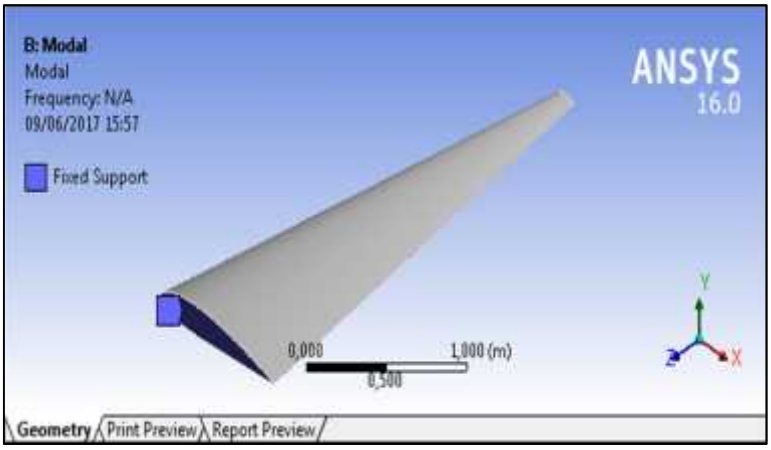

- **Solution**
  Solution →deformation → total→ Mode 1
  (name it mode shape one)
  Solution →deformation → total→Mode 2
  (name it mode shape two)
  Solution →deformation → total→Mode 3
  (name it mode shape three)
  Solution →deformation → total→Mode 2(name it mode shape four)

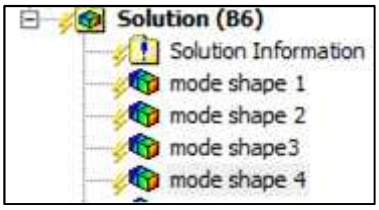

- Finally click on **solve** to get the result.

Appendix 06: Static structural analysis

for the static structural analysis, it is the same as the modal analysis for the geometry and the engineering data.

For the model, it is the same but we add the force in modal.

- Modal → Loads →Force
  Force →Defined by → Components

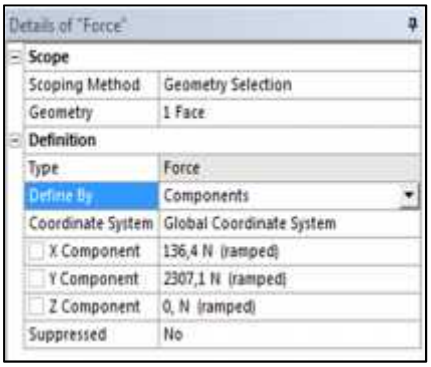

➢ **Solution**

- Solution → Deformation →Total
  Solution → Strain → Equivalent (von-Mises)
  Solution → stress → Equivalent (von-Mises)
  Solution → Energy → Strain Energy
- Finally click on **solve** to get the result.